Functional characterization of coronavirus non-structural proteins

Chen, Bo

2008

Chen, B. (2008). Functional characterization of coronavirus non-structural proteins. Doctoral thesis, Nanyang Technological University, Singapore.

https://hdl.handle.net/10356/39373

https://doi.org/10.32657/10356/39373

FUNCTIONAL CHARACTERIZATION OF CORONAVIRUS NON-STRUCTURAL PROTEINS

CHEN BO

SCHOOL OF BIOLOGIAL SCIENCES

NANYANG TECHNOLOGICAL UNIVERSITY

2008

FUNCTIONAL CHARACTERIZATION OF CORONAVIRUS NON-STRUCTURAL PROTEINS

CHEN BO

SCHOOL OF BIOLOGICAL SCIENCES

A THESIS SUBMITTED TO THE NANYANG TECHNOLOGICAL UNIVERSITY IN FULFILLMENT OF THE REQUIREMENT FOR THE DEGREE OF DOCTOR OF PHILOSOPHY

2008

This dissertation is dedicated to those people in my life who have made it possible, especially to my parents, my husband, and my son.

ACKNOWLEDGEMENTS

When I start wrote this chapter, I found it is the easiest and hardest chapter that I have to write. It will be simple to name all the people that helped me to get this work done, but it will be tough to thank them enough.

There are number of people who have helped me both personally and professionally during the past five years. Their help has taken me to complete my Ph.D. I would like to express my heartfelt thanks to those who have helped me to reach this point.

First of all, I would like to express my deepest appreciation to my supervisor, Dr. Dingxiang Liu, for his excellent scientific and technical guidance. This thesis would not have been possible without his great support, the trenchant critiques, the probing questions, cracking-of-the-whip and the remarkable patience. His precise and serious-minded attitude to science impresses me deeply.

I would like gratefully acknowledge my co-supervisor Prof. James P. Tam. He gave me the opportunity to pursue research work, the encouragement to face the hard work with a smile on the lips and confidence to deal with the politics of science.The help he have given to me have been invaluable over the years.

There were a number of pals and colleagues in Dr. Liu's lab and Prof. Tam's lab with whom I worked closely and would like to acknowledge here. They are Frank Li Qisheng, Li Yanning, Liao Ying, Wang Jibin, Wang Li, Yuan Quan and Wu Zhihao. I deeply

appreciate their constant help and friendship over the past five years. I would also like to thank Ji zhe for his assistance with all types of technical problems at all times. I have greatly benefited from his invaluable and honest help. Many thanks also to members in Dr. Liu's lab in IMCB whose guidance have ensured that my experiments went as smoothly as possible.

Sincere thanks to all members in my dissertation committee for their valuable comments and suggestions.

My final words go to my family. I am proud to dedicate this dissertation to my husband and my son for the incredible quantity of their love. Their love is the source of all my courage and the motivation for my progress in science. Their support was critical to this thesis work. Thanks to them for their understanding, endless patience and encouragement when it was most required.

This work was supported by the Agency for Science, Technology and Research, Singapore, and grants from the Biomedical Research Council, Agency for Science, Technology and Research, Singapore.

ABSTRACT

Genetic manipulation of the RNA genomes by reverse genetics is a powerful tool to study the molecular biology and pathogenesis of RNA viruses. During construction of an infectious clone from a Vero cell-adapted coronavirus infectious bronchitis virus (IBV), we found that a G - C point mutation at nucleotide position 15526, causing Arg-to-Pro mutation at amino acid position 132 of the helicase protein, is lethal to the infectivity of IBV on Vero cells. When the in vitro-synthesized full-length transcripts containing this mutation were introduced into Vero cells, no infectious virus was rescued. Upon correction of the mutation, infectious virus was recovered. Further characterization of the in vitro-synthesized full-length transcripts containing the G15526C mutation demonstrated that this mutation may block the transcription of subgenomic RNAs. Substitution mutation of the Arg132 residue to a positively charged amino acid Lys affected neither the infectivity of the in vitro-synthesized transcripts nor the growth properties of the rescued virus. However, mutation of the Arg132 residue to Leu, a conserved residue in other coronaviruses at the same position, reduced the recovery rate of the in vitro-synthesized transcripts. The recovered mutant virus showed much smaller-sized plaques. On the contrary, a G - C and a G - A point mutations at nucleotide positions 4330 and 9230, respectively, causing Glu - Gln and Gly - Glu mutations in or near the catalytic centers of the papain-like (Nsp3) and 3C-like (Nsp5) proteinases, did not show detectable detrimental effect on the rescue of infectious viruses and the infectivity of the rescued viruses.

Coronaviruses devote more than three quarters of their coding capacity to encode two large polyproteins (1a and 1ab polyproteins), which are proteolytically processed into 15-16 mature, nonstructural replicase proteins (nsp1 to 16). These cleavage products are believed to play essential roles in replication of the giant RNA genome of ~30 kb and transcription of a nested set of 5 to 9 subgenomic RNA species by a unique discontinuous transcription mechanism. In this report, one of these replicase proteins, nsp9 of the coronavirus infectious bronchitis virus (IBV) is systematically studied using both biochemical and reverse genetics approaches. The results showed that substitution of a conserved Gly (G98) residue in the C-terminal α-helix with an Asp greatly destabilized the IBV nsp9 homodimer and abolished its RNA-binding activity. Introduction of the same mutation into an infectious IBV clone system showed that the mutation totally abolishes the transcription of subgenomic RNA and no infectious virus could be recovered. Mutation of a semi-conserved Ile (I95) residue in the same region showed moderately destabilizing effect on the IBV nsp9 homodimer but minimal effect on its RNA-binding activity. Introduction of the mutation into the IBV infectious clone system showed recovery of a mutant virus with severe growth defects, supporting that dimerization is critical for the function of this replicase protein. Meanwhile, mutations of some positively charged residues in the β-barrel regions of the IBV nsp9 protein significantly reduced its RNA-binding activity, but with no obvious effect on dimerization of the protein. Introduction of these mutations into the viral genome showed only mild to moderate effects on the growth and infectivity of the rescued mutant viruses.

TABLE OF CONTENTS

LIST OF TABLES

LIST OF FIGURES

LIST OF ABBREVIATIONS

aa.....amino acids

A.....alanine

ACE2.....angiotensin converting enzyme 2

APN.....canine aminopeptidase N

APV.....avian pneumovirus

Arg.....arginine

BAC.....bacterial artificial chromosome

BCoV.....bovine coronavirus

bp.....base pair

C.....cysteine

CCoV.....canine coronavirus

CEACAM1.....carcinoembryonic antigen-cell adhesion molecule

CECoV.....canine enteric coronavirus

3CLpro.....3C-like protein

CMC.....carboxymethy cellulose

CoV.....coronavirus

CPEs.....cytopathic effects

CRCoV.....canine respiratory coronavirus

C-terminal.....carboxy-terminal

DCoV.....duck coronavirus

DMEM.....dulbecco's modified eagle medium

DMVs.....double-membraned vesicles

DNaseI..... deoxyribonuclease I

DTT.....dithiothreitol

E protein.....coronavirus envelope protein

EAV.....equine arteritis virus

EGFP.....enhanced green fluorescent protein

ER.....endoplasmic reticulum

ERGIC.....ER-to-Golgi intermediate compartment

ExoN.....exonuclease

FBS..... fetal bovine serum

FCoV.....feline enteric coronavirus

FIPV.....feline infectious peritonitis virus

GCoV..... goose coronavirus

Gln.....glutamine

Glu.....glutamic acid

Gly.....glycine

HCV..... .....heptatis C virus

HCoV.....human coronavirus

HCoV OC43..... .....human coronavirus OC43

HE.....haemagglutinin

HEV.....porcine haemagglutinating encephalomyelitis coronavirus

His.....histidine

HIV-1.....human immunodeficiency virus type 1

HR.....heptad repeat

HRV14.....human rhinovirus 14

HS.....heparan sulfate

IBV.....infectious bronchitis virus

Ile.....isoleucine

IPTG.....isopropyl-b-D-thiogalactopyranoside

Kb.....kilo-base

kDa.....kilo-dalton

Leu.....leucine

Lys.....lysine

M protein.....membrane protein

MCS.....multiple cloning site

MEM.....modified eagle medium

MHV.....mouse heptatis virus

ml.....milliliter

mM.....millimolar

MW.....molecular weight

N48.....asparagine 48

N66..... asparagine 66

NDV.....Newcastle disease virus

N protein.....coronavirus nucleocapsid protein

nsp.....non-structural protein

nt.....nucleotide

µl.....microliter

OB.....oligonucleotide-oligosaccharide binding

ONPG.....orthonitro-phenyl-beta-D-galactopyranoside

ORFs.....open reading frames

p65..... passage 65

PAGE.....polyacrylamide gel electrophoresis

PBS.....phosphate buffered saline

PEDV..... porcine epidemic diarrhoea coronavirus

PFU.....plaque forming unit

PhCoV..... .....pheasant coronavirus

PiCoV.....pigeon coronavirus

Pro.....proline

PVDF.....polyvinylidene difluoride

RBD..... .....receptor-binding domain

RDRP..... .....RNA dependent RNA polymerase

RT-PCR.....reverse transcriptase-PCR

S protein.....spike protein

SARS .....severe acute respiratory syndrome

SARS-CoV.....severe acute respiratory syndrome coronavirus

SDS.....sodium dodecyl sulfate

TCoV.....turkey coronavirus

TGEV.....transmissible gastroenteritis virus

TRSs.....transcription regulating sequences

Tyr.....tyrosine

UTR.....untranslated region

v/v.....volume/volume

w/v.....weight/volume

VLP.....virus-like particle

vTF7-3..... vaccinia virus-T7

CHAPTER I INTRODUCTION

1.1. Taxonomy

Coronaviruses are grouped in the order Nidovirales. Other families in the Nidovirales order are Arteviridae (Snijder and Meulenberg, 1998) and Roniviridae (Cowley et al., 2000; Dhar et al., 2004), which include viruses that infect swine and equine, and invertebrates. Nidovirals have common features which set them apart from other nonsegmented positive-strand RNA viruses. The most salient features include gene expression through transcription of a set of multiple 3'-nested subgenomic RNAs; expression of the replicase polyprotein via ribosomal frameshifting; unique enzymatic activities among the replicase protein products. In contrast to their commonalities, nidovirus families differ from one another in distinct ways, most conspicuously in the numbers, types, and sizes of the structural proteins in their virions and in the morphologies of their nucleocapsids (Masters, 2006).

Members of the coronavirus family are assigned to three groups (Table 1), were initially based on antigenic relationships (McKintosh et al., 1969; Bradburne, 1970; Pensaert et al., 1981). This classification was subsequently supported by gene sequencing. Almost all group I and group II viruses have mammalian hosts, with human coronaviruses falling into each of these two groups. Viruses in group 3, by contrast, have been isolated solely from avian hosts.

Viruses in Group I do not have the hemagglutinin-esterase (HE) protein; the membrane (M) protein is N-glycosylated and the spike (S) protein is not cleaved.

Most of Coronaviruses in Group II have an HE protein; the M protein is O-glycosylated and S protein is cleaved into two subunits. Viruses in Group III do not have an HE protein; the M protein is N-glycosylated and S protein is cleaved.

In February 2003, severe acute respiratory syndrome (SARS) in humans was reported in Guangdong Province, the People's Republic of China. The disease spread to over 24 countries in only a few months, infecting 8098 people worldwide and killing 774 (World Health Organization, http://www.who.int/csr/sars/en/; Goldsmith et al., 2004; Marra et al., 2003; Rota et al., 2003). The etiological agent of SARS was quickly identified as a newly emerged coronavirus. Masked palm civets were suspected as the origin of the SARS outbreak in 2003 and was confirmed as the direct origin of SARS cases with mild symptom in 2004. Sequence analysis of the SARS coronaviurs (SARS-CoV)-like virus in masked palm civets indicated that they were highly homologous to human SARS-CoV with nucleotide identity over 99.6%, indicating the virus has not been circulating in the population of masked palm civets for a very long time (Shi and Hu. 2007).

Based on sequence analysis of the polymerase protein, SARS-CoV has been placed as a distant member of the Group II coronaviruses. Although it lacks genes that are common in group II viruses, like the papain-like proteinase 1 ($PL1^{pro}$) and

HE genes, but it possesses distant homologues of cellular RNA processing enzymes and four of them are conserved in SARS-CoV (Snijder et al., 2003). Currently available evidence best supports the conclusion that it is closely allied with the group II coronaviruses.

However, like Group III avian coronaviruses, it does not have an HE protein, and the SARS-CoV membrane protein is N-glycosylated and S protein was shown to be cleaved in vitro (Voss et al., 2006; Wu et al., 2004). It is also interesting to note that the gene organization of the 3' end of the SARS-CoV genome is most similar to the Group III avian viruses.

1.2. Virion Morphology, Structural Proteins, and Accessory Proteins

1.2.1. Virion morphology

Coronaviruses are roughly spherical and moderately pleiomorphic (Fig1.1). Virions have been reported to have average diameters of 80–120 nm, but extreme sizes as small as 50 nm and as large as 200 nm are occasionally given in the older literature (Oshiro, 1973; McIntosh, 1974). The surface spikes or peplomers of these viruses were described as club-like, pear-shaped, or petal-shaped and project some 17–20 nm from the virion surface (McIntosh, 1974), they had a thin base that swells to a width of about 10 nm at the distal extremity (Sugiyamaand et al.,

1981). For some coronaviruses a second set of projections, 5–10-nm long, forms an undergrowth beneath the major spikes (Guy et al., 2000; Patel et al., 1982; Sugiyamaand et al., 1981). These shorter structures are now known to be HE protein that is found in a subset of group 2 coronaviruses. A lipid bilayer comprising S protein, M protein and the envelope protein (E) cloaks the helical nucleocapsid, which consists of the nucleocapsid protein (N) that is associated with the viral RNA. In the case of coronaviruses, the lipid envelope is derived from intracellular membranes (Fig 1. a and b).

Table 1.1. Coronavirus Species and Groups

Group 1
Subgroup 1a
Porcine transmissible gastroenteritis coronavirus (TGEV)
Canine enteric coronavirus (CECoV)
Feline coronavirus (FCoV)
Subgroup 1b
Porcine epidemic diarrhoea coronavirus (PEDV)
Human coronavirus 229E (HCoV) and other species (e.g. NL-63)
Bat coronavirus
Group 2
Subgroup 2a
Murine hepatitis coronavirus (MHV)
Human coronavirus OC43 (HCoV OC43) and other species
Bovine coronavirus (BCoV)
Canine respiratory coronavirus (CRCoV)
Porcine haemagglutinating encephalomyelitis coronavirus (HEV)
Puffinosis coronavirus (from a shearwater, Puffinus puffinus)
Subgroup 2b
SARS-coronavirus (SARS-CoV)b
Group 3
Infectious bronchitis coronavirus (IBV)
Turkey coronavirus (TCoV)
Pheasant coronavirus (PhCoV)
Goose coronavirus (GCoV)
Duck coronavirus (DCoV)
Pigeon coronavirus (PiCoV)

Cavanagh, D.（2005）Coronaviruses in poultry and other birds. *Avian Pathol.* 34 (6): 439-448.

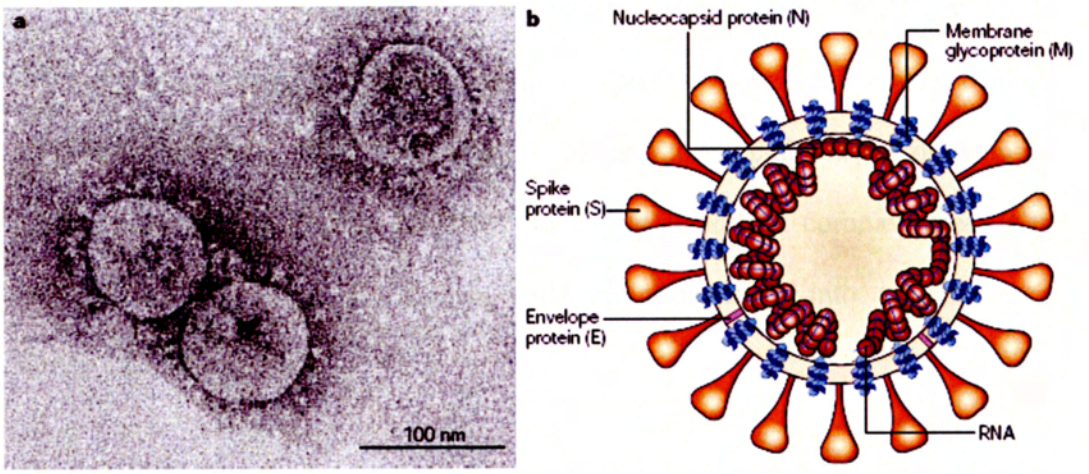

Fig.1.1. Morphology of the SARS coronaviurs. **a.** Electron micrograph of the virus that was cultivated in Vero cells. (Image courtesy of Dr L. Kolesnikova, Institute of Virology, Marburg, Germany). **b.** Schematic representation of the virus. (Konrad Stadler, Nature Reviews Micorbiology, 2003 1:209-218)

1.2.2. Structural features of coronaviruses

1.2.2.1 Spike protein (S)

All coronaviruses possess four structure proteins (S, E, M and N). The order of the structural protein genes within the genome is the same for all coronaviruses (Fig.1.1). The most entirely studied coronavirus structural protein is S protein. It is a very large, N-exo, C-endo transmembrane protein that assembles into trimers (Delmas and Laude, 1990; Song et al., 2004) and forms club-shaped projections on the surface of the virus particles. In Group II and III coronaviruses, it is posttranslationally cleaved by host cell serine proteases into two subunits designated S1 and S2.

Studies with some coronaviruses have shown that the S protein mediates receptor attachment, viral and host cell membrane fusion (Cavanagh et al., 1995; Collins et al., 1982). Coronaviruses can bind to specific host cell receptors. Some receptors have been identified; for example, SARS-CoV binds to angiotensin converting enzyme 2 (ACE2). When the S protein binds to its specific cell receptor it undergoes a conformational change involving two heptad repeat regions that bring the S protein fusion peptide close proximity to the viral transmembrane segment, which facilitates membrane fusion and virus entry into the cell (Bosch et al., 2004).

The S protein is a determinant of host range and pathogenicity (de Haan et al., 2002; Haijema et al., 2004; Boursnell et al., 1989; Lai et al., 2001; Weiss et al., 2005). A receptor-binding domain (RBD) within the N-terminal region of S protein forms part of the globular head of the mature protein. Changes in S protein and specifically in the RBD can alter host cell specificity and mediate shift in viral pathogenesis (Hodgson et al., 2004; Kuo et al., 2000; Sanchez et al., 1999). For example, when the MHV S protein gene was substituted for the FIPV S protein using targeted recombination, the recombinant feline MHV containing the feline S-glycoprotein was now capable of infecting feline cells and lost its ability to infect murine cells (Kuo et al., 2000). A host shift was also observed in TCoV, which is closely related to IBV (Jackwood et al., 2004). However, pathogenicity does not appear to be solely related to the S glycoprotein in some coronaviruses. In the case of IBV, the S protein is possibly a determinant but is not necessarily a determinant of pathogenicity. When S gene of the non-pathogenic Beaudette strain was replaced with that of the pathogenic M41 strain, the host range of Beaudette was altered in vitro: the virus no longer replicated in Vero cells (Casais et al., 2001, 2003), but no difference in pathogenicity was observed between the recombinant and the parental strain (Hodgson, T et al., 2004).

1.2.2.2 Membrane protein (M)

The M protein is the most abundant constituent of coronaviruses (Sturman, 1977; Sturman et al., 1980) and gives the virion envelope its shape (Fig.1.1). It is a multi-spanning membrane protein with a small, amino-terminal domain located on the exterior of the virion, or, intracellularly, in the lumen of the ER. M protein within each coronavirus group is moderately well conserved, but is quite divergent across the three groups.

The most conservative region of M protein is a segment of some 25 residues encompassing the end of the third trans-membrane domain and the start of the endodomain (den Boon et al., 1991). The ectodomain of the M molecule is glycosylated. For most group 2 coronaviruses, glycosylation is O-linked, but the M protein of MHV strain 2 (Yamada et al., 2000) and SARS-CoV (Nal et al., 2005) is N-linked glycosylated. Group 1 and group 3 coronavirus M proteins, by contrast, exhibit N-linked glycosylation exclusively (Cavanagh and Davis, 1988; Garwes et al., 1984; Jacobs et al., 1986; Stern and Sefton, 1982). Although the role of M protein glycosylation is not fully understood, the glycosylation status of M can influence both organ tropism in vivo and the capacity of some coronaviruses to induce alpha interferon in vitro (Charley and Laude, 1988; de Haan et al., 2003a; Laude et al., 1992). It shows that M protein may play a role in viral pathogenesis.

Most M proteins do not possess a cleaved amino-terminal signal peptide (Cavanagh et al., 1986b; Rottier et al., 1984), and for both IBV and MHV it was demonstrated that either the first or the third transmembrane domain alone is sufficient to function as the signal for insertion and anchoring of the protein in its native orientation in the membrane (Krijnse et al., 1992b; Machamer and Rose, 1987; Mayer et al., 1988). M protein of group 1 coronaviruses (TGEV, FIPV, and CCoV) each contains a cleavable amino-terminal signal sequence (Laude et al., 1987), but this element may not be required for membrane insertion (Kapke et al., 1988; Vennema et al., 1991).

M protein plays many important biological functions in the viral life cycle. Physical interactions between M protein of SARS-CoV and other viral proteins, including N (Fang et al., 2005; He et al., 2004; Kuo et al., 2002), S (Yue et al., 2004), 3a (Tan et al., 2005), and 7a (Fielding et al., 2006) which involve in viral replication, have been elucidated. Recently, SARS-Cov M protein has also been reported to induce apoptosis through the modulation of the cellular Akt pro-surviral pathway and mitochondrial cytochrome C release. All these studies provide some potential functions in regulating viral replication and packing genomic RNA into viral particles.

1.2.2.3 Envelope protein (E)

All coronavirus E proteins are small integral membrane proteins with rather long hydrophobic domains (Arbely et al., 2004; Corse et al., 2000; Raamsman et al.,

2000). It is only a minor constituent of virions and varies in size from 76 to 109 amino acids. But all E proteins have the same general architecture: a short hydrophilic amino terminus, followed by a large hydrophobic region containing two to four cysteines, and a hydrophilic carboxy-terminal tail. The E protein of IBV has been shown to be palmitoylated on one or both of its two cysteine residues (Corse and Machamer, 2002), but it is not currently clear whether this modification is a general characteristic. Functionally, coronavirus E protein plays a pivotal role in viral morphogenesis, assembly and budding. Co-expression of MHV E and M was shown to result in the production of virus-like particles, roughly the same size and shape as virions (Madan et al., 2005; Wilson et al 2005). The same phenomena were also observed in other coronaviruses, such as SARS-CoV and IBV (Corse et al., 2003; Ho et al., 2004). More recently, the SARS-CoV E protein was found to permeabilize bacterial cells as well as to form pores in artificial membranes (Liao et al., 2004, 2006; Wilson et al., 2004). It was also reported that MHV E protein could modify the membrane permeability in both Escherchia coli and mammalian cells (Madan et al., 2005). The viroporin activity of Coronaviruses E protein can enhance membrane permeability and promote virus budding. However, many viroporins are not required for viral replication, although their presence significantly increases the formation of virus particles (Hatta et al., 2003; Klimkait et al., 1990; Loewy, 1995; Madan et al., 2004; McInerney et al., 2004; Watanabe et al., 2001).

1.2.2.4 Nucleocapsid protein (N)

Coronavirus N protein, which ranges from 43 to 50 kDa, has a structural role as it forms a ribonucleoprotein complex with gRNA in a beads-on-a-string fashion (Laude and Masters, 1995) (Fig.1.1). In addition to its structural role, the N protein also participates in viral RNA transcription, replication and in modulating the metabolism of host cells (Almazan et al., 2004; Baric et al., 1988; Chang et al., 2005; Chang et al., 1996; Eleouet et al., 2000; He et al., 2003, 2004; Li et al., 2005; Schelle et al., 2005; Surjit et al., 2004).

Although N proteins from different coronaviruses are variable in length and primary sequence, a conserved three-domain organization was proposed (Parker and Masters, 1990). Domains 1 and 2 are rich in arginines and lysines which are typical of many viral RNA-binding proteins. In contrast, the short, carboxy-terminal domain 3 has a net negative charge resulting from an excess of acidic over basic residues. People believe that domain 3 constitutes a separate domain (Hurst et al., 2005; Koetzner et al., 1992), little is known about the structure of the other two putative domains. Domain II is more conserved than domains I and III, especially in a serine-rich region that is important for the biological function of N protein.

The main function of N protein is to bind the viral RNA. Specific RNA substrates that have been identified for N protein include the positive sense transcription regulating sequence (Chen et al., 2005; Nelson et al., 2000; Stohlman et al., 1988),

regions of the 3' UTR (Zhou et al., 1996) and N gene (Cologna et al., 2000), and the genomic RNA packaging signal (Cologna et al., 2000; Molenkamp and Spaan, 1997). The nucleocapsid N protein of coronavirus infectious bronchitis virus (IBV) is highly sensitive to proteolysis. Like the N-terminal RNA binding domain (SARS-N45-181) of the severe acute respiratory syndrome virus (SARS-CoV) N protein, the crystal structure of the IBV-N29-160 fragment at 1.85A° resolution reveals a protein core composed of a five-stranded antiparallel b sheet with a positively charged b hairpin extension and a hydrophobic platform that are probably involved in RNA binding (Fan et al., 2005).

In addition, N proteins of some coronaviruses, including IBV, TGEV and MHV, are localized to both cytoplasm and nucleolus, and the presence of N in the nucleolus may be important for the synthesis of viral RNA (Hiscox et al., 2001; Wurm et al., 2001). For SARS-CoV N protein, it has been reported to be found in the cytoplasm and nucleus of SARS-CoV infected cells (Chang et al., 2004; Zeng et al., 2004a).

N protein has also been found to be able to enhance the efficiency of replication of replicon or genomic RNA in reverse genetic systems in which infections are initiated from engineered viral RNA (Almazan et al., 2004; Schelle et al., 2005; Thiel et al., 2001a; Casais et al., 2001; Yount et al., 2000, 2002; Youn et al., 2005a, 2005b). This may be indicative of a direct role of N in RNA replication,

but it remains possible that the enhancement actually results from the sustained translation of a limiting replicase component.

1.2.3. Accessory proteins of coronaviruses

Each coronavirus encodes different numbers of accessory proteins (Table II) and the predicted sequences of these proteins do not share high level of homology, although there may be some degree of conservation within each subgroup of coronaviruses (Brown and Brierly, 1995). These "extra" genes can fall in any of the genomic intervals among the canonical genes, and also called "group specific

gene". For example, the SARS-CoV genome encodes eight putative accessory proteins (i.e. ORFs 3a, 3b, 6, 7a, 7b, 8a, 8b and 9b) varying in length from 39aa to 274aa, as shown in Fig.1.2. While the SARS-CoV replicase genes and structural proteins share some degree of sequence homology with those of other coronaviruses, the accessory proteins do not show significant homology, at the amino acids level, to viral proteins of known coronaviruses. However, emerging evidence suggests that some of SARS-CoV accessory proteins, like 3a, 3b, are strongly conserved and they may share some structural and biological features with other coronaviral proteins.

In the SARS CoV, 3a was demonstrated to be a novel coronavirus structural protein and can associate with virions purified from SARS CoV infected cell. It is incorporated into viral-like particles when co-expressed with M and E in the baculolviurs system, (Ito et al., 2005; Shen et al., 2005) and can interact with other structural proteins, such as M, E and S protein (Tan et al., 2004c). Over-expression of 3a in Vero E6 cells can also trigger apoptosis via a caspase-8 dependent pathway (Law et al., 2005). For 3b protein which is the second ORF in subgenomic RNA3, much less information is available. But it has been demonstrated that the over-expression of 3b can induce cell cycle arrest at the G0/G1 phase and apoptosis (Yuan et al., 2005b). However, it was not determined if apoptosis was occurring via a caspase-dependent pathway or if it is the consequence of the cell cycle arrest.

TABLE II
CORONAVIRUS ACCESSORY PROTEINS

Group	Virus species	Accessory genes (Proteins)*
1	TGEV	[rep] - [*S*] - 3a, 3b - [*E*] - [*M*] - [*N*] - 7
	FIPV	[rep] - [*S*] - 3a, 3b, 3c - [*E*] - [*M*] - [*N*] - 7a, 7b
	HCoV-229E	[rep] - [*S*] - 4a, 4b - [*E*] - [*M*] - [*N*]
	PEDV	[rep] - [*S*] - 3 - [*E*] - [*M*] - [*N*]
	HCoV-NL63	[rep] - [*S*] - 3 - [*E*] - [*M*] - [*N*]
2	MHV	[rep] - 2a, 2b(HE) - [*S*] - 4 - 5a, [*E*] - [*M*] - [*N*], 7b(I)
	BCoV	[rep] - 2a - 2b(HE) - [*S*] - 4a(4.9k), 4b(4.8k) - 5(12.7k) [*E*] - [*M*] - [*N*], 7b(I)
	HCoV-OC43	[rep] - 2a - 2b(HE) - [*S*] - 5(12.9k) - [*E*] - [*M*] - [*N*], 7b(I)
	SARS-CoV	[rep] - [*S*] - 3a, 3b - [*E*] - [*M*] - 6 - 7a, 7b - 8a, 8b - [*N*], 9b(I)
	HCoV-HKU1	[rep] - 2(HE) - [*S*] - 4 - [*E*] - [*M*] - [*N*], 7b(I)
	Bat-SARS-CoV	[rep] - [*S*] - 3 - [*E*] - [*M*] - 6 - 7a, 7b - 8 - [*N*], 9b(I)
3	IBV	[rep] - [*S*] - 3a, 3b, 3c - [*E*] - [*M*] - 5a, 5b - [*N*]

(Paul S. Masters, *Adv. Virus Res.* 66 p212)

Table.I.2. Coronavirus Assessory Proteins. Accessory genes and proteins are listed only for coronaviruses for which a complete genomic sequence is available. The protein product is indicated in parentheses in cases where it has a different designation than the gene. Products of separate transcripts are separated by hyphens; the transcription of accessory genes may vary among different strains of the same virus species (O'Connor and Brian, 1999). The canonical coronavirus genes are indicated in brackets; rep denotes replicase.

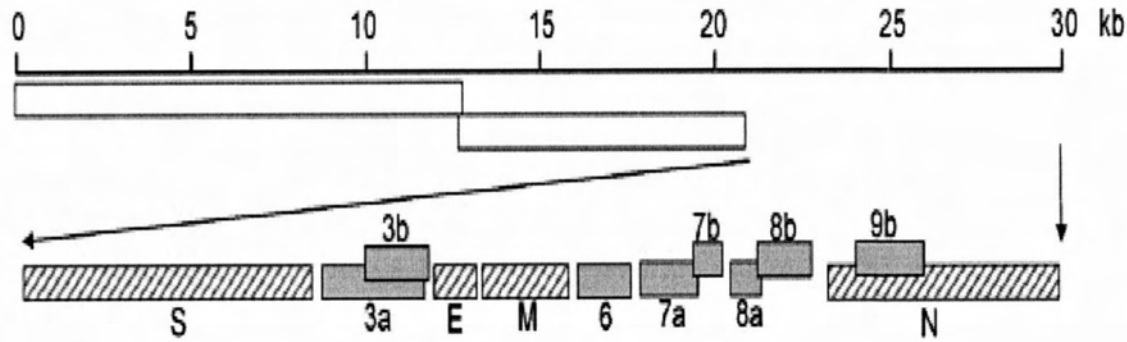

(Yee-Joo Tan et al. 2006 Antiviral Research 72, 78–88)

Fig.1.2. Schematic diagram showing the location of the accessory proteins in the severe acute respiratory syndrome coronavirus (SARS-CoV) genome. Open reading frames (ORFs) in the last 1/3 of the SARS-CoV genome are translated from eight subgenomic mRNAs. Four of these encode the structural proteins (checked boxes), spike (S), membrane (M) and envelope (E) and nucleocapsid (N). Another eight SARS-CoV-unique ORFs (grey solid boxes) encode accessory proteins (3a, 3b, 6, 7a, 7b, 8a, 8b and 9b) with no significance sequence homology to viral proteins of other coronaviruses.

1.3. Genome of coronaviruses

The coronavirus genome contains a single stranded, positive-sense RNA of 27 000 to 32 000 nucleotides, which is the largest viral RNA genome known. They all have the same general genome organization (Cavanagh et al., 2005; Lai., 1997; Weiss., 2005). The invariant gene order in all members of the coronavirus family is 5'-replicase-S-E-M-N-3', where the UTR are untranslated regions (each ~500 nucleotides in IBV). The 5' end of coronavirus genome is capped, and starts with a leader sequence of 65-98 nucleotides, which is also present at the 5' end of mRNAs, followed by a 200-to 400-mucleotide untranslated region (UTR). At the termini of the genome is a 3' UTR, ranging from 270 to 500 nucleotides followed by a poly (A) tail (Lai and Stohlman., 1978, 1981; Lomniczi et al., 1977; Schochetman et al., 1977; Wege et al., 1978) (Fig.1.3).

Almost two-thirds of the entire RNA is occupied by the polymerase gene, which comprises two overlapping ORFs, 1a and 1b (Thiel et al., 2003). Expression of the ORF 1b-encoded region of pp1ab involves ribosomal frameshifting into the −1 frame just upstream of the ORF 1a translation termination codon (Thiel et al., 2003). Proteolytic processing of these polyproteins is mediated by viral cysteine proteinases and produces 13-16 non-structural proteins (also called nsp's), some of which are responsible for replicating the viral genome and/or generating a nested set of subgenomic mRNAs to express all the ORFs downstream of ORF 1b (Ziebuhr et al., 2000).

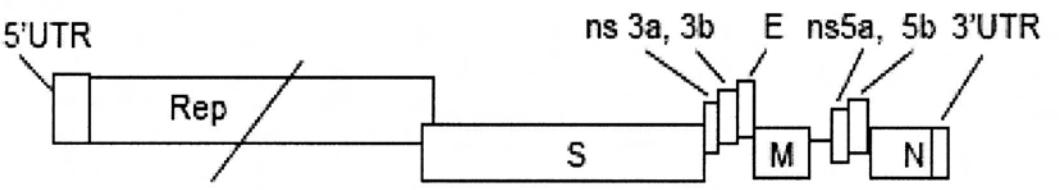

Dave Cavanagh. 2005. Avian Pathlolgy. 34 (6), p441

Fig.1.3. Coronavirus genomic organization. The layout of the IBV genome is shown as an example. Gene 1, which accounts for approximately two-thirds of the genome, encodes many proteins that are associated with RNA replication and transcription. All coronaviruses have the structural protein genes S, E, M and N in the same order. Where the genomes of coronaviruses differ is in respect of the number and location of genes that encode non-structural proteins (nsp) that are situated among the structural.

1.4. Coronavirus Replication Cycle

1.4.1. Virus entry and receptors

The infection cycle of the coronavirus starts with the binding of the virion to specific virus receptors on the cell surface (Fig.1.4). Virus-receptor interaction triggers the fusion of the viral envelope and the host cell membrane, which results in virus entry. Next, the virus disassembles, releasing its genomic RNA into the cytoplasm of the host cell.

Translation of the replicase genes produces two large precursor proteins (pp1a and pp1ab), many cleavage products of which collectively constitute the functional replication–transcription complexes on double-membraned vesicles (DMVs). Genes located downstream of the replicase genes are expressed from a 3′-coterminal nested set of subgenomic mRNAs, each of which contains a short 5′ leader sequence derived from the 5′ end of the genome (Fig.1.4). Many copies of N protein package the genomic RNA into a helical nucleocapsid. The envelope proteins (S, E and M) are inserted into the ER membrane, and accumulate in the ER-to-Golgi intermediate compartment (ERGIC) to meet the nucleocapsid and, subsequently, to assemble into particles by budding. Finally, the complete virions are transported out of the cell via smooth-walled vesicles.

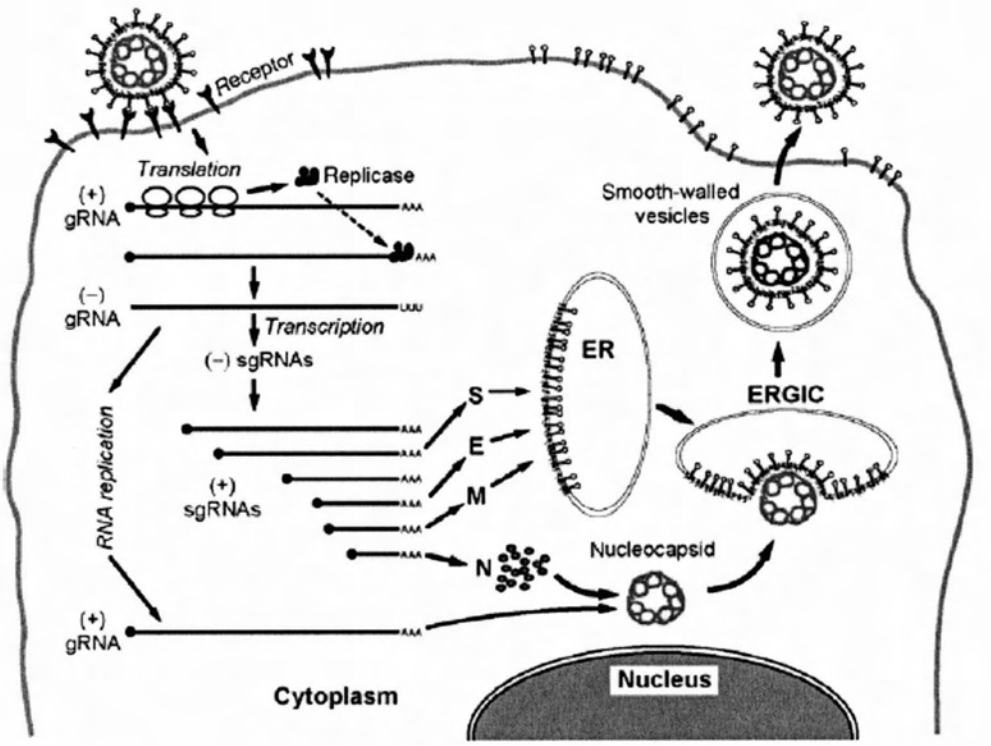

Fig.1.4. Cornavirus life cycle.

(Paul S. Masters. Advances in virus research. Vol 66)

Interaction with receptor is the first step leading to a successful entry and productive replication. Binding of the S protein to the receptor triggers a series of conformational changes that ultimately results in the structural rearrangements in the S protein. These structural rearrangements can generate the energy which drives the fusion of the viral and cellular lipid membrane. In contrast to other viral families that utilize a universal receptor to gain entry into host cells, members in the coronavirus family use a variety of cellular proteins and/or cofactors.

Group 1 CoVs – including HCoV-229E, FIPV, TGEV and CCV – utilize human, feline, porcine, and canine aminopeptidase N (APN) as functional receptors during virus entry (Yeager et al., 1992; Delmas et al., 1992; Tresnan et al., 1996). But HCoV-NL63 utilizes ACE2. In group 2 CoV, MHV of group 2a and SARS-CoV of group 2b independently utilize carcinoembryonic antigen-cell adhesion molecule (CEACAM1) and ACE2 to mediate infection (Nash et al., 1996; Li et al., 2003). However, other group 2a CoVs, including HCoV-OC43 and BCoV recognize N-acetyl-9-Oacetylneuraminic acid as a functional receptor (Schwegmann et al., 2006). Receptors for group 3 CoVs are still undetermined.

1.4.2. Virion assembly and release

In virus-infected cells, the assembly of virus particles takes place through a series of cooperative interactions that occur in the ER and the ERGIC among the structural proteins, S, M, E, and N. It is clear that the M protein, a triple spanning

membrane protein, is the key player in coronavirus assembly. The M protein exerts its central role in assembly by selecting and organizing the viral envelope components at the assembly sites and by mediating the interactions with the nucleocapsid to allow the budding of virions. Despite its dominant role, however, M protein alone is not sufficient for virion formation. Independent expression of M protein does not result in its assembly into virion-like structures.

There are two types of interactions which affect the incorporation of the nucleocapsid into the virion: protein–protein interactions between the M protein and the N protein and protein–RNA interactions between the M protein and the viral genome. At the level of the membrane the M protein interacts with itself, to generate the basic molecular framework of the envelope; with the E protein, to induce the budding and release of the M protein-modified membrane; and with the S protein, to assemble the spikes into the viral envelope. Although the S protein is not required for virus-like particle (VLP) formation, it does become incorporated into VLPs if coexpressed with M and E proteins (Bos et al., 1996; Vennema et al., 1996). In addition, the SARS-CoV M protein interacts with the 3a protein, resulting in its incorporation into particles (Ito et al., 2005). Such VLPs independently formed by N protein, E and M are the minimally required proteins (Vennema *et al.*, 1996; de Haan and Rottier, 2005). This has also been reported for the SARS-CoV (Mortola and Roy, 2004; Hsieh *et al.*, 2005), although some studies have claimed the M and N proteins to be necessary and sufficient for formation of virus-like particles (Huang *et al.*, 2004).

1.5. Coronavirus RNA Synthesis

1.5.1. RNA replication and transcription

The process of coronavirus replication and transcription is very complex. There are two reasons for such a complexity. One is the generation of multiple subgenomic mRNAs and the process of discontinuous transcription during minus-strand synthesis demand complex replication transcription machinery. Another one is the large size of the coronavirus genome demands unusual activities to maintain genetic stability.

CoV genome replication is mediated through the synthesis of a negative-strand RNA, which in turn is the template for the synthesis of progeny virus genomes (Fig.1.5) (Baric and Yount, 2000; Sethna et al., 1989, 1991). Each positive-sense subgenome- length mRNA contains a 70–100-nt leader RNA which is derived from the 5' end of the genomic RNA. The 5' leader is joined to the body of the sgRNA which is identical to the 3' end of the genome. The 3'-nested set of sgRNAs, with or without a leader sequence, is a defining feature of the order Nidovirales (Enjuanes et al., 2000a; Van et al., 2002).

Coronavirus replication and transcription require recognition of the 5'and 3'ends of the RNA genome by viral and cellular proteins. Both ends are necessary for positive-strand synthesis, whereas only the last 55 nt from the 3' end and the poly (A) tail are required for the synthesis of negative-strand (Lin et al., 1994). During

the synthesis of the positive strand RNA the 3'end of the genome is the last region reached by the viral polymerase, the replication signal at the 3'end of the genome may interact with signals at the 5' end to exert its effect on RNA synthesis (Huang et al., 2001; Lai et al., 1998). For TGEV and IBV, the minimal replication signals at 5' end are limited to 1348 and 544 nucleotides, respectively (Dalton et al., 2001; Izeta et al., 1999). Although there is no apparent sequence complementarity between the 5' and 3' ends of the CoV genome, a direct interaction between the 5' and 3'ends is mediated by proteins through RNA-protein and protein-protein interactions (Huang et al., 2001).

The sites of leader-to-body fusion in the sgRNAs contain a short run of sequence that is identical, or nearly identical, to the 3' end of the leader RNA (Fig.1.5). These sites are called transcription-regulating sequences (TRSs), TRSs are fairly well conserved within each coronavirus group. The core consensus TRS is 5' AACUAAAC-3' for group 1; 5'-AAUCUAAAC-3' for group 2 (except for SARS-CoV, for which it is 5'-AAACGAAC-3'); and 5'-CUUAACAA-3' for group 3 (Thiel et al., 2003a; van der Most and Spaan, 1995). Not every TRS in a given virus conforms exactly to the consensus sequence; a number of allowable variant bases are found in individual TRSs.

The discontinuous step in sgRNA synthesis occurs during negative-strand RNA synthesis (Fig.1.6) (Sawicki and Sawicki, 1998, 2005). During RNA synthesis, the viral polymerase, starting from the 3' end of a genomic template, switches

templates at an internal TRS and resumes synthesis at the homologous TRS sequence at the 3' end of the genomic leader RNA. The resulting negative-strand sgRNA, in association with positive-strand gRNA, then serves as the template for synthesis of multiple copies of the corresponding positive-strand sgRNA (Sethna et al., 1989; Chang et al., 1994; Baric and Yount, 2000; Sawicki and Sawicki, 1990; Sawicki et al., 2001; Schaad and Baric, 1994).

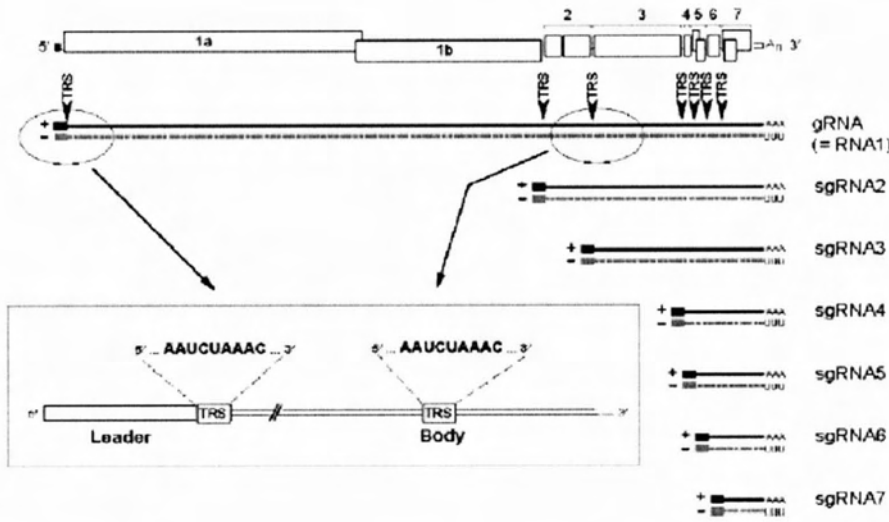

Fig.1.5. Coronavirus RNA synthesis. The nested set of positive- and negative-strand RNAs produced during replication and transcription are shown, using MHV as an example. The inset shows details of the arrangement of leader and body copies of the transcription-regulating sequence (Picture adapted from Masters, P. S. Advances in Virus Research, VOL 66).

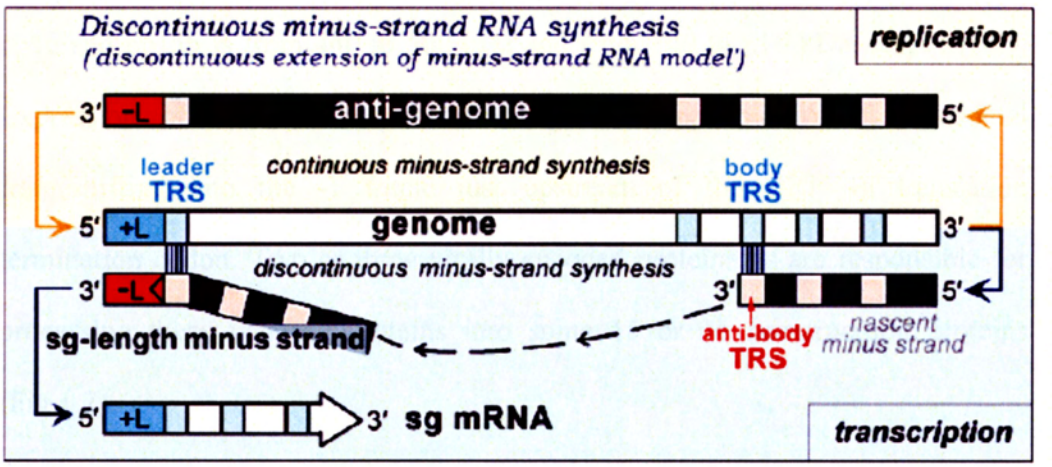

Fig.1.6. Model for discontinuous negative-strand transcription (Sawicki and Sawicki, 1998, 2005). Negative-strand sgRNAs are initiated at the 3' end of the gRNA template. The body TRSs in the genome would act as attenuation signals for minus-strand RNA synthesis, A strand-switching event then occurs, pairing the newly transcribed negative-sense body TRS with the leader copy of the TRS, from which point transcription resumes. A complex of the (+) gRNA and the (-) sgRNA then serves as the template for synthesis of multiple (+) sgRNAs. (Picture adapted from Alexander O et al., 2006)

1.5.2. Replicase proteins

The 5' two-thirds of the genome of coronavirus contain two open reading frames (ORFs), pp1a and pp1ab, coding for two very large polyproteins that are cleaved into proteins to enable the viral RNA to replicate and transcribe. The range of pp1a and pp1ab is from 440 to 500 kDa and from 740 to 810 kDa, respectively. Expression of the ORF 1b-encoded region of pp1ab involves ribosomal frameshifting into the -1 frame just upstream of the ORF 1a translation termination codon. Two or three virally encoded proteinases are responsible for processing these two polyproteins into some 15 or 16 nonstructural proteins (Fig.1.7).

Nsp1–nsp11 is derived from pp1a, whereas nsp1–nsp10 and nsp12–nsp16 are derived from pp1ab. The products that are unique to pp1ab carry out the actual catalysis of RNA replication and transcription. Sequence analysis of the nsp1 to 16 proteins predicts that they have at least eight enzymatic activities (Snijder et al., 2003). The enzymatic activities and characteristics of these protein domains are listed in Fig.1 7. Among the replicase proteins, the crystallographic or nuclear magnetic resonance structures of the PLpro and nsp3, nsp5, nsp7, nsp8, nsp9, nsp10 and nsp15 have been reported (Anand et al., 2003; Joseph et al., 2006; Peti et al., 2005; Ratia et al., 2006; Saikatendu., 2005; Sutton et al., 2004; Zhai., 2005; Ricagno et al., 2006).

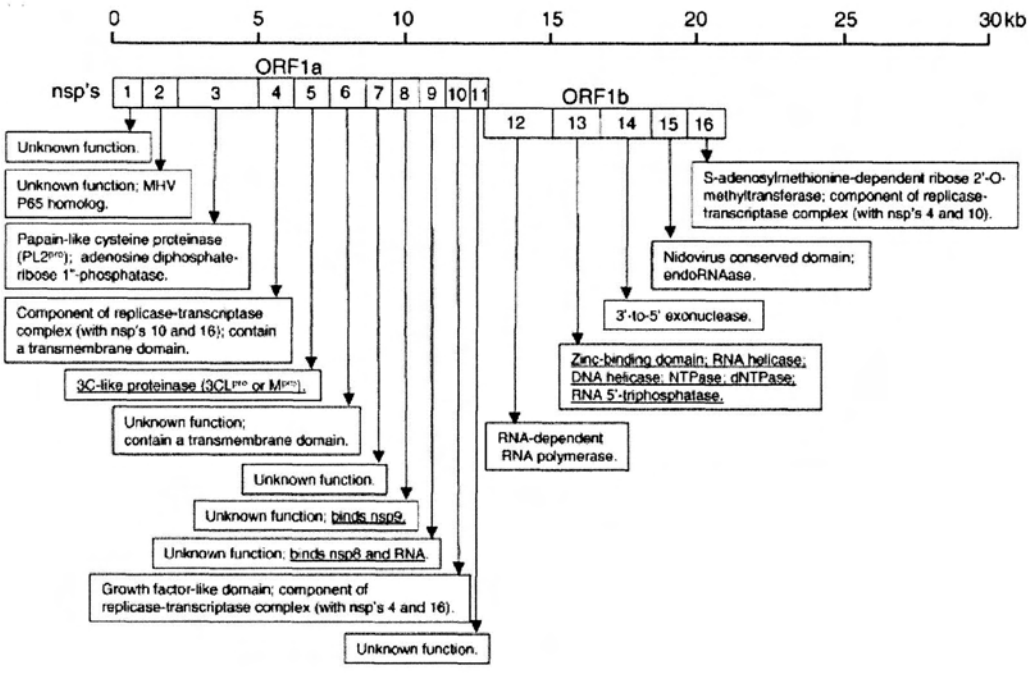

Fig.1.7. Protein products of the replicase gene. Cleavage sites and processed products of pp1a (nsp1–nsp11) and of pp1ab (nsp1–nsp10, nsp12–nsp16) are shown using SARS as an example. Predicted and/or experimentally demonstrated activities are indicated (Tan et al., 2004).

A number of other features, including domains with conserved cysteine and histidine residues (C/H domains in nsp3, nsp13, and nsp14), putative transmembrane domains (TM domains in nsp3, nsp4, and nsp6), and domains with conserved features (the A [acidic] and Y domains within nsp3) have also been identified in coronavirus nonstructural proteins (Ziebuhr, 2005).

In addition to the proteins for which enzymatic functions have been predicted or demonstrated, the structures of four other coronavirus nonstructural proteins have been also reported.

First, the SARS CoV proteins nsp7 and nsp8 cocrystallize to produce a supercomplex that can be viewed as a hollow, cylinder-like structure assembled from eight copies of nsp8 and eight copies of nsp7. This complex has a central channel with positive electrostatic properties favorable for nucleic acid binding. It has been suggested that the role of this structure may be to confer processivity to the viral RdRp (Peti et al., 2005; Zhai et al., 2005).

Second, the crystal structure of SARSCoV nsp9 has been shown as comprising a single ß-barrel with a fold that resembles a carboxyl-extended oligonucleotide-oligosaccharide binding (OB) fold (Fig.1.8). The crystal structure suggests that the protein is dimeric, and gel shift assays show that it is able to bind single-stranded RNA (Egloff et al., 2004; Sutton et al., 2005).

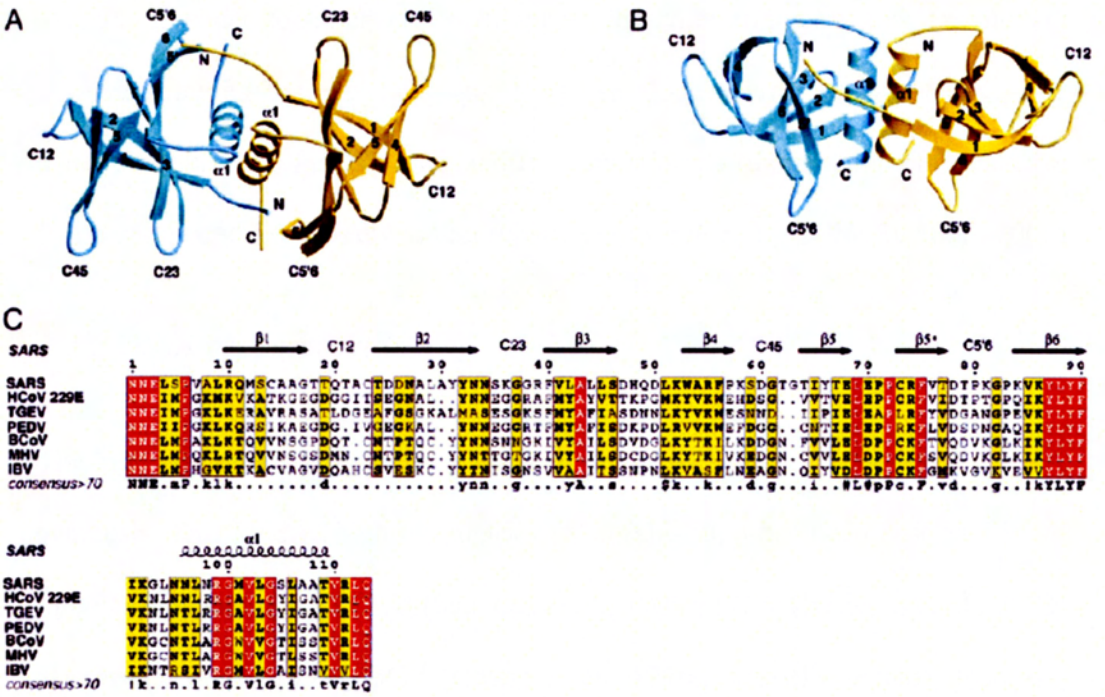

Fig.1.8. Crystal structure and sequence of SARS-CoV nsp9. (*A*) Ribbon representation of SARS-CoV nsp9. One molecule of the dimer is gold and the other is cyan. Loops between strands x and y are labeled C. (*B*) A 90° view of *A*. (*C*) Multiple alignment of nsp9 sequences from SARS-CoV National Center for Biotechnology Information (NCBI) accession no. AY291315, and several related CoVs (Egloff et al. 2004).

Third, some studies have reported the crystal structure of the SARS CoV nsp10 protein (Joseph et al., 2006). The structure predicts a single domain protein consisting of a pair of antiparallel amino-terminal helices stacked against an irregular ß -sheet, together with a coil-rich carboxyl terminus and two zinc fingers. Twelve subunits assemble to form a unique dodecameric superstructure. The nsp10 protein is the first representative of a new family of zinc-finger proteins. So far, it was found exclusively in coronaviruses (Joseph et al., 2006; Su et al., 2006).

1.5.3. RNA recombination

The high rate of RNA recombination is an important feature of coronavirus RNA synthesis. This kind of high frequency of recombination has been observed in all three groups including TGEV (Sanchez et al., 1999), FIPV (Haijema et al., 2003; Herrewegh et al., 1998), BCV (Chang et al., 1996), and IBV (Cavanagh et al., 1992; Kottier et al., 1995; Kusters et al., 1990; Wang et al., 1993).

Viral RNA recombination has three mechanistic requirements (Lai, 1992). First, the RNA polymerase must pause during synthesis. It has been shown that MHV RNA synthesis normally pauses at certain sites on the RNA genome (Baric et al., 1987). The nascent, incomplete RNA transcripts may dissociate from the template RNA and then re-bind to the template to resume RNA synthesis. When the nascent RNA binds to a different template, the resumed RNA synthesis will result in a recombinant RNA. This may be an intrinsic property of the enzyme, or it may

result from the enzyme encountering a template secondary structure that exceeds a certain stability threshold (Masters, 2006). Second, a new template must be in physical proximity. Third, some property of the new template must allow the transfer of the nascent RNA strand and the resumption of RNA synthesis. Recombination can occur not only during positive strand RNA synthesis but can also take place during negative strand RNA synthesis (Liao and Lai, 1992).

Recombination is one of the most unique aspects of coronavirus biology. It can potentially provide a genetic mechanism by which coronaviurses maintain their sequence integrity. For the large size of the coronavirus RNA which would contain mutations due to the high error frequencies of RNA polymerases, recombination may provide a repair mechanism for the virus (Lai, 1992).

1.6. Reverse genetics

Analysis of recombinant viruses with specific genetic changes has proved to be a powerful method for understanding the molecular biology of RNA viruses and for studying the role of individual genes in pathogenesis. The first reverse genetic system for a positive strand RNA virus, the transcription of infectious RNA from a full-length cDNA copy of the viral genome, was established more than two decades ago with poliovirus (Racaniello and Baltimore, 1981). It became possible only recently to apply this scheme to coronaviruses. Because coronavirus contains the longest viral RNA genome known so far, and may be one of the most stable

RNAs in nature (Lai and Cavanagh, 1997; Siddell., 1995), the large size of coronavirus RNA presented several obstacles to construct an infectious cDNA or RNA transcript.

First, long RNA sequences make the synthesis of a faithful cDNA molecular difficult, because the fidelity of reverse transcriptase-PCR (RT-PCR) for the amplification of cDNA inevitably decreases in proportion to the RNA length.

Second, the high instabilities of various regions of the replicase gene when they were propagated as cloned cDNA in E. coli, because long RNA sequences are more likely to contain fortuitous poison sequences, which make the cDNA sequences in plasmids unstable.

Third, it is difficult to find a suitable vector that can accommodate large foreign cDNA inserts. Now three methods were developed to overcome these obstacles.

In the first method, a full-length cDNA copy of the TGEV genome was assembled in a low copy-number bacterial artificial chromosome (BAC) vector (Enjuanes et al., 2005). This method ensured complete capping of the viral RNA, and it also bypassed potential limitations of the system arising from the efficiency of in vitro transcription of genomic RNA.

In the second method, full-length genomic cDNAs were assembled by in vitro ligation of smaller, more stable subcloned cDNAs (Yount et al., 2000, 2002, 2003; Youn et al., 2005; Baric and Sims, 2005). Infectious RNA was transcribed in vitro

from the ligated products. The advantage of this method is to easily allow manipulation of the viral genome by site-directed mutagenesis and interrupt regions of the cloned cDNA with low stability.

In the third method, entire coronavirus cDNAs generated by long range RT-PCR (Thiel et al., 1997) were inserted into a unique restriction site in the genome of vaccinia virus (Thiel and Siddell, 2005). In this scheme, coronavirus genome cDNAs which were contained in a huge cloning vector did not exhibit the instabilities encountered in E. coli plasmids. Site-directed mutagenesis could be easily manipulated in this system. Infectious RNA was produced by in vitro transcription from purified vaccinia virus DNA (Thiel et al., 2001a).

A number of important findings have been made using reverse genetic system already. Reverse genetics has been used to confirm the involvement of coronavirus nonstructural proteins in RNA synthesis and to discriminate between essential and nonessential functions (Baric et al., 2005; Enjuanes et al., 2005; Thiel et al., 2005). For example, mutation at the active site of the HCoV-229E nsp15 NendoU domain or the active site of the HCoV-229E nsp14 3'- to -5' exonuclease (ExoN) domain suggests that these functions are essential for virus RNA synthesis in cell culture (Ivanov et al., 2004). In contrast, mutation of the active site of the HCoV-229E nsp3 ADRP domain had no significant effect on virus RNA synthesis (Putics et al., 2005).

Reverse genetics has been used to show that the MHV and SARS-CoV nsp2 proteins are not essential for virus replication but that their deletion attenuates virus growth and virus RNA synthesis (Graham et al., 2005). Using reverse genetics, an extensive deletion and site-specific mutagenesis study of the MHV nsp1 has identified domains and residues that are important for processing of polyprotein and virus RNA synthesis system (Brockway et al., 2006).

Reverse genetics has also been used to show that some group-specific genes of coronavirus are not essential for virus replication but that their mutation can affect virus growth and infectivity. For example, neither the RNA nor the proteins of ORF 3a, 3b and 5a, 5b of IBV are essential for replication (Hodgson et al., 2005; Casais., 2005). In contrast, the accessory proteins, i.e., 3a/3b and 7a/7b, could play an important role during the replication cycle of the SARS-CoV (Sara et al., 2006). In all three full-length cDNA systems (Almazan et al., 2004; Schelle et al., 2005; Thiel et al., 2001a; Yount et al., 2002), N protein are confirmed to greatly enhance recovery of recombinant coronaviruses.

As reviewed above, many nonstructural proteins of coronavirus are involved in virus RNA replication and transcription, and become components of the replication complex. But the roles some of them play in virus replication are still an open question. In this study, we focused on replicase protein nsp9 and nsp13 to investigate their functions during virus RNA synthesis using IBV as a model. In general, IBV shares close similarities in genome organization, gene expression,

and RNA replication with other coronaviruses, but is non-infectious to human. These properties make IBV an attractive model system for studying the biology and pathogenesis of coronavirus.

1.7. Coronavirus Avian Infectious Bronchitis Virus (IBV)

IBV was the first coronavirus to be isolated, in the 1930s. It is, by definition, the coronavirus of the domestic fowl. Although it does indeed cause respiratory disease, it also replicates at many non-respiratory epithelial surface, where it may cause pathology. Avian viral respiratory infections caused by avian influenza virus, IBV, avian pneumovirus (APV) and Newcastle disease virus (NDV) result in considerable economic losses to the poultry industry worldwide (Cavanagh, 2003). IBV is one of the major respiratory viruses of chickens that are endemic in all chicken producing countries (Cavanagh, 2003), causing an acute and highly contagious upper respiratory tract infection. The virus has been recovered from trachea, bronchus, lungs, esophagus, proventriculus, duodenum, jejunum, caecal tonsils, kidney and cloaca of experimentally infected birds with the most persistent infection in kidney and caecal tonsils. The endemic nature of infection, lack of effective vaccines due to the absence of inter-strain cross protection and circulation of various IBV strains and genotypes in poultry flocks makes the control of IBV infection a challenging task (Farsang et al.2002).

IBV, a group 3 coronavirus, contains a 27.6 kb single-stranded, positive-sense RNA genome. In the virus-infected cells, six mRNA species, including the genome-length mRNA 1 and five subgenomic mRNAs (mRNA 2 - 6), are produced by a discontinuous RNA transcription mechanism (Fig.1.6). Each mRNA species possesses a 64 nucleotides leader sequence derived from the 5'end of the genome (Boursnell et al., 1987). Subgenomic mRNAs 2, 3, 4, and 6 encode the four structural proteins, i.e., S protein, E protein, M protein, and N protein. The 5' two-third region of mRNA 1 comprises two large ORFs, 1a and 1b which encode two polyproteins respectively (Fig.1.9). The two polyproteins are proteolytically cleaved by two virus-encoded proteinases, the papain-like and 3C-like proteinases, into 15 functional proteins (Nsp2 - Nsp16) (Lim and Liu, 1998a, 1998b; Lim et al., 2000; Liu et al., 1995, 1997, 1998; Ng and Liu, 1998, 2000, 2002; Xu et al., 2001) (Fig.1.9).Compared to other coronaviruses, Nsp1 is absent in IBV but Nsp2 is considerably larger (Lim and Liu, 1998a, 1998b; Liu et al., 1995).

In addition, IBV has two of group-specific genes, called genes 3 and 5. Gene 3 has three ORFs, encoding proteins 3a, 3b and 3c, where 3c is the E protein. Gene 5 encodes two proteins, 5a and 5b. These genes are located thus: -S-3a, b, c (E)-M-5a, b –N-. Neither the IBV 3a nor 3b protein is essential for replication (Teri et al., 2006). IBV 5a is also not essential for viral replication (Soonjeon, 2004). But

for the SARS-CoV, 3a and 3b could play an important role during the replication cycle (Sara et al., 2006).

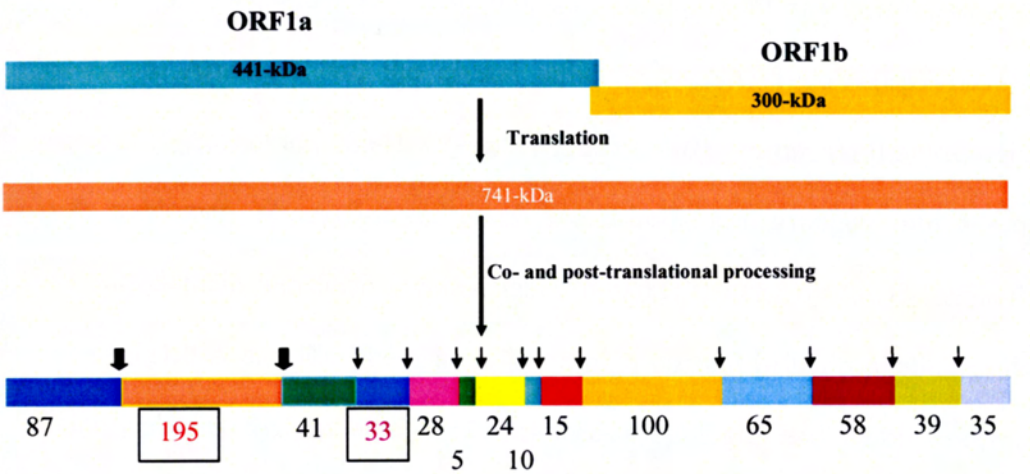

(Liu et al., 1994, 1995abc, 1997, 1998; Liu & Brown, 1995; Lim & Liu, 1998, 2000; Ng & Liu, 1998, 2000; etc.)

Fig.1.9. Protein products of the replicase gene of IBV. Cleavage sites and processed products of pp1a (nsp1-nsp11) and of pp1ab (nsp1-nsp15) are shown. Experimentally demonstrated protein molecular weights are indicated.

1.8. Nsp9 of Coronavirus

Most of replicase cleavage products of coronaviurs assemble into a membrane-associated viral replication/ transcription complex. There are four small replicase proteins nsp7, nap8, nsp9 and nsp10 at the carboxy-terminal (C-terminal) end of la region. Among them, the crystal structure of SARS-CoV nsp9 has been reported (Egloff et al., 2004). Crystals contain a dimer in the asymmetric unit, in each monomer, seven ß-strands and one α-helix are arranged into a single compact domain and form a cone-shaped ß-barrel flanked by the C-terminal α-helix (Fig1.8 A and B). The α-helix has a high content of hydrophobic residues which yield two hydrophobic sides. One faces the ß-barrel and the other interacts with the second crystallographic monomer of α-helix (Egloff et al., 2004) (Fig1.8 A and B). This dimer is therefore assembled by hydrophobic interactions which effectively lock them together.

Structural homologues of nsp9 have been shown that it displays the same characteristics with OB-fold proteins which can bind nucleic acids. Usually OB-fold proteins has a network of positively charged amino acids that defines a positive track suitable for binding the phosphate backbone to the protein surface (Fig.1.8 A and B). Some residues are conserved in all CoV nsp9 sequences, such as: Arg-10, Lys-52, Trp-53, Arg-55, Arg-74, Phe-75, Lys-86, Tyr-87, Phe-90, Lys-92, Arg-99, and Arg-111 (Fig.1.8 C). These data further show that nsp9 is a nucleic acid-binding protein and has nonspecific RNA-binding activity (Marie-

Pierre et al.,2004). Biophysical evidence has also been presented for an interaction between nsp9 and nsp8 (Sutton et al., 2004). Nsp9 corresponds to a 12 kDa cleavage product in the related MHV that is most prominent in discrete foci in the perimuclear region of infected cells and colocalize with other proteins, such as, 3C-like protein (3CLpro), N, nsp7, nsp8, nsp9 and nsp13 that are the components of the viral replication complex (Bost et al., 2000), suggesting its involvement (directly or indirectly) in viral RNA metabolism.

1.9. Nsp13 of Coronavirus

Nsp13 of coronaviurs contains multiple activities that have been extensively characterized for HCoV 229E and SARS-CoV (Ivanov and Ziebuhr, 2004; Ivanov et al., 2004a; Seybert et al., 2000). These activities include RNA and DNA duplex-unwinding activities, NTPase and dNTPase activities which probably provide the energy for its translocation along RNA templates, and an RNA 5′-triphosphatase activity that might be involved in the formation of the 5′-cap structure of viral RNAs (Ivanov et al., 2004).

The protein is comprised of two domains: a putative N-terminal zinc binding domain, which spans the N terminal region of the protein from approximately amino acids 1 to 77, and a C-terminal helicase domain covering the C-terminal part of the protein from amino acids 279 to the C terminal end (Ivanov et al., 2004). The zinc-binding domain of the RNA helicase protein of coronaviurs

Which is equal to the arterivirus nsp10 helicase was shown previously to be involved in diverse processes of the viral life cycle (van Dinten et al., 2000). A Ser–Pro substitution located immediately downstream of the putative zinc binding domain of Nsp10 of equine arteritis virus (EAV) caused defect in subgenomic mRNA transcription (van Dinten et al., 1997). More detailed analysis of the zinc binding domain of Nsp10 from EAV and Nsp13 from human coronavirus 229E by mutagenesis studies showed that this domain could modulate the enzymatic activities of the helicase domain (Seybert et al., 2005). Through this regulatory role and some yet to be discovered mechanisms, the zinc binding domain is shown to be critically involved in the replication and transcription of coronavirus RNA.

1.10. Objectives of This Study

The objectives of present study which focus on replicase proteins of coronavirus infectious bronchitis virus were as follows:

(1). Investigate the importance of an amino acid in the domain which locates outside the two function domains of helicase protein during virus replication cycle using full-length infectious clone system.

(2). Study whether the single strand RNA binding function of nsp9 may be restricted to specific residues of the genome.

(3). Study whether nsp9 protein is directly involved in viral replication through interacting with other proteins which are components of viral replication complex.

(4). Investigate the relationship between the dimerization function and the RNA binding activity of nsp9.

(5). Explore the possibility in which nsp9 may not only form dimers but also form polymers.

In construction of an infectious IBV clone by in vitro assembly of five cloned RT-PCR fragments from a Vero cell adapted IBV Beaudette strain, a G–C (G15526C) point mutation at nucleotide position 15,526 was found to be lethal to the infectivity of IBV on Vero cells. No infectious virus could be rescued from Vero cells electroporated with in vitro-synthesized full-length transcripts containing this mutation. As this mutation causes Arg132–Pro mutation in a domain with unknown function within the helicase protein (Nsp13), it implies that this region might play certain roles in the functionality of the helicase protein.

On the contrary, a G–C (G4330C) and a G–A (G9230) point mutations at nucleotide positions 4330 and 9230, respectively, causing Glu–Gln and Gly–Glu mutations in or near the catalytic centers of the papain-like (Nsp3) and 3C-like (Nsp5) proteinases, did not impair the infectivity of the in vitro synthesized transcripts containing these mutations. Further characterization of the in vitro-synthesized full-length transcripts containing the G15526C mutation

demonstrated that this mutation blocks the transcription of subgenomic RNAs. Substitution mutation of the Arg132 residue to a positively charged amino acid (Lys) affected neither the infectivity of the in vitro-synthesized transcripts nor the growth properties of the rescued virus.

However, mutation of the Arg132 residue to a Leu, which is conserved in most of other coronaviruses at the same position, reduced the viral recovery rate of the in vitro-synthesized full-length transcripts. The mutant virus showed much smaller-sized plaques. This study reveals the essential role of a domain with previously unassigned functions within the helicase protein in coronavirus replication.

So far, whether the ssRNA-binding function of nsp9 is restricted to specific residues of the genome or is complemented with other proteins which are involve in viral replication cycle and whether nsp9 can directly interact with RNA dependent RNA polymerase (RDRP) or nsp13 which are also the components of the viral replication complexes remain unknown.

According to structural hypothesis, we chose to mutate a number of evolutionarily conserved residues in different domains of IBV nsp9 to assess their roles in viral replication and viral genomic RNA binding. We introduced these mutations into an infectious cDNA clone system derived from the genomic RNA of IBV to assess their effects on viral replication and infectivity. Subsequently, Immunoblotting, gel filtration assay and chemical cross linking assay were used to confirm the dimerization and RNA binding activity of mutant nsp9. Purified

recombinant wild type and mutant proteins expressed in Escherichia coli were used for RNA binding assays to compare their RNA binding activity. Co-immunoprecipitation was used to confirm the direct interaction between RDRP, nsp13 and nsp9. The results of our studies led to the identification of an amino acid residue essential for its dimerization and the RNA-binding activity, and no distinctly direct relationship between RDRP, nsp13 and nsp9.

We also identified a residue Gly-98 which was mutated to aspartic acid yields a severe abolishment of RNA binding and a concomitant reduction in virus replication. In addition, the dimerization of nsp9 does have absolute correlation with the RNA binding of nsp9. This study thus identifies residues critical for RNA binding at IBV nsp9 and presents biochemical and genetic evidence that directly links the RNA binding capacity of IBV nsp9 protein to virus replication and the viral infectivity in cultured cells. This information would be useful in development of preventive and treatment approaches against coronavirus infection.

CHAPTER 2

MATERIALS AND METHODS

2.1 Materials

2.1.1 Virus

Avian infectious bronchitis virus (IBV)

The IBV (strain Beaudette) is an embryo-adapted virus that has extended species tropism in cell culture. The S protein sequence of Beaudette strain contains a putative heparan sulfate (HS)-binding site compared with other strains, indicating that the Beaudette virus may use HS as a selective receptor. It may explain in part the extended tropism of IBV Beaudette (Madu, *et al.*, 2007). In this study, a Vero cell-adapted IBV Beaudette strain [65 passages on Vero cells (p65)] (Shen et al., 2003, 2004; Fang et al., 2005) was propagated in Vero cells in fetal bovine serum - free (FBS) MEM.

Recombinant vaccinia virus (vTF-3)

The Bacteriophase T7 polymerase gene was inserted into the vaccinia virus genome. This recombinant vaccinia virus can express T7 RNA polymerase in infected cells. The T7 RNA polymerase produced by the recombinant vaccinia virus can express target gene in very high efficiency.

2.1.2 Cells

Vero cells

The Vero cell was isolated from kidney epithelial cells extracted from African green monkey. The Vero cell lineage is continuous and aneuploid. A continuous cell lineage can be replicated through many cycles of division and will not become senescent. The cells were grown at 37 °C in 5 % CO_2 and maintained in Glasgow's modified Eagle's medium supplemented with 10% fetal calf serum.

HeLa cells

HeLa cell is an immortal cell line derived from cervical cancer cells taken from Henrietta Lacks, who died in 1951 (Masters., 2002; Valen et al., 1991). HeLa cells have an active version of the enzyme telomerase during cell division, which prevents the incremental shortening of telomeres that is implicated in aging and eventual cell death. In this way, HeLa cells circumvent the Hayflick Limit, which is the limited number of cell divisions that most normal cells can undergo before dying out in cell culture. HeLa cells were cultured in complete Dulbecco's modified Eagle's medium (Invitrogen) supplemented with 10 % FBS and 1 % penicillin (100 units/ml) (Invitrogen) and maintained at 37 °C in 5 % CO_2.

H1299 cells

H1299 cell line is an adherent epithelial cell line that is derived from human lung carcinoma. H1299 cells lack endogenous p53. H1299 cells were grown at 37 °C in 5 % CO_2 and maintained in Hyclone's RPMI-1640 medium supplemented with 10 % fetal calf serum and 1 % penicillin.

2.1.3 Bacterial strains

Competent cell of *E coli* strain DH5α

Competent cell of *E coli* strain DH5α is one of the standard competent cells for molecular biology applications. The DH5α cell has mutation of φ80*lacZ*ΔM15 and lacks *laq*Iq gene, which allows blue-white color screening of transformants with X-gal (IPTG is not required) (Product information of subcloning competence DH5α from BioDynamics Laboratory Inc).

Competent cell of *E coli* strain BL 21

BL21 (DE3) is DE3 lysogens containing the T7 RNA polymerase gene under control of the lacUV5 promotor. Induction with IPTG allows production of T7 RNA polymerase which then directs the expression of the target gene located downstream of the T7 promotor in the expression vector (Novagen).

2.1.4 Plasmid vectors

pKT0

pKT0 origins from pING14 by inserting a T7 RNA polymerase promoter sequence in it (Liu and Inglis, 1991) and is ampicillin resistant.

pXJ-40

pXJ-40 was constructed by replacing the SV40 early promoter with the human cytomegalovirus early promoter in pSG5 and is ampicillin resistant.

pFlag

pFlag was derived from pXJ-40 by inserting a flag tag (MDWKDDDDK) sequence downstream of the *NcoI* restriction endonuclease site and is ampicillin resistant.

p-Myc

p-Myc was derived from pXJ-40 by inserting a c-myc tag (MEQKLISEEDL) sequence downstream of the *NcoI* restriction endonuclease site and is ampicillin resistant.

pCR-XL-TOPO

pCR-XL-TOPO contains a T7 Polymerase promoter site flanking a multiple cloning site (MCS) for in vitro RNA transcription and it contains 3'-T overhangs for cloning RCR products produced by most thermostable polymerase mixtures (Invitrogen).

pGEM-T Easy The pGEM-T Easy Vectors contain T7 and SP6 RNA Polymerase promoters flanking a MCS within the a-peptide coding region of the enzyme ß-galactosidase. Insertional inactivation of the a-peptide allows recombinant clones to be directly identified by color screening on indicator plates (Promage).

pET-16b

The pET-16b vector carries an N-terminal His tag sequence followed by a Factor Xa and three cloning sites (invitrogen).

2.1.5 Antibodies

Polyclonal anti-IBV M antibody raised from Rabbit

Polyclonal anti-IBV N antibody raised from Rabbit

Polyclonal anti-IBV S antibody raised from Rabbit

Polyclonal anti-IBV E antibody raised from Rabbit

Monoclonal anti-Flag antibody Stratagene Inc

Monoclonal anti-Myc antibody Stratagene Inc

Polyclonal goat anti-Rabbit immunoglobulins HRP DAKO

Polyclonal rabbit anti-Mouse immunoglobulins HRP DAKO

2.1.6 Commercial kits:

QIAprep Miniprep kits QIAGEN Ltd

HiSpeed plasmid Midi kits QIAGEN Ltd

QIAquick PCR purication kits QIAGEN Ltd

QIAquick gel extraction kits QIAGEN Ltd

Quickchange site-directed mutagenesis kit Stratagene Inc

mMessage mMachine T7 Ambion Inc

Lipofectamine 2000 Invitrogen life technologies

ECL plus western blotting detection system Amersham. Pharmacia biotech

Supersignal west pico chemiluminescent substrate Pierce Biotechnology

2.1.7 Chemicals

Cytochalasin D Sigma-Aldrich Co

Cytomatin fluorescent mounting medium DAKO

Low-range rainbow molecular weight markers Amersham Bioscience

Dulbecco's modified eagle medium Hyclone

RPMI-1640 Hyclone

Alexa fluor 488 phalloidin Invitrogen life technologies

2.1.8 Enzymes

Pfu DNA polymerase New England Biolabs Inc

T4 ligase Fermentas Inc

T7 transcriptase Ambion Inc

Restriction endonuclease New England Biolabs Inc

Turbo Pfu DNA polymerase Stratagene Inc

Proteinase K New England Biolabs Inc

2.1.9 Buffers

2.1.9.1 Buffers for western Blot

1.5 M Tris-Cl (pH 8.8)

Tris (MW 121.1): 36.3 g, add H_2O to 200 ml. Adjust pH to 8.8 with HCl.

0.5 M Tris-Cl (pH 6.8)

Tris (MW 121.1): 6.06 g, add H_2O to 100 ml. Adjust pH to 6.8 with HCl.

10 % SDS

SDS: 10 g, add H_2O to 100 ml.

10 % Ammonium persulphate

Ammonium persulphate: 1 g, add H_2O to 10 ml, Prepare freshly. (can be stored at 4 °C for a few days).

2X Sample buffer (with β-ME)

0.5 M Tris-Cl (pH 6.8): 2.5 ml, 10 % SDS: 4 ml, Glycerol: 2 ml, 2-Mercaptoethanol: 1 ml, Bromophenol Blue: 0.1 mg, add H_2O to 10 ml. Divide into 1 ml aliquots and freeze.

5X Running buffer

Tris (MW 121.1): 60 g, Glycine: 288 g; SDS: 10 g, add H_2O to 2 Liter. The pH of the solution does not need to be adjusted.

2.1.9.2. Buffers for northern blot

1% Formaldehyde gel

1.52 g agarose, 113 ml H_2O Microwave to melt, add 15.2 ml 10 x MOPS Buffer, 24.65 ml Formaldehyde, total volume 152 ml

Running buffer

1 x MOPS Buffer (not DEPC-treated, no formaldehyde)

10 x MOPS

0.4 M Morpholinopropanesulfonic acid (free acid); 0.1 M Na-acetate-3 x H_2O; 10 mM EDTA; adjust to pH 7.2 with NaOH; store dark in fridge. [500 ml: 41.9 g MOPS, 6.8 g NaAc, 10 ml 0.5 M EDTA]

Loading buffer

1×MOPS; 18.5 % Formaldehyde; 50 % Formamide; 4 % Ficoll 400; Bromophenolblue; stored at -20 °C. [1 ml: 100 µl 10 x MOPS, 500 µl Formamide, 185 µl Formaldehyde, 40 mg Ficoll400, Bromophenolblue, 215 µl H_2O]

Prehybridization-buffer

5 x SSC; 50 % Formamide; 5 x Denhardt's solution; 1 % SDS; 100 µg/ml heat-denatured sheared non-homologous DNA (Salmon sperm DNA or yeast tRNA). [100 ml: 25 ml 20 x SSC, 50 ml Formamide, 5 ml 100 x Denhardt's, 1 g SDS, 1 ml 10 mg/ml DNA]

Hybridization-buffer

Prehybridization buffer with 5 % Dextransulfate (Na-salt, MW 500,000, 50 % stock-solution) and without non-homologous DNA.

20 x SSC

3 M NaCl; 0.3 M Na-citrate. [1 l: 175.3 g NaCl, 88.2 g NaCitrate]

Strip-solution

5 mM Tris pH 8; 0.2 mM EDTA; 0.05 % Na-pyrophosphate; 0.1 x Denhardt's solution. [500 ml: 2.5 ml 1 M Tris, 200 µl 0.5 M EDTA, 5 ml 5 % NaPP, 1 ml 50 x Denhardt's]

2.1.9.3 Buffers for northern western blot

1.5 M Tris-Cl (pH 8.8)

Tris (MW 121.1): 36.3 g, add H_2O to 200 ml. Adjust pH to 8.8 with HCl.

0.5 M Tris-Cl (pH 6.8)

Tris (MW 121.1): 6.06 g, add H_2O to 100 ml. Adjust pH to 6.8 with HCl.

10 % SDS

SDS: 10 g, add H_2O to 100 ml.

10 % Ammonium persulphate

Ammonium persulphate: 1 g, add H_2O to 10 ml. Prepare fresh (can be stored at 4°C for a few days).

2X Sample buffer (with β-ME)

0.5 M Tris-Cl (pH 6.8): 2.5 ml, 10 % SDS: 4 ml, Glycerol: 2 ml, 2-Mercaptoethanol: 1 ml, Bromophenol Blue: 0.1 mg, add H_2O to 10 ml. Divide into 1 ml aliquots and freeze.

5X Running buffer

Tris (MW 121.1): 60 g, Glycine: 288 g; SDS: 10 g, add H_2O to 2 Liter. The pH of the solution does not need to be adjusted.

Probe buffer

1 × Denhardt's reagent; 1 mM EDTA; 10 mM Tris-Hcl, PH 7.5; 50 mM NaCl.

Blocking buffer

5-10 % milk (fat free) solution (milk powder in 1 x maleic acid solution).

Washing buffer

1 x maleic acid; 0.3 % Tween 20.

Strip-solution

5 mM Tris pH 8; 0.2 mM EDTA; 0.05 % Na-pyrophosphate; 0.1 x Denhardt's solution. [500 ml: 2.5 ml 1 M Tris, 200 µl 0.5 M EDTA, 5 ml 5 % NaPP, 1 ml 50 x Denhardt's]

2.1.9.4 Buffer for others

LB/Amp plates

10 g/L bactotryptone, 5 g/L yeast extract, 10 g/L NaCl, 16 g/L bactoagar. Autoclave and when cooled add ampicillin to 100 µg/ml.

Cell freezing medium

50 % DMEM, 10 % DMSO and 40 % FBS.

2.2 Methods

2.2.1 Competent cells

Take 100 ml aliquot of frozen cells from the -80 °C and innoculate about 500 ml to 1 L sterile LB medium. Grow the cells on a shaker at 37 °C until they reach an OD 600 nm of 0.6. Cells were collected by centrifugation at 5000 rpm for 10 minutes (min) at 4 °C and ice down 100 mM $CaCl_2$ and 100 mM $MgCl_2$ solutions at this point. Gently resuspend the bacteria pellet on ice in 1/4 volume of ice cold $MgCl_2$, Centrifuge the cell suspension at 4,000 rpm for 10 min. Resuspend the bacteria pellet on ice in 1/20 volume of ice cold $CaCl_2$ and then add an additional 9/20 volume of $CaCl_2$. Keep this suspension on ice for at least 20 min. Centrifuge the cell suspension at 4,000 rpm for 10 minutes and resuspend the cell pellet in 1/50 volume of ice cold, sterile 85 mM $CaCl_2$ in 15 % glycerol w/v. Dispense in 100 ml aliquots and freeze cells at -80 °C.

2.2.2 Bacteria transformation

1-2 µl of DNA was added to 50 µl competent cells, which was incubated on ice for 30 min. The mix was incubated on ice for 5 min after heat shock at 42 °C for 1 - 2 min. 1 ml of LB was added to the mix, incubated at 37 °C for 1 hour. The cells were spun at 800 rpm for 5 minutes. The cells were resuspent in the remaining LB after pouring off the supernatant. Plate the entire volume of resuspended cells on LB plate containing antibiotic.

2.2.3 Agarose gel electrophoresis

To prepare 50 ml of 1 % agarose solution, measure 0.5 g agarose into a glass beaker or flask and add 50 ml 1 X TAE or TBE buffer. Microwave or stir on a hot plate until agarose is dissolved and the solution is clear. Allow the solution to cool to about 55 °C before pouring (Ethidium bromide can be added at this point to a concentration of 0.5 μg/ml). The comb was placed after adding the gel in gel mold. Load samples and run at 100 V until the running dye reaches the end of the gel. If the gel was not stained with ethidium during the run, stain the gel in 0.5 μg/ml ethidium bromide until the DNA has taken up the dye and is visible under short-wave UV light.

2.2.4 DNA ligations

100-1000 ng DNA fragments, 2 μl cloning vector (10 ng/μl), 10X ligation buffer and 1 μl T4 DNA ligase (400 U/μl) were combined in a microcentrifuge tube and topped up with sterile H_2O to 10 μl, incubated overnight at 16 °C or room temperature. Control ligation reactions were incubated without insert DNA.

2.2.5 Polymerase chain reaction (PCR)

1 μl template DNA, 5 μl reaction buffer,1 μl 10 uM forward primer, 1 μl 10 uM reverse primer, 4 μl 2.5 mM dNTP and 1 μl of enzyme (*Taq, Pfu etc.*) were added to a microcentrifuge tube and added water to make up to 50 μl. The PCR cycling

scheme was as follows: first denaturation at 94 °C for 2-5 min, denaturation at 94 °C for 30-90 sec, annealing at 55 °C (or -5° Tm) for 0.5-2 min, extension at 72 °C for 1 min. (1 min / kb), final last extension at 72 °C for 5-10 min and repeat cycles for 30 times.

2.2.6 Cell culture

The cells were sub-cultured during cell maintaining. The medium was removed and the cells were washed twice with PBS. Pipette trypsin/EDTA onto the washed cell monolayer and incubating about 2-5 min, the cells were resuspended in a small volume of fresh serum-containing medium to inactivate the trypsin. Cells were transferred to a new labeled flask containing appropriate medium. The flask was incubated at 37 °C in 5 % CO_2.

2.2.7 Preparation and resuscitation of frozen cell line stock

Cells in 75 cm^2 flask were detached by trypsin / EDTA at 37 °C incubator, resuspended by cell freezing medium and aliquoted. The tubes were stocked at -80 °C overnight and then kept at -150 °C for longer storage.

For resuscitation of frozen cells, cells were collected from liquid nitrogen storage wearing appropriate protective equipment. Thaw and transferred it into the flask containing appropriate medium and incubated at the appropriate temperature for species and appropriate concentration of CO_2 in atmosphere.

2.2.8 Construction of an infectious IBV clone, introduction of mutations into the clones and rescue of recombinant viruses

2.2.8.1 Reverse transcription (RT)-polymerase chain reaction (PCR), cloning, and sequencing

Five fragments spanning the entire IBV genome were obtained by RT-PCR from Vero cells infected with the Vero cell-adapted IBV p65 at a multiplicity of approximately 1. Briefly, total cellular RNA was extracted from the infected Vero cells with TRI Reagent (Molecular Research Center, Inc.), according to the manufacturer's instructions. Reverse transcription was performed with Expand Reverse Transcriptase (Roche) using reverse primers IBV-5753R, IBV-8694R, IBV-15532R, IBV-20930R, and IBV-27608R (Table 1). Each cDNA fragment was amplified from RT products by PCR using KOD Hot Start DNA polymerase according to the manufacturer's instructions (Novagen).

The PCR products were purified from agarose gels and cloned into pCR-XL-TOPO (Invitrogen) or pGEM-T Easy (Promage) vectors. Subsequently, fragment A was removed from pCR-XL-TOPO by digestion with *NheI* and *EcoRI* and subcloned into pKT0 vector. Two to three independent clones of each fragment were selected and sequenced by automated sequencing using specific primers and the ABI dye termination sequencing method. Sequence comparison, assembly, and analysis were performed by using BLAST and DNA STAR software.

2.2.8.2 PCR mutagenesis

Mutations were introduced into the corresponding fragments by using Quick Change site-directed mutagenesis kit (Stratagene) and confirmed by sequencing of the whole fragments.

2.2.8.3 In vitro assembly of full-length cDNA clones

Plasmids were digested with either *BsmBI* (fragment A) or *BsaI* (fragments B, C, D, and E). The digested plasmids were separated on 0.8 % agarose gels containing crystal violet. Bands corresponding to each of the fragments were cut from the gels and purified with QIAquick gel extraction kit (QIAGEN Inc.). Fragments A and B, and fragments C, D, and E were first ligated with T4 DNA ligase at 4 °C overnight. The two reaction mixtures were then mixed and further ligated at 4 °C overnight. The final ligation products were extracted with phenol/chloroform/ isoamyl alcohol (25:24:1), precipitated with ethanol, and detected by electrophoresis in 0.4 % agarose gels overnight at 15 V.

2.2.8.4 In vitro transcription

Full-length transcripts were generated in vitro using the mMessage mMachine T7 kit (Ambion, Austin, TX) according to the manufacturer's instructions with certain modifications. Briefly, 30 µl of transcription reaction with a 1:1 ratio of GTP to cap analog was sequentially incubated at 40.5 °C for 25 min, 37.5 °C for 50 min, 40.5 °C 25 min and 37.5 °C for 20 min. The N transcripts were generated

by using a linearized pKTO-IBVN containing IBV N gene and the 3′-UTR region as templates. A 1:2 ratio of GTP to cap analog was used for the transcription of IBV N gene. Finally, post-transcription products were detected by electrophoresis in 0.8 % agarose gels.

2.2.8.5 Introduction of in vitro-synthesized transcripts into Vero cells by electroporation

The in vitro-synthesized full-length and N transcripts were treated with *DNaseI* and purified with phenol/chloroform. Vero cells were grown to 90 % confluence, trypsinized, washed twice with cold PBS, and resuspended in PBS. RNA transcripts were added to 400 µl of Vero cell suspension in an electroporation cuvette and electroporated with one pulse at 450 V, 50 µF with a Bio-Rad Gene Pulser II electroporator. The transfected Vero cells were cultured overnight in 1 % FBS-containing MEM in a 60 mm dish or a six-well plate and further cultured in MEM without FBS.

2.2.8.6 Analysis of the negative strand and subgenomic RNAs by RT-PCR

Total RNA was extracted from Vero cells electroporated in vitro-synthesized transcripts after treatment with DNaseI, using TRI Reagent (Molecular Research Center, Inc.) at 48 h post-electroporation. Reverse transcription was performed with Expand Reverse Transcriptase (Roche) using equal amount of RNA.

2.2.9 Construction of plasmids for nsp9 of IBV

PCR products covering the IBV sequence from 11542-11880 nt were amplified by using the forward primer 5'-CGCGGATCCAATAATGAGCTTATGCCA-27 and the reverse primer 5'-CCGCTCGAGCTAAGACTGTAAGACAAC-27. The PCR fragments were digested with *BamHI* and *XhoI*, and ligated into these two enzyme digested pXL 40 to form plasmid pXL-nsp9. For the plasmid pET-nsp9, the IBV sequence from 11542-11880nt were amplified by using the forward primer 5'-GGGAATTCCATATGAATAATGAGCTTATGCCA-3' and the reverse primer 5'-CGCGGATCCTTAAGACTGTAAGACAACAAC-3'. The PCR fragments were digested with *NdeI* and *BamHI*, and ligated into plasmid pET-16 which was digested by *NdeI* and *BamHI* to form plasmid pET-nsp9. Each mutation was introduced by two round PCR and the mutation introduced was confirmed by automated nucleotide sequencing.

2.2.10 Transient expression of viral protein in mammalian cells

IBV wild type nsp9 and mutants were placed under the control of a T7 promoter and transiently expressed in mammalian cells using a vaccinia virus-T7 system. Briefly, semiconfluent monolayers of HeLa cells were infected with 10 plaque forming units/cells of recombinant vaccinia virus (vTF7-3), which expresses the T7 RNA polymerase gene, for 2 h at 37 °C prior to transfection. The plasmid DNA (pXL-nsp9) was transfected into vTF7-3-infected cells using Effectene

transfection reagent according to the manufacturer's instructions (Qiagen). Cells were harvested at 12 h to 24 h posttransfection.

2.2.11 Expression, purification and characterization of IBV nsp9 protein in E.coli

His-tagged wild type and mutant IBV nsp9 protein were expressed in E.coli BL-21 by induction with 1mM isopropyl-b-D-thiogalactopyranoside (IPTG) at 30 °C for 4 h. Cells were lysed by sonication, purified by metal affinity chromatography with Protino-Ni 150 kit (Macherey Nagel) and confirmed by mass spectroscopy.

2.2.12 Co-immunoprecipitation analysis

Transiently transfected HeLa cells in 60-mm dishes were lysed in 1 ml of lysis buffer (150 mM NaCl, 1 % NP-40, and 50 mM Tris–HCl, pH 8.0) with 0.5 % protease inhibitor cocktail (Sigma). The lysates were centrifuged at 12000 rpm for 30 min at 4 °C. The supernatants were added with anti-Flag (Biomed Diagnostics) antibodies at 4 °C for 2 h. Protein-A agarose beads (30 ul) (KPL) were added to the lysates and incubated with shaking for 1 h at 4 °C. The beads were collected by centrifugation and washed for three times with RIPA buffer (150 mM NaCl, 1 % NP-40, 0.5 % sodium deoxycholate, 0.05 % SDS, and 50 mM Tris–HCl, pH 8.0). Proteins binding to the beads were eluted by adding 2 × SDS loading buffer and analyzed by Western blotting with anti-Flag or anti-Myc antibody.

2.2.13 Synthesis of RNA probes

PCR fragments covering the IBV genome from 27100 nt to 27608 nt were cloned into a plasmid pGEM in either forward or reverse orientation under the control of a T7 promoter. The Dig-labeled sense (+) and anti-sense (-) RNA probes were made in vitro using the DIG RNA labeling kit according to the instructions of the manufacturer (Roche).

2.2.14 Northern blot analysis

Vero cells were infected with wild type and mutant viruses at a multiplicity of approximately 1, and total RNA was extracted from the infected cells. Ten micrograms of RNA was added to a mixture of 1× MOPS, 37 % formaldehyde, and formamide and incubated at 65 °C for 20 min before subjected to gel electrophoresis. The segregated RNA bands were transferred onto a Hybond N+ membrane (Amersham Biosciences) via capillary action overnight and fixed by UV crosslinking (Stratalinker). Hybridization of Dig-labeled DNA probes was carried out at 50 °C in hybridization oven overnight. Membranes were washed 3 times for 15 min each with the probe buffer, before proceeding to detection with CDP-Star (Roche) according to the manufacturer's instructions.

2.2.15 Northwestern blot analysis

Three micrograms of purified proteins were resolved on an SDS 15 %

polyacrylamide gel and transferred onto nitrocellulose membranes (Hybond C-Extra, Amersham Biosciences) using a semi-dry transfer apparatus. Membranes were washed for 10 min with the probe buffer (1×Denhardt's Reagent, 1 mM EDTA, 10 mM Tris–HCl (pH 7.5) and 50 mM NaCl), blocked for 1 h with 25 mg/ml yeast tRNA (Ambion) and subsequently incubated with 10 mg of DIG-labeled RNA probe in the same probe buffer for 1 h. Membranes were washed three times for 15 min each with the probe buffer, before proceeding to detection with CDP-Star (Roche) according to the manufacturer's instructions.

2.2.16 Western blot analysis

Vero cells were infected with wild type and mutant viruses at a multiplicity of approximately 1. Total proteins extracted from the infected Vero cells were lysed with 2 × SDS loading buffer in the presence of 200 mM DTT plus 10 mM of iodoacetamide and subjected to SDS-PAGE. Proteins were transferred to PVDF membrane (Stratagene) and blocked overnight at 4 °C in blocking buffer (5 % fat free milk powder in PBST buffer). The membrane was incubated with 1:2000 diluted primary antibodies in blocking buffer for 2 h at room temperature. After washing three times with PBST, the membrane was incubated with 1:2000 diluted anti-mouse or anti-rabbit IgG antibodies conjugated with horseradish peroxidase (DAKO) in blocking buffer for 1 h at room temperature. After washing three times with PBST, the polypeptides were detected with a chemiluminescence

detection kit (ECL, Amersham Biosciences) according to the manufacturer's instructions.

2.2.17 Size-exclusion chromatography assay

The gel-filtration assay was performed using BioSuite™ 250 HR SEC column (7.8×300 mm, Waters) on Shimadszu chromatograph (LC-10ATvp) equipped with a photodiode array detector (SPD-M20A). The column was equilibrated at a flow rate of 1 mL/min with PBS buffer at room temperature. The protein sample (300 μL) was injected at a given concentration and detected.

2.2.18 Chemical cross-linking assay

The chemical cross-linking experiment was carried out using purified proteins which were also digested by DNAase and RNAase to get rid of the possible binding nucleic acids. Glutaraldehyde (25 %, Sigma) was diluted to a series of concentrations (2 %, 4 %, 8 %, 10 %, 20 %) by distilled water. The proteins in PBS buffer were reacted with glutaraldehyde at 16 °C for 30 min. The reactions were stopped by adding SDS PAGE loading buffer and heated at 100 °C for 10 min.

2.2.19 Indirect immunofluorescence assay

H1299 cells were grown to 60-70 % confluence on 4-well chamber slides (IWAKI), and transfected with plasmids containing the interesting protein gene.

After 16 h, the media was aspirated, and the cells were fixed with 4 % paraformaldehyde for 15 min at room temperature and permeabilized with 0.2 % Triton X-100. Cells were rehydrated in PBS for 30 min, and blocked in buffer comprised of PBS with 5% bovine serum albumin. After blocking, cells were incubated in primary antibody in 1:200 dilution for 1 h. Cells were then washed in PBS wash buffer three times at 10 min/wash. Next, cells were incubated with FITC-conjugated anti-rabbit secondary antibodies (DAKO) in fluorescence dilution buffer at 4 °C for 1 h. Next, cells were washed three times at 10 min/wash in PBS. Cells were mounted and then visualized by confocal immunofluorescence microscopy using a Zeiss LSM 510 laser scanning confocal microscope at 488 nm and 543 nm with a final magnification of 40 X with the oil immersion lens.

2.2.20 Growth curve and plaque sizes of the recombinant viruses on Vero cells

2.2.20.1 IBV growth analysis

Confluent monolayers of Vero cells on six-well plates were infected with wild-type and mutant viruses at a multiplicity of ~1 PFU/cell. After 1 h of incubation at 37 °C, cells were washed twice with PBS and cultured in 2 ml of MEM containing 0.5 % carboxymethy cellulose for 3-5 days. The cells were fixed and stained with 0.1 % toluidine. The plaque-forming units per ml of each sample

were determined by infecting Vero cells on 6-well plates in duplicate with 10-fold serial dilution of each viral stock.

2.2.20.2 TCID 50 (the 50 % tissue culture infective doses)

Vero cells were put in 96 well plates at 5000 cells/well in DMEM with 10 % FCS for about 1-2 days. In a separate 96 well plate, virus was diluted in a serial 10 × dilution. 100 µl of each dilution was transferred to the plate with Vero cells to make a total of 200 µl per well (leaving columns 1 and 2 without virus as the negative control). The plates were put in incubator at 37 °C in 5 % CO_2 for approximately 5 days and check daily. Virus titer was calculated in PFU/ml. Growth curve of the virus was drawn according to the virus titer at each time point. Viral stocks were prepared by freezing/thawing of the cells three times.

2.2.20.3 Purification and plaque sizes of the recombinant viruses

Serial 10-fold dilutions of media supernatants sampled in IBV growth analyses were made. 200 µl of each dilution was added (each sample was assayed in duplicate) to the monolayer of Vero cells grown on six-well plates and incubated at 37 °C in 5 % CO_2. After 1 h, the inoculum was removed. The infected cells were washed twice with PBS, and overlaid with 1 % low-melting agarose. After 4 days, single plaque was picked up and propagated in Vero cells. 200 µl of 10-fold serial dilutions of virus was added to Vero cells. 1 h later, the cells were overlaid with 3.5 ml of DMEM containing 0.5 % carboxymethy cellulose (CMC) (Purified

Agar, SPD) and 1 % FBS after removing the inoculum. Five days later, the plaques were fixed with 4 % formaldehyde (BDH) in PBS for 15 min, and visualized by staining the intact cells with 0.1 % toluidine blue (Sigma) for 30 min.

2.2.21 Structure predication of IBV nsp9

JIGSAW server, MOLMOL and PYMOL viewer were used to predict tertiary protein structure of IBV nsp9.

CHAPTER 3 RESULTS

3.1 Establishment of the Infectious Clone System

3.1.1 In vitro assembly of full-length cDNA clone derived from a Vero cell-adapted IBV Beaudette strain.

To construct a full-length IBV clone, five fragments (A to E) spanning the entire IBV genome were obtained by RT-PCR of total RNA extracted from Vero cells infected with a Vero cell-adapted IBV Beaudette strain (p65) (Shen et al., 2003, 2004; Fang et al., 2005). To facilitate the assembly of the full-length cDNA in vitro, restriction sites for either *BsmBI* or *BsaI* were introduced into both the 5′ and 3′ ends of the fragments (Fig.3.1a). In fragment A, a 19-nucleotide sequence corresponding to the T7 RNA promoter (Table.3.1) was inserted into the 5′ end of the IBV genome to facilitate in vitro transcription using the T7 polymerase (Fig.3.1a). The primers used to amplify these fragments are listed in Table.3.2. The PCR products were purified from agarose gel and cloned into either pCR-XL-TOPO (Invitrogen) or pGEM-T Easy (Promage) vectors. For the convenience of digestion using the restriction enzyme *BsmBI,* the *NheI*- and *EcoRI*-digested fragment A was subcloned into pKT0 which contains a *BsmBI* site 400 bp upstream of the T7 promoter sequence (Fig.3.1a). Two to three independent clones for each construct were selected for sequencing. The complete sequences of the five fragments, determined by automated nucleotide sequencing, are summarized in Table.3.2.

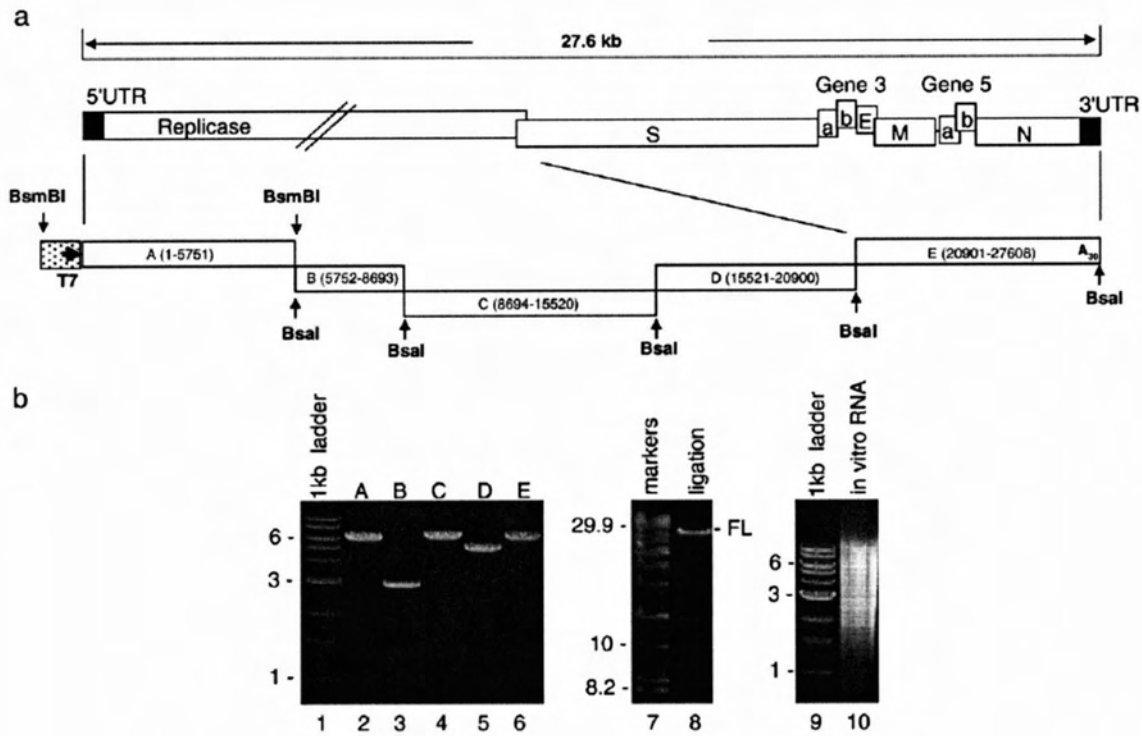

Fig.3.1. In vitro assembly of full-length cDNA clone derived from a Vero cell-adapted IBV Beaudette strain. (**a**) Diagram of the genome organization of IBV. The regions coding for the replicase polyproteins, the structural proteins S, E, M, and N, the accessory proteins 3a, 3b, 5a, and 5b, and the 5′- and 3′-UTR are shown. Also shown are the regions of the five RT-PCR fragments, the T7 promoter at the 5′-end of fragment A, and the 30 As at the 3′-end of fragment E. (**b**) Preparation of the five cDNA fragments, assembly of the five fragments into a full-length cDNA clone, and in vitro transcription of the full-length transcripts. The five cDNA fragments covering IBV sequences from nucleotides 1–5751 (lane 2), 5752–8693 (lane 3), 8694–15,520 (lane 4), 15,521–20,900 (lane 5), and 20,901–27,608 (lane 6), respectively, were obtained by digestion of corresponding plasmid DNA with either *BsmBI* or *BsaI,* purified from agarose gel, and analyzed on a 0.8% agarose gel (lanes 2–6). Equal amounts of the purified fragments were ligated using T4 DNA ligase (lane 8) and analyzed on a 0.4% agarose gel. The in vitro assembled full-length cDNA was used as templates for generation of the full-length in vitro transcripts, which were analyzed on a 0.8% agarose gel (lane 10). Lanes 1, 7, and 9 show DNA markers, and numbers on the left indicate nucleotides in kilobases.

Table.3.1

Primers used to construct the full-length IBV clone

Clone	Primer	Nucleotide sequence	Location
A	T7-IBV	5′-CGCTAGCTAATACGACTCACTATAGGACTTAAGATAGATATTAATA-3′	1–20
	IBV-5753R	5′-CGGGATCCGTCTCGCGACAACACTCTTAAC-3′	5737–5753
B	IBV-5748F	5′-ATTATGGTCTCTGTCGCTAGCTATAAGACCG-3′	5748–5768
	IBV-8694R	5′-GGGTCTCGGCCTCAAATTTATCACCTATC-3′	8673–8694
C	IBV-8689F	5′-CGGGATCCGGTCTCGAGGCCTACCTTTCAGCG-3′	8689–8706
	IBV-15532R	5′-GCAAAAGGTCTCAATGAATCAC-3′	15,511–15,532
D	IBV-15511F	5′-CGGGATCCGTGATTCATTGAGACCTTTTGC-3′	15,511–15,532
	IBV-20930R	5′-ACACCTGCAGATGTAACATC-3′	20,911–20,930
E	IBV-20887F	5′-GTTTACACCTCTAATGAGACCATAG-3′	20,887–20,911
	IBV-27608R	5′-GGAATTCGGTCTCG$(T)_{30}$TGCTCTAACTCTATACTAGC-3′	27,589–27,608

Table.3.2

Comparison of IBV sequences between Vero cell-adapted strain (p65) and the cloned fragments

Position (nt)	p65		Clone	
	nt	aa	nt	aa
Nsp2 (p87)				
2015	A	D	G	G[a]
Nsp3 (p195)				
4330	G	E	C	Q
4481	C	T	A	N
Nsp5 (3CLP)				
9230	G	G	A	E
9701–3	-GTG	-G	GTG	G[b]
Nsp6				
10,253	G	S	A	N
10,540	G	D	A	N
10,594	G	E	A	K
Nsp8 (p24)				
10,942	A	T	C	P
11,362	C	H	T	Y
Nsp13 (helicase)				
15,526	G	R	C	P
Nsp14 (p58)				
17,033	C	D	T	D
17,674	C	S	T	L
18,195	T	Y	C	H
18,430	C	S	T	F
N				
26,398	G	A	T	S

[a] Unique mutations found only in the cloned fragments.

[b] Same as the published sequences but different from p65.

The five fragments were then prepared by digestion of the corresponding constructs with either *BsmBI* or *BsaI* and purified (Fig.3.1b, lanes 2–6). The full-length clone was made by ligation of the purified fragments in vitro (Fig.3.1b, lane 8) and used as the template for in vitro transcription.

The full length in vitro-synthesized transcripts were generated using the mMessage mMachine T7 kit (Ambion, Austin, Tex) (Fig.3.1b, lane 10). As coronavirus N gene transcripts were shown to enhance the recovery of the rescued virus from the in vitro synthesized full-length transcripts (Casais et al., 2001; Youn et al., 2005a, 2005b; Yount et al., 2000, 2002), the N transcripts were generated from a linearized pKT0-IBV N construct containing IBV N gene and the 3′-UTR region. The full-length transcripts together with the N transcripts were introduced into Vero cells by electroporation. However, it was consistently observed that no infectious virus could be recovered from cells transfected with the full-length transcripts together with the N transcripts.

3.1.2 Rescue of infectious virus by correction of a point mutation (G15526C) located in a domain with unknown function within the helicase protein (Nsp13)

Sequencing comparison of the five fragments with the Vero cell-adapted IBV strain (p65, accession no. DQ001339) shows nucleotide changes at 16 positions (Table.3.2). Among them, 11 caused unique amino acid changes (Table.3.2). To

assess the deleterious effects of these mutations on the infectivity of the full-length clone, correction of some of the mutations was carried out by site-directed mutagenesis. Three point mutations, G4330C, G9230A, and G15526C, were chosen based on the fact that they are located either in or near the catalytic centers of the two viral proteinases or in a region of the RNA helicase protein with undefined functions. Four full-length cDNA clones either with correction of the mutations at all three positions (rIBV) or combination of two positions (e.g., G4330C containing G–C mutation at nucleotide position 4330 but without mutations at the other two positions) were constructed. RNA transcripts generated from the four full-length cDNA clones were introduced into Vero cells together with the N transcripts by electroporation. At 2 days post-electroporation, a typical CPE of the Vero cell-adapted IBV, the formation of giant syncytial cells (Fang et al., 2005), was observed in cells transfected with transcripts generated from cDNA clones rIBV, G4330C, and G9230A. CPE was extended to almost the whole monolayers at 3 days post-electroporation (Fig.3.2a). No CPE was observed in cells transfected with transcripts generated from clone G15526C (Fig.3.2a). RT-PCR analysis of the subgenomic mRNA 5 was performed to confirm if CPE observed is caused by the replication of IBV. Sequencing of the RT-PCR fragment generated from cells transfected with rIBV showed correct sequence in the leader/body junction region of the subgenomic mRNA (Fig.3.2b). Further sequencing of the RT-PCR fragments covering regions with unique amino

acid mutations confirmed the recovery of IBV (rIBV) from the in vitro-synthesized full length transcripts.

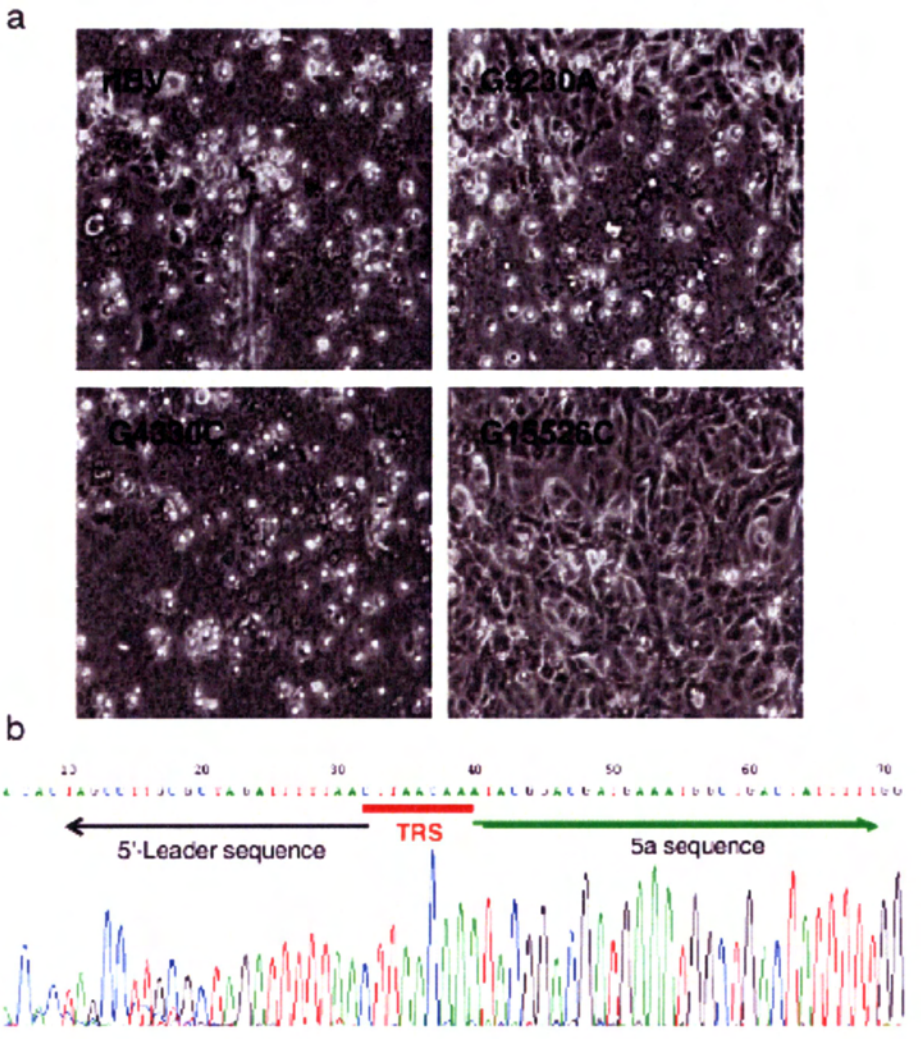

Fig.3.2. Recovery of infectious viruses from cells electroporated with in vitro-synthesized full-length transcripts. (**a**) Vero cells electroporated with in vitro synthesized transcripts derived from the in vitro assembled full-length clones with or without a point mutation at one of the three positions (G4330C, G9230A, or G15526C). Images were taken at 3 days post-electroporation. (**b**) Nucleotide sequencing of the leader/body junction of the subgenomic mRNA 5. Total RNA was prepared from Vero cells infected with the recombinant virus rescued from the in vitro-synthesized full-length transcripts 24 h post-infection. The 5′ 400-nucleotide region of the subgenomic mRNA 5 was amplified by RT-PCR and sequenced by automated nucleotide sequencing. The 70 nucleotides flanking the transcription regulatory sequence (TRS) for mRNA 5 are shown.

3.1.3 Characterization of the rescued IBV virus (rIBV)

Compared to the parent IBV strains, rIBV contains 8 amino acid mutations (Table.3.2). To test if these mutations may affect the growth properties and genetic stability of the rescued virus, rIBV was propagated on Vero cells for 5 passages, and the plaque sizes and growth kinetics were determined and compared with wild type IBV p65. In cells infected with rIBV, the average plague size is 0.56±0.028 mm, which is slightly smaller than the average plaque size of 0.68±0.034 mm in cells infected with wild type IBV (Fig.3.3). Analysis of the growth curves demonstrated that rIBV exhibited very similar growth properties as the wild type virus (Fig.3.3). Further characterization of rIBV was carried out by analysis of viral RNAs and structural proteins. Northern blot and Western blot analyses showed the presence of very similar amounts of viral RNAs (Fig.3.4a), and S, N, and M proteins (Fig.3.4b) in cells infected with wild type and rIBV, respectively, at 24 h post-infection. When probing with anti-N protein antibodies, other species migrating faster than the full length products on SDS-PAGE were also observed (Fig.3.4b). They may represent premature termination and cleavage products of N protein (unpublished observation). It was also noted that variable amounts of these species were detected in cells infected with wild type and rIBV (Fig.3.4b). The significance of these variations is unclear at the moment. Taken together, these results confirm that rIBV is stable and possesses very similar growth properties as wild type IBV.

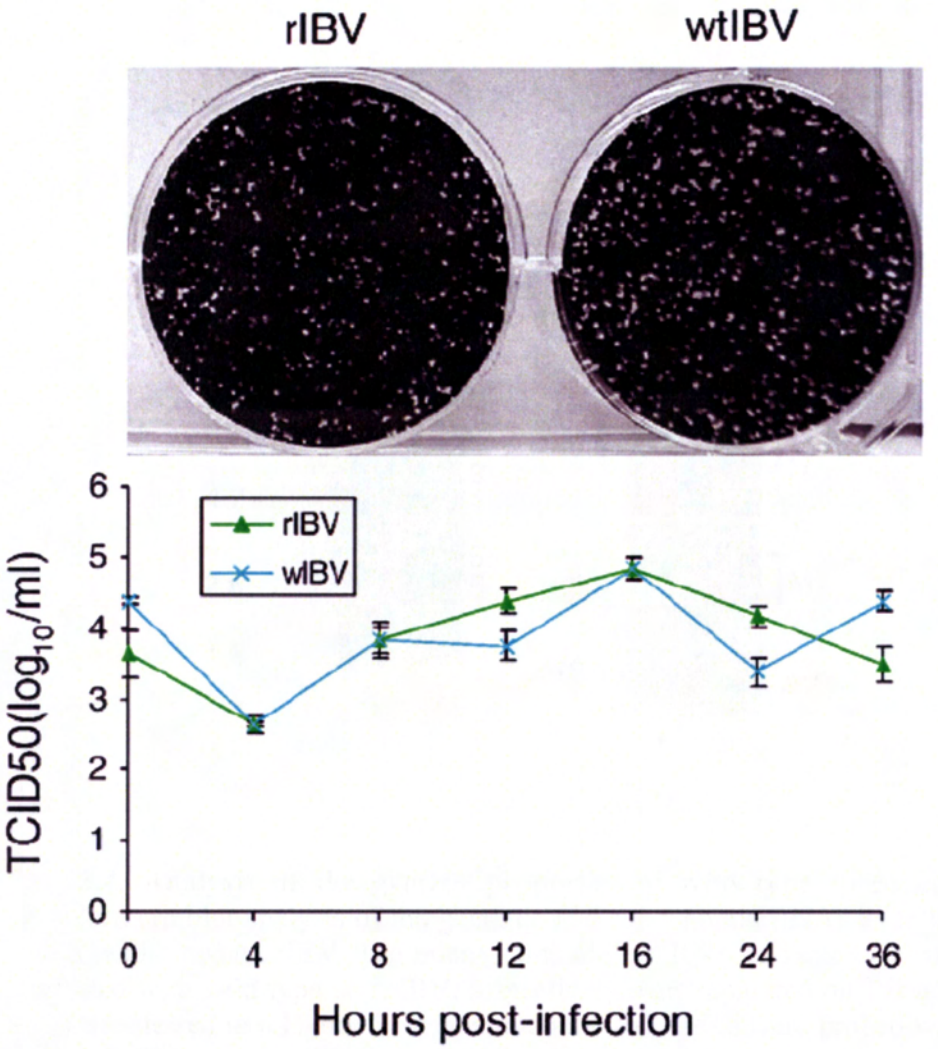

Fig.3.3. Analysis of the growth properties of wild type (p65) and rIBV. Plague sizes and one-step growth curves of wild type and rIBV. Monolayers of Vero cells on a 6-well plate were infected with 100 µl of 1000-fold diluted virus stock and cultured in the presence of 0.5% carboxymethy cellulose at 37 °C for 3 days. The cells were fixed and stained with 0.1% toluidine. To determine the one-step growth curves of wild type and rIBV, Vero cells were infected with the viruses and harvested at 0, 4, 8, 12, 16, 24, and 36 h post-inoculation, respectively. Viral stocks were prepared by freezing/thawing of the cells three times, and TCID50 of each viral stock was determined by infecting five wells of Vero cells on 96-well plates in triplicate with 10-fold serial dilution of each viral stock. Error bar shows standard error of the mean.

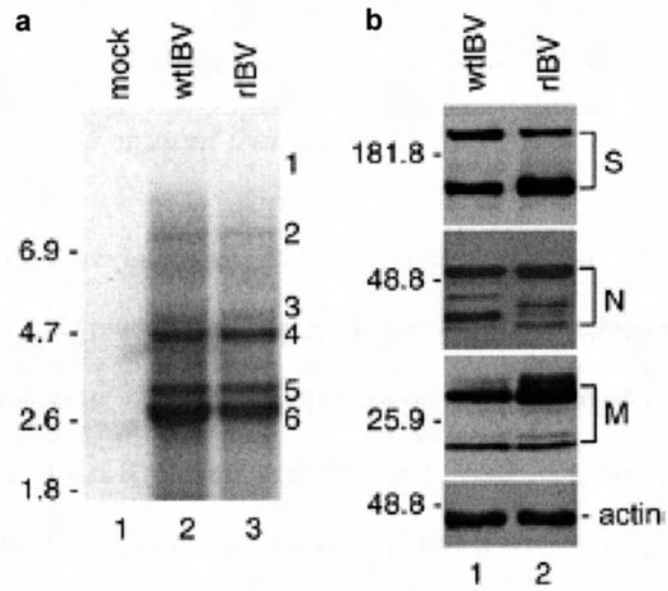

Fig.3.4. Analysis of the growth properties of wild type (p65) and rIBV. (**a**)Northern blot analysis of the genomic and subgenomic RNAs in cells infected with wild type and rIBV. Ten micrograms of total RNA extracted fromVero cells infected with wild type and rIBV, respectively, was separated on 1% agarose gel and transferred to a Hybond N+ membrane. Viral RNAs were probed with a Dig-labeled DNA probe corresponding to the 3-end 680 nucleotides of the IBV genome. Total RNA extracted from mock-infected cells was included as negative control. Numbers on the left indicate nucleotides in kilobase, and numbers on the right indicate the genomic and subgenomic RNA species of IBV. (**b**)Western blot analysis of viral protein expression in cells infected with wild type and rIBV. Vero cells infected with wild type (lane 1) and rIBV(lane 2)were harvested, lysates prepared and separated on SDS-10% polyacrylamide gel. The expression of S, N, and M proteins was analyzed by Western blot with polyclonal anti-S, anti-N, and anti-M antibodies, respectively. The same membrane was also probed with antiactin antibody as a loading control. Numbers on the left indicate molecular masses in kilodaltons.

3.2 Mutational Analysis and Functional Characterization of the R132 Residue of the helicase protein

3.2.1 Absence of subgenomic RNA transcription in cells transfected with G15526C mutant transcripts

As described previously, no infectious virus was recovered from cells transfected with G15526C mutant transcripts. To check if RNA replication occurred in these transfected cells, RT-PCR amplification of the negative strand RNA was performed. Total RNA was extracted from Vero cells transfected with wild type and G15526C mutant transcripts at 24 and 48 h post-electroporation, respectively. Reverse transcription was performed by using equal amount of RNA and the sense-primer IBV14931-F (5′-$_{14,931}$GCTTATCCACTAGTACATC$_{14,949}$-3′), and PCR was carried out by using the sense-primer IBV14931-F and the antisense primer IBV15600-R (5'-$_{15,600}$CTTCTCGCACTTCTGCACTAGCA$_{15,578}$-3'). If replication of viral RNA occurred, a 670 bp PCR fragment would be expected. As shown in Fig.3.5a, RT-PCR fragments amplified from negative strand RNA templates were obtained from cells transfected with both wild type (lanes 2 and 4) and the mutant transcripts (lanes 3 and 5). Sequencing of the PCR fragments confirmed that they represent the correct sequences. As a negative control, the in

vitro-synthesized transcripts were mixed with total RNA extracted from normal Vero cells and were used as a template for RT-PCR. No RT-PCR fragment was detected (Fig.3.5a, lane 6), confirming that the detection of negative strand RNA from cells transfected with mutant transcripts is due to the replication of viral RNA. Further quantitation of the negative strand RNA transcription in cells transfected with wild type and G15526C mutant transcripts was carried out by real-time RT- PCR. At 24 and 48 h post-electroporation, transcription of the negative RNA in cells electroporated with wild type transcripts was 24.76- and 945.54- fold, respectively, higher than that in cells electroporated with the G15526C mutant transcripts. These results confirm that transcription of the negative strand RNA has taken place in cells transfected with the mutant transcripts, but with much lower efficiency.

RT-PCR amplification of subgenomic mRNAs was carried out to check if a low level of subgenomic mRNA synthesis could occur in cells transfected with the mutant transcripts. Total RNA prepared from the transfected cells 2 days post-electroporation was used in the RT reaction with the sense-primer IBV-leader (5′-26CTATTACAC TAGCCTTGCGCT 46-3′) for the detection of negative-stranded sgRNA, and the antisense primer IBV 24803-R (5′-24,803 CTCTGGATCCAATAACCTAC 24,784-3′) for the detection of positive-stranded sgRNA. The two primers were then used for PCR. If transcription of subgenomic mRNAs did occur, a 415 bp PCR product corresponding to the 5′-terminal region

of the subgenomic mRNA 4 and a 1010 bp fragment corresponding to the 5′-terminal region of the subgenomic mRNA 3 would be expected.

As shown in Fig.3.5b, a dominant 415 bp band and a weak 1010 bp band were observed in cells electroporated with wild type full-length transcripts at 2 days post-electroporation (lanes 2 and 5). Sequencing of the PCR fragments confirmed that they represent the correct sequences of the corresponding regions of the subgenomic mRNAs 3 and 4, respectively. However, the same PCR products were not detected in cells electroporated with the mutant transcripts (Fig.3.5b, lanes 3 and 6). As a negative control, the amplified fragments were not detected in cells without electroporation (Fig.3.5b, lane 4). The failure to detect both negative- and positive-stranded sgRNAs in cells transfected with the mutant transcripts show that the G15526C mutation leads to the disruption of subgenomic RNA transcription.

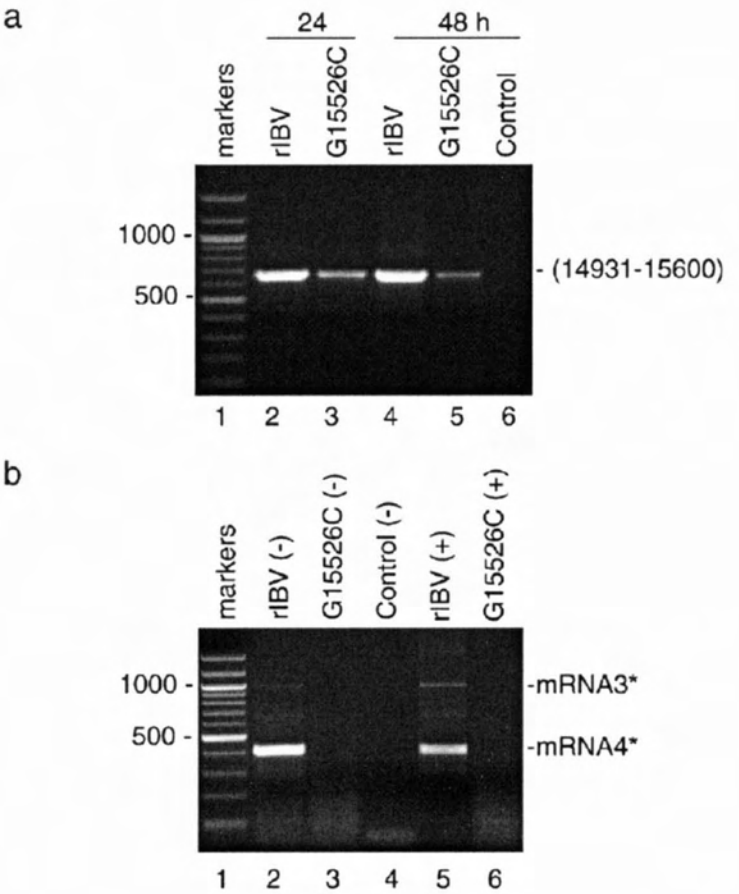

Fig.3.5. Analysis of RNA replication in cells electroporated with G15526C mutant transcripts. (**a**) Detection of negative strand RNA synthesis in cells electroporated with wild type (lanes 2 and 4) and G15526C mutant (lanes 3 and 5) transcripts. Total RNA was prepared from Vero cells electroporated with in vitro-synthesized full-length transcripts at 24 and 48 h post-electroporation, respectively. Region corresponding to nucleotides 14,931–15,600 of the negative (−) sense IBV genomic RNA was amplified by RT-PCR and analyzed on 1.2% agarose gel. Lane 1 shows DNA markers, and lane 6 shows negative control. Numbers on the left indicate nucleotides in bases. (**b**) Detection of the negative and positive strand subgenomic RNA synthesis in cells electroporated with wild type (lanes 2 and 5) and G15526C mutant (lanes 3 and 6) transcripts. Total RNA was prepared from Vero cells electroporated with in vitro synthesized full-length transcripts 2 days post-electroporation. Regions corresponding to the 5′-terminal 415 and 1010 nucleotides of the subgenomic mRNA 4 and 3, respectively, were amplified by RT-PCR and analyzed on 1.2% agarose gel. Lane 1 shows DNA markers, and lane 4 shows negative cell control. Numbers on the left indicate the length of DNA in bases.

To further demonstrate that the failure to rescue infectious virus from the G15526C mutant transcripts is due to a defect in subgenomic RNA transcription, the full-length clones with and without the G15526C mutation were used to generate recombinant IBV expressing the enhanced green fluorescent protein (EGFP) by replacing the 5a gene with EGFP. Full-length transcripts containing EGFP were synthesized in vitro and introduced into Vero cells together with the N transcripts by electroporation. At 2 days post electroporation, single CPE with the expression of EGFP was observed in cells transfected with the full-length transcripts without the G15526C mutation (Fig.3.6). Gradually increased CPE and fluorescent cells were observed from 3 to 5 days post-electroporation (Fig.3.6). At 5 days post-electroporation, CPE and fluorescent cells were extended to almost the whole monolayer (Fig.3.6). However, it was consistently observed that much less infectious virus was recovered from cells transfected with this construct.

Furthermore, the recombinant virus rapidly lost infectivity when passaged on Vero cells; the recovered virus maintains minor infectivity only for one passage. In cells transfected with the full length transcripts containing the G15526C mutation, neither CPE nor cells expressing EGFP were observed (Fig.3.6), demonstrating that G15526C mutation led to total demolition of the EGFP expression. As EGFP could be expressed only if subgenomic RNAs were synthesized but can be observed even if a single cell was transfected and expressed the protein to a certain level, these results reinforce the conclusion that the G15526C mutation blocks subgenomic RNA transcription.

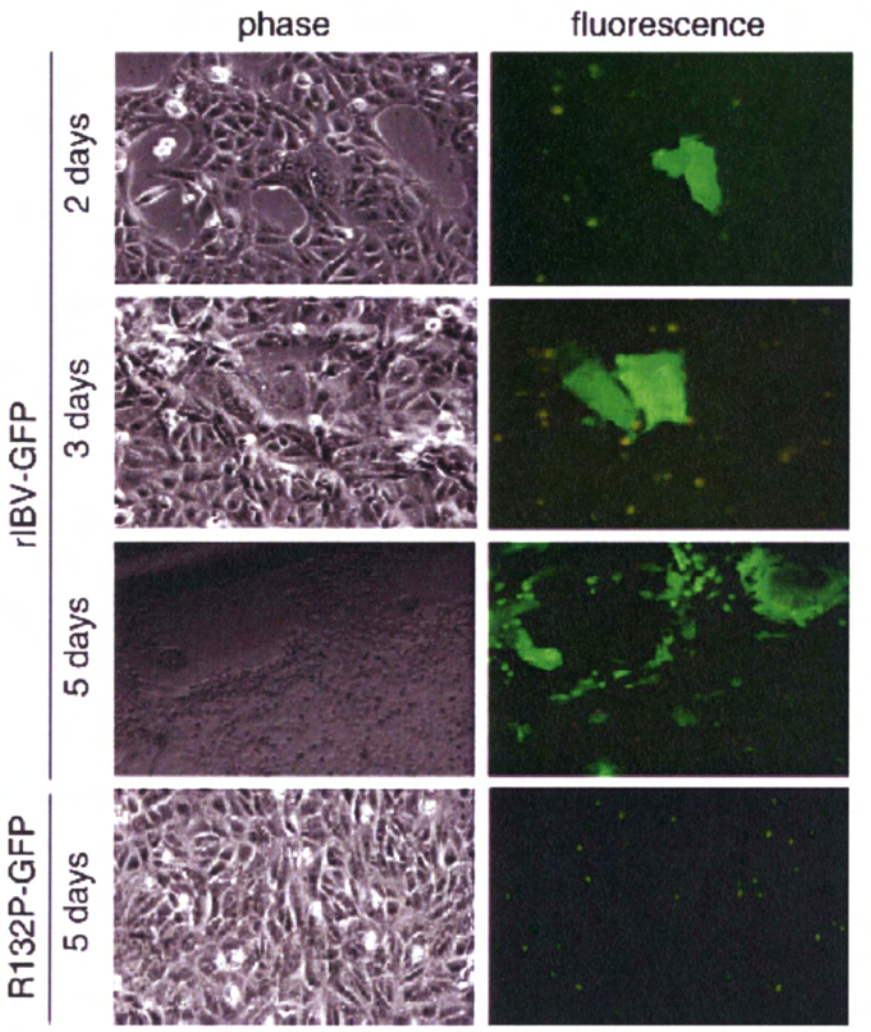

Fig.3.6. Analysis of RNA replication in cells electroporated with G15526C mutant transcripts. Construction of a recombinant IBV expressing EGFP and further analysis of the effect of G15526C mutation on subgenomic transcription using the recombinant virus. Vero cells electroporated with in vitro-synthesized transcripts derived from the in vitro assembled full-length clones containing EGFP either with or without G15526C mutation. Phase-contrast and fluorescent images were taken 2, 3, and 5 days post-electroporation, respectively.

3.2.2 Mutational analysis of the R132 residue of the helicase protein

G15526C mutation resulted in the substitution mutation of the R132 with a Pro (R132P) of the helicase protein. Sequence comparison of the IBV helicase protein with other known coronaviruses showed that R132 residue is located adjacent to a conserved motif (Fig.3.7a). In all sequenced coronaviruses, only IBV has a charged amino acid (R132) at this position (Fig.3.7a). To assess if a positive charge amino acid at this position is essential for the function of the protein, mutation of R132 to a Lys (R132K) was carried out. Meanwhile, a conserved Leu residue (Ile in the case of TGEV) was found at this position in all other coronaviruses, mutation of R132 to a Leu (R132L) was also included.

In vitro full-length transcripts containing the R132K and R132L mutations were electroporated into Vero cells. As shown in Fig.3.7b, transcripts generated from wild type (R132) and R132K mutant constructs showed very similar infectivity after introduction into Vero cells. Typical CPE was observed in large areas of the monolayers at 3 days post-electroporation (Fig.3.7b), and recombinant viruses were recovered. However, R132L transcripts were found to be less infectious. In cells electroporated with transcripts generated from this mutant, typical CPE was observed in much restricted areas of the monolayer at 3 days post-electroporation (Fig.3.7b).

a

```
                 80         90         100        110        120        130        140
IBV              FCGNHKPKLSIPLVSNGTVFGIYRANCAGSENVDDFNQLATTNWSTVEPYILANRCSDSLRRFAAETVKA
SARS-CoV         YCKSHKPPISFPLCANGQVFGLYKNTCVGSDNVTDFNAIATCDWTNAGDYILANTCTERLKLFAAETLKA
MHV              YCEDHKPQYSFKLVMNGMVFGLYKQSCTGSPYIEDFNKIASCKWTEVDDYVLANECTERLKLFAAETCKA
BCV              YCEDHKPQYSFKLVMNGMVFGLYKQSCTGSPYIDDFNRIASCKWTEVDDYILANECTERLKLFAAETCKA
HCoV-229E        YCVDHKPHYSFPLCSNGNVFGLYKSSALGSMDIDVFNKLSTSDWSEIRDYKLANDAKESLRLFAAETVKA
TGEV             YCMNHKPQLSFPLCANGNVFGLYKSSAVGSEAVEDFNKLAVSDWTEVEDYKLANNVKESLKIFAAETIKA
PEDV             WCHEHKPRLAFPLCSAGNVFGLYKNSATGSPDVEDFNRIATSDWTEVSDYRLANDVKDSLRLFAAETVKA
```

b

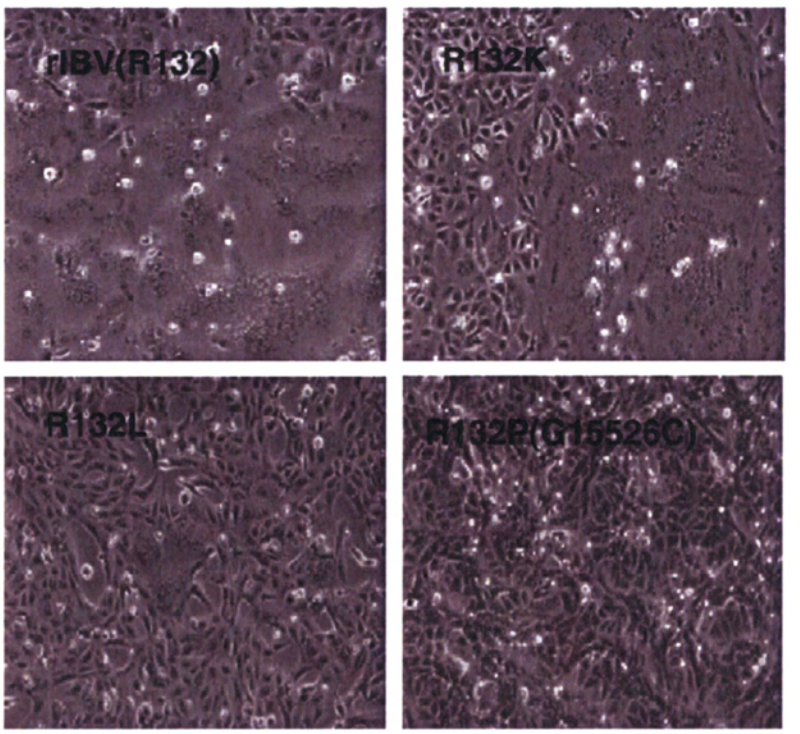

Fig.3.7. Mutational analysis of the R132 residue of the helicase protein. (**a**) Sequence comparison of the region between amino acids 70 and 140 of helicase proteins from seven different coronaviruses. The identical amino acids are shown in bold, and the last Cys/His residues of the zinc-binding domain are shown in bold and underlined. Also shown are the R132 residue in IBV and the equivalent amino acids in other coronaviruses (boxed). (**b**) Vero cells electroporated with in vitro synthesized transcripts derived from wild type recombinant IBV (rIBV), R132K, R132L, and R132P (G15526C) constructs. Phase-contrast images were taken 3 days post-electroporation.

3.2.3 Genetic stability and growth kinetics of R132K and R132L mutant viruses

The growth properties of the R132K and R132L mutant viruses on Vero cells were tested by analysis of plaque sizes and growth curves of passage 5 mutant viruses. Compared to cells infected with wild type recombinant virus (average plaques size is 0.56±0.028), plaques with similar size were observed in cells infected with the R132K mutant virus (Fig.3.8). The average plaque size in cells infected with R132K mutant virus is 0.59±0.029 mm. In cells infected with the R132L mutant virus, much smaller-sized plaques were observed (Fig.3.8). The average plaque size in cells infected with this mutant virus is 0.24±0.017 mm. However, analysis of the growth curves of wild type and mutant viruses demonstrated that the mutant viruses exhibited very similar, or even better, growth properties as the wild type recombinant virus (Fig. 3.8).

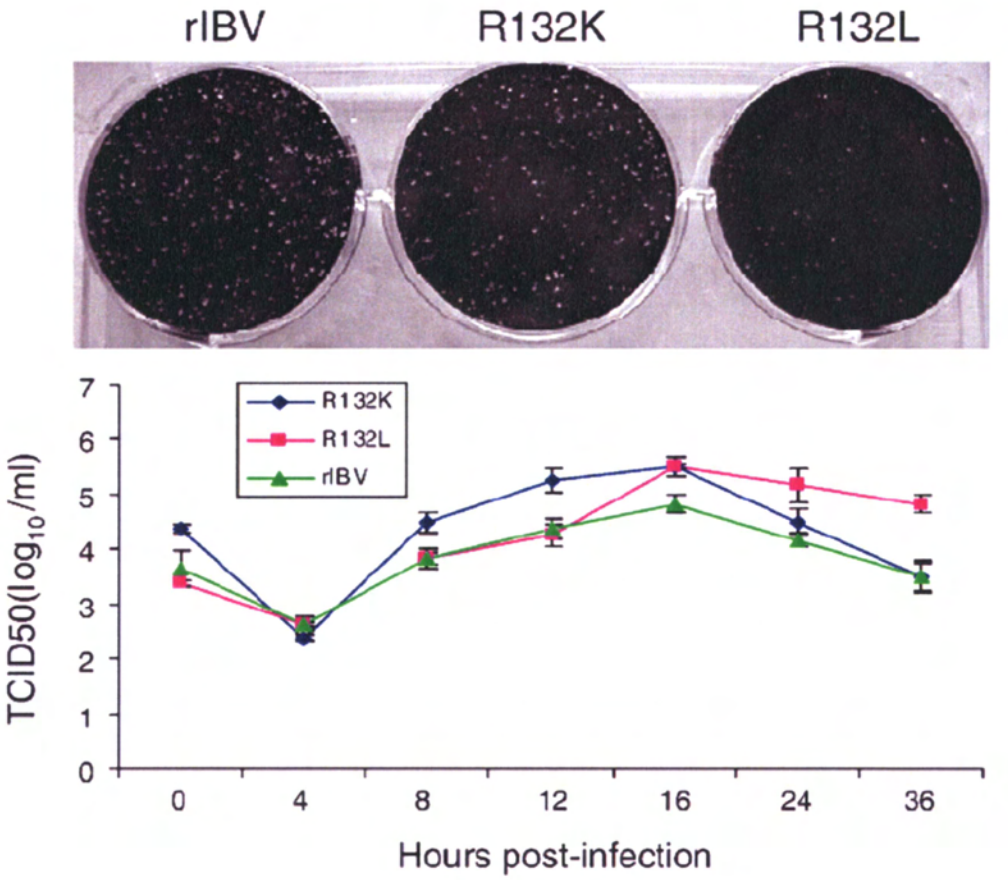

Fig.3.8. Analysis of the growth properties of rIBV, R132K, and R132L mutant viruses. Plague sizes and one-step growth curves of rIBV, R132K, and R132 mutant viruses. Monolayers of Vero cells on a 6-well plate were infected with 100 µl of 100-fold diluted virus stock and cultured in the presence of 0.5% carboxymethy cellulose at 37 °C for 3 days. The cells were fixed and stained with 0.1% toluidine. To determine the one-step growth curves of rIBV, R132K, and R132L mutant viruses, Vero cells were infected with the viruses and harvested at 0, 4, 8, 12, 16, 24, and 36 h postinoculation, respectively. Viral stocks were prepared by freezing/thawing of the cells three times, and TCID50 of each viral stock was determined by infecting five wells of Vero cells on 96-well plates in triplicate with 10-fold serial dilution of each viral stock. Error bar shows standard error of the mean.

The R132K and R132L mutant viruses were subsequently characterized by analysis of viral RNAs and structural proteins. Northern blot analysis showed the detection of very similar amounts of genomic and subgenomic RNAs in cells infected with rIBV and the two mutant viruses at 24 h post-infection (Fig.3.9a). Similarly, Western blot analysis of cells infected with rIBV, R132K, and R132L mutant viruses showed that similar amounts of S, N and M proteins were detected at 24 h post-infection (Fig.3.9b, lanes 1-3). When probing with anti-N protein antibodies, other species migrating faster than the full-length products on SDS-PAGE were also observed (Fig.3.9b). They may represent premature termination and cleavage products of N protein (unpublished observation). It was also noted that variable amounts of these species were detected in cells infected with wild type and different mutants (Fig.3.9b).

The genetic stability of R132K and R132L mutant viruses was tested by propagation of the viruses on Vero cells for 5 passages. Sequencing analysis of the fifth passages of the two mutant viruses showed that the mutations are stable. No reversion to the original sequences or mutation to other nucleotides was found in the position.

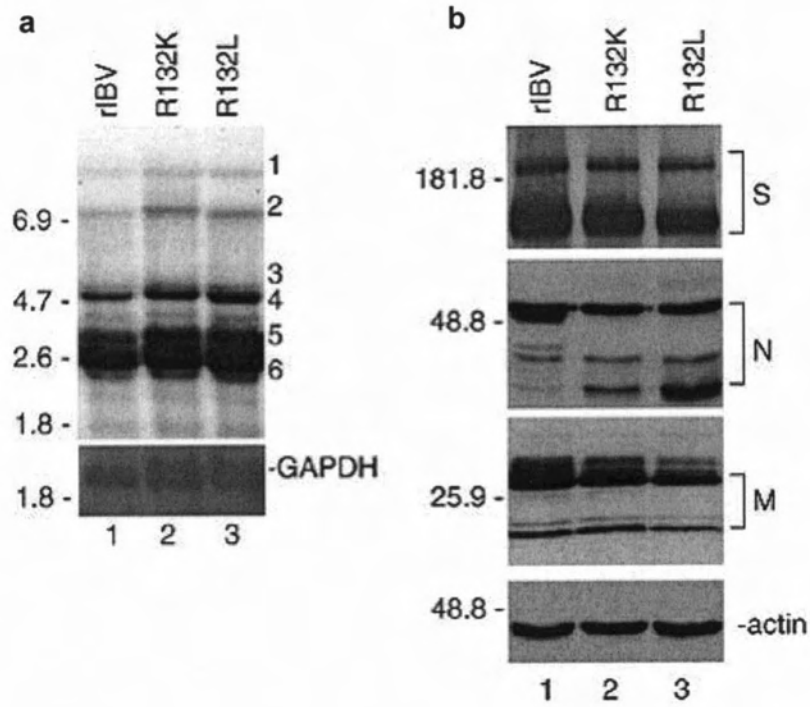

Fig.3.9. Analysis of the growth properties of rIBV, R132K, and R132L mutant viruses. (**a**) Northern blot analysis of the genomic and subgenomic RNAs in cells infected with rIBV, R132K, and R132L mutant viruses. Ten micrograms of total RNA extracted from Vero cells infected with rIBV, R132K, and R132L mutant viruses, respectively, was separated on 1% agarose gel and transferred to a Hybond N+ membrane. Viral RNAs were probed with a Dig-labeled DNA probe corresponding to the 3-end 680 nucleotides of the IBV genome. Numbers on the left indicate nucleotides in kilobase, and numbers on the right indicate the genomic and subgenomic RNA species of IBV. (**b**) Western blot analysis of viral protein expression in cells infected with wild type and R132 mutant viruses. Vero cells infected with wild type recombinant IBV (lane 1), R132K (lane 2), and R132L (lane 3) were harvested, lysates prepared, and separated on SDS-10% polyacrylamide gel. The expression of S, N, and M proteins was analyzed by Western blot with polyclonal anti-S, anti-N, and anti-M antibodies, respectively. The same membrane was also probed with anti-actin antibody as a loading control. Numbers on the left indicate molecular masses in kilodaltons.

3.3 Functional Analysis of the IBV Nsp9 Protein in Viral Replication and Infectivity.

3.3.1 Overview of the structure and RNA-binding properties of the coronavirus nsp9 protein

Determination of the crystal structure of SARS-CoV nsp9 has shown that the nsp9 crystals contain a dimer in the asymmetric unit (Fig.3.10). In each monomer, seven-β strands and one α-helix form a cone-shaped β-barrel flanked by the C-terminal α-helix (Fig.3.10). The C-terminal α-helix has a high content of hydrophobic residues, yielding two hydrophobic sides. One side faces the β-barrel and the other interacts with the C-terminal α-helix of the second crystallographic monomer to form the homodimer (Fig.3.10). This homodimer is therefore assembled by hydrophobic interactions (Egloff et al., 2004; Sutton et al., 2004). Analysis of the purified SARS-CoV nsp9 protein by surface plasmon resonance demonstrated that it is a single strand RNA-binding protein (Egloff et al., 2004). This single strand RNA-binding activity was further confirmed by fluorescence experiments (Egloff et al., 2004).

Multiple alignment of the nsp9 sequences from SARS-CoV (accession No. AY291315) and IBV (accession No. NP-040829) shows that the two proteins share 70% similarity at the amino acid level（Fig.3.11). By structural modeling,

the IBV nsp9 protein was found to adopt a very similar folding as the SARS-CoV nsp9 protein (Fig.3.10). Based on this structural model, systematic mutagenesis of the IBV nsp9 protein was carried out to identify amino acid residues critical for the dimerization and the RNA-binding activity of the protein. The effect of these mutations on the infectivity and replication of IBV was studied by using an infectious IBV cloning system.

3.3.2 Introduction of single amino acid substitutions into nsp9 and analysis of their effects on the replication and infectivity of IBV

By structural modeling, the IBV nsp9 protein was found to adopt an identical folding as the SARS-CoV nsp9 protein (Fig.3.10). To study the biochemical properties and functions of IBV nsp9 protein in viral replication, systematic mutagenesis was carried out based on the IBV nsp9 structure model (Fig.3.12). Seven point mutations, K10A, Y31A, K51A, Y87A, K90A, I95N and G98D (Fig. 3.12), were made and introduced separately into the infectious IBV clone. The in vitro transcribed full-length RNA derived from wild type and the mutant constructs were generated by in vitro transcription using the T7 RNA polymerase in the presence of a cap analog. Electroporation of wild type RNA transcripts together with an RNA fragment covering the N protein region into Vero cells showed the formation of massive CPE at 2 days post-electroporation (Fig.3.13). Similarly, typical CPEs were observed in cells transfected with mutant transcripts derived from K10A, Y31A, K51A and K90A constructs at 2 days post

electroporation and recombinant viruses were recovered (Fig.3.13). In cells electroporated with the I95N transcripts, a typical CPE was observed at 3 days post-electroporation (Fig.3.13). Re-infection of fresh Vero cells with medium collected from total cell lysates prepared by freezing and thawing cells transfected with these mutant transcripts showed the formation of typical CPE, indicating that the minute viruses rescued from the initially transfected cells maintain infectivity in subsequent passages.

In contrast, no CPE formation was observed in cells transfected with transcripts derived from Y87A and G98D mutant constructs up to 5 days post-electroporation (Fig.3.13). Subsequent infection of fresh cells with cell lysate preparations by freezing and thawing the initially transfected cells showed no sign of IBV infection (data not shown), suggesting that no infectious virus could be rescued from these mutant transcripts. These results indicate that Y87A and G98D mutations may abolish the infectivity of the in vitro synthesized full-length IBV transcripts.

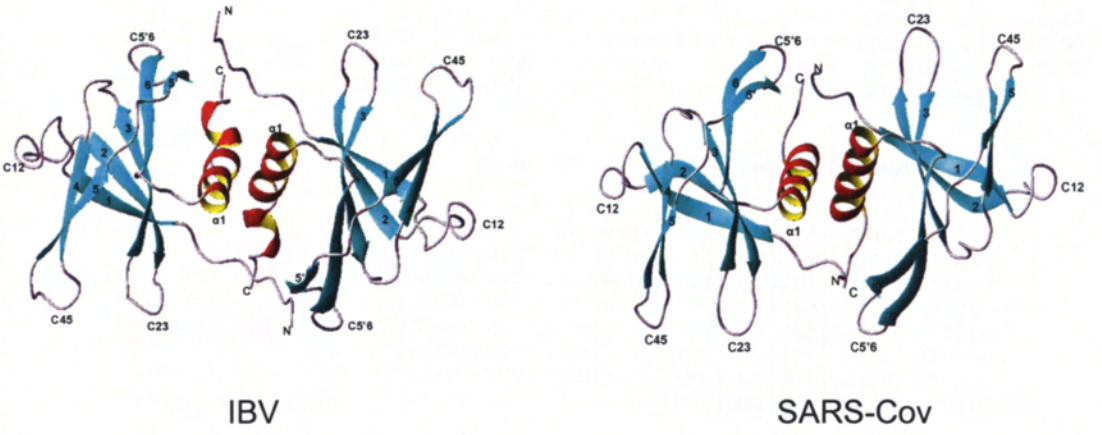

IBV SARS-Cov

Fig.3.10. Crystal structure, topology of SARS-CoV nsp9 and the structure predication of IBV nsp9. Ribbon representation of IBV and SARS-CoV nsp9 protein. The IBV nsp9 structure was presented based on structural modeling using JIGSAW server, MOLMOL and PYMOL viewer.

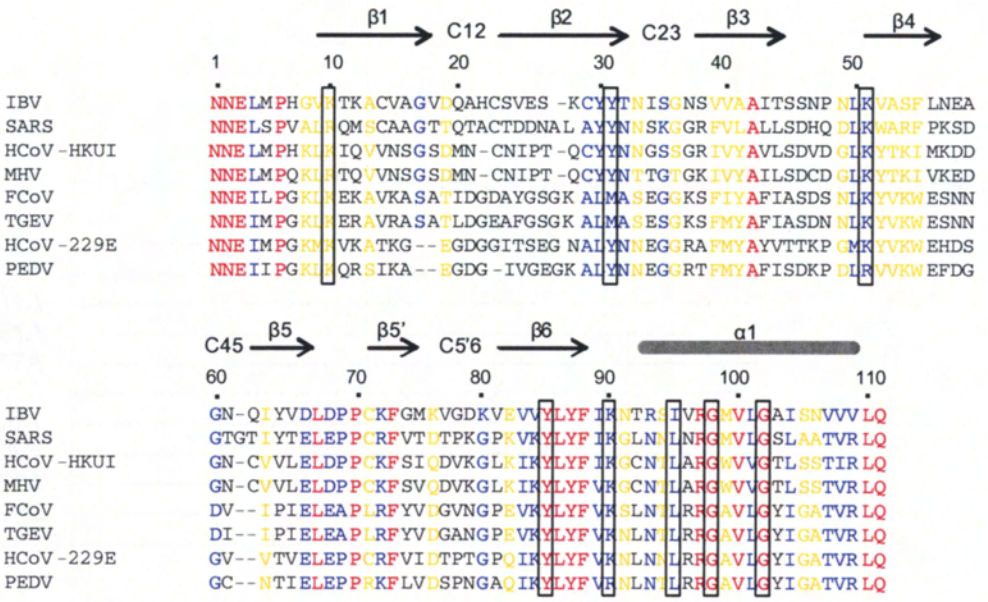

Fig.3.11. Multiple alignment of nsp9 of coronaviruses sequences. Structure-Based alignment of coronavirus nsp9 protein. Secondary structure elements are labeled above the sequence for IBV, based on the structural of SARS-CoV nsp9 protein. Sequences of IBV (infectious bronchitis virus, strain Beaudette, NP_040838); H-CoV (Human Coronavirus, strain HKU1, YP_173242); MHV (Murine Hepatitis Virus, strain 1, AAA46439); TGEV (Porcine Transmissible Gastroenteritis Virus, strain RM4, AAG30228); and SARS (SARS-Coronavirus, 1SSK_A) were obtained from GenBank. The identical residues are marked in red and the similar residues are in blue. The amino acid residues chosen for mutational analysis in this study are boxed.

	1---10 ------ 31 -------- 51 -------- 87- 90 - 95 - 98--102 ----111	**Virus Recovery**
WT	---- K ------- Y -------- K ----------Y-- K --- I --- G -- G ---------	Y
K10A	---- A ----------	Y
Y31A	---------- A ----------	Y
K51A	---------- A ----------	Y
Y87A	---------- ---------- A ----------	N
K90A	---------- A ----------	Y
I 95A	---------- ------ A ----------	Y
I 95N	---------- N ----------	Y
G98A	---------- A ----------	Y
G98D	---------- D ----------	N
G102D	---------- --- D --------	N

Fig.3.12. The amino acid substitutions in each mutate construct and viral recovery in this study. WT represents wild type nsp9. Mutate construct K10A is mutation of Lys10 to an Ala. Y31A is mutation of Tyr 31 to an Ala. K51A is mutation of Lys 51 to an Ala. Y87A is mutation of Tyr 87 to an Ala. K90A is mutation of Lys 90 to an Ala. I95N is mutation of Ile 95 to an Asn. G98D is mutation of Gly 98 to an Asp.

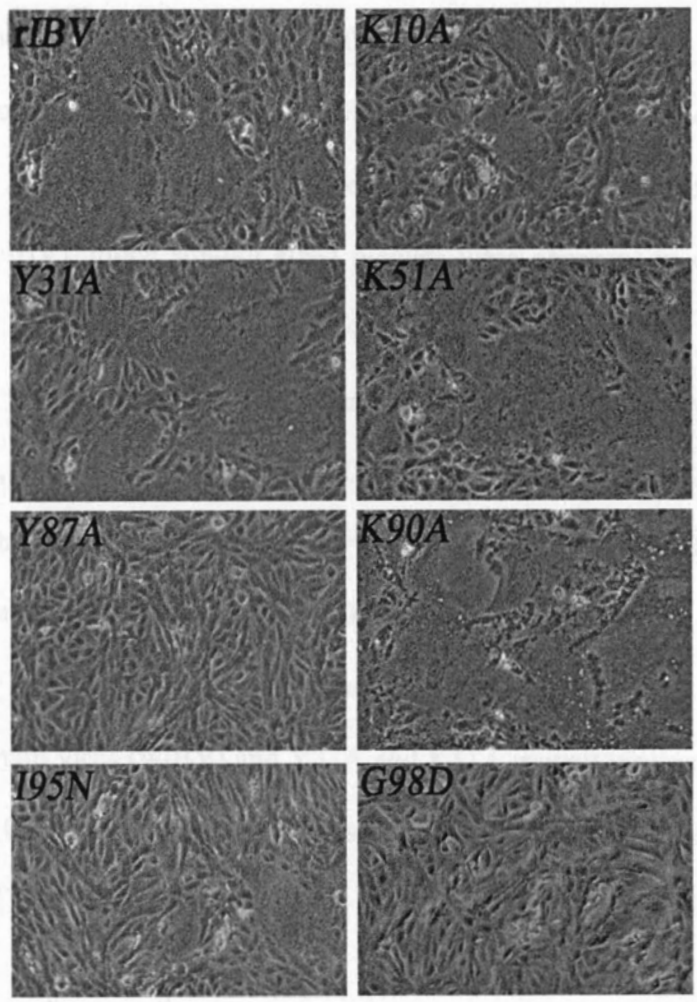

Fig.3.13. Introduction of single amino acid mutations into the IBV genome and recovery of infectious mutant viruses. Vero cells electroporated with the in vitro synthesized transcripts derived from an in vitro assembled full-length clone containing the mutation K10A, Y31A, K51A, Y87A, K90A, I95N, G98D and the full-length wild type IBV (wIBV).

3.3.3 Phenotype and growth properties of the mutant viruses

The growth properties of the K10A, Y31A, K51A, K90A, and I95N mutant viruses on Vero cells were tested by analysis of plaque sizes and growth curves of passage 3 mutant viruses. Compared to cells infected with wild type recombinant virus (wIBV), much smaller sized plaques were observed in cells infected only with the I95N mutant virus (Fig.3.14). The average plaque size for I95N is 0.43 ± 0.07mm (n=10) which is significantly smaller than that of wild type (1.24 ± 0.20mm, n=10; unpaired T-test P=0.001). Plaques size for K10A, Y31A, Y51A and K90A were 0.79 ± 0.08mm (n=10), 1.22 ± 0.12mm (n=10), 1.17 ± 0.16mm (n=10) and 0.73 ± 0.12mm (n=10) respectively. As shown in Fig. 3a, very similarly sized plaques were observed in cells infected with wild type recombinant virus (wIBV) and Y31A and K51A mutant viruses. In cells infected with K10A, K90A mutant viruses, plaques with slightly smaller size were observed (Fig.3.14).

Analysis of the growth curves of wild type and mutant viruses demonstrated that the Y31A and K51A exhibited similar growth kinetics as wild type virus, reaching the peak at 16 hours post-infection (Fig.3.15). At this time point, the titers of the two mutant viruses were approximately 5 fold lower than that of wild type virus (Fig.3.15). The other three mutant viruses, K10A, K90A and I95N, grew slightly more slowly than wild type virus, reaching the peak at 24 hours post-infection (Fig.3.15). The titers of these mutant viruses were approximately

20 to 100 fold lower than that of wild type virus (Fig.3.15). Among them, the titer of the I95N mutant virus was the lowest (Fig.3.15).

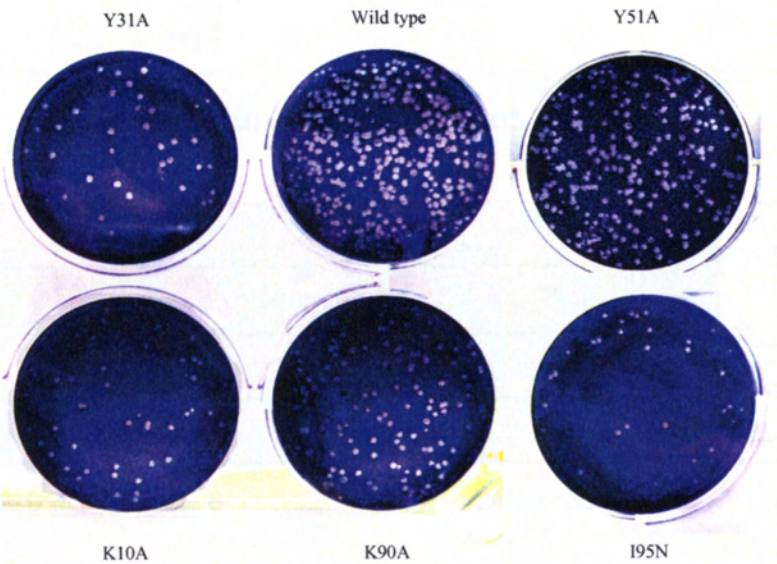

Fig.3.14. Analysis of the growth properties of wild type and mutant viruses through their plaque sizes. Plague sizes of wild type and K10A, Y31A, K51A, K90A and I95N mutant viruses. Monolayers of Vero cells on a 6-well plate were infected with 100 µl of 1000-fold diluted virus stock and cultured in the presence of 0.5% carboxymethy cellulose at 37°C for 3 days. The cells were fixed and stained with 0.1% toluidine.

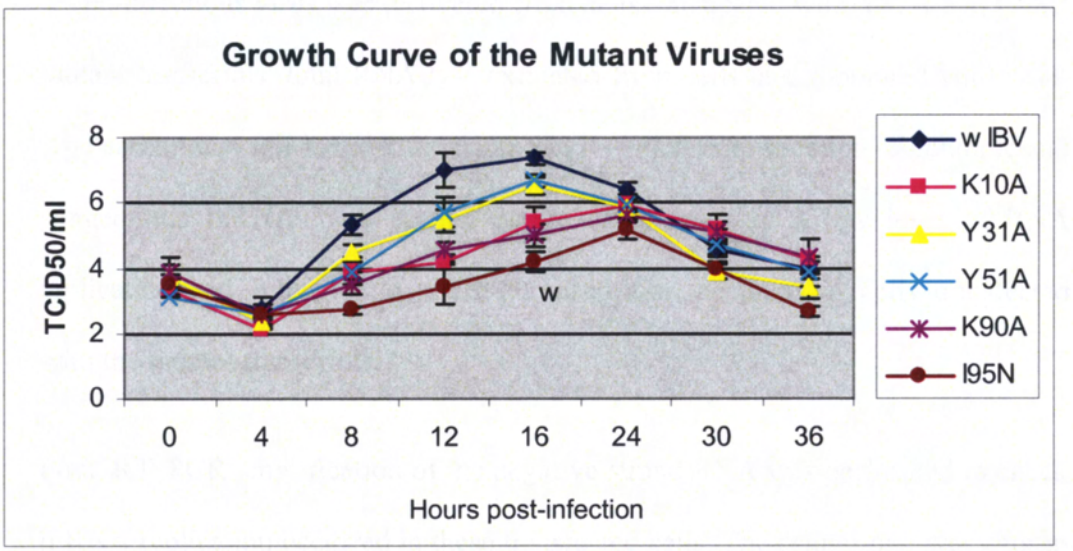

Fig.3.15. Analysis of the growth properties of wild type and mutant viruses through their one-step growth curves. Growth curves of wild type and mutant viruses. Vero cells were infected with wild type and K10A, Y31A, K51A, K90A and I95N mutant viruses, and harvested at 0, 4, 8, 12, 16, 24, 30 and 36 hours post-inoculation, respectively. Viral stocks were prepared by freezing/thawing of the cells three times and TCID50 of each viral stock was determined by infecting five wells of Vero cells on 96-well plates in triplicate with 10-fold serial dilution of each viral stock.

3.3.4. Analysis of negative-strand RNA replication and subgenomic RNA transcription in cells transfected with wild type and mutant full-length transcripts

As no infectious virus was recovered from cells transfected with Y87A and G98D mutant transcripts, total RNA was extracted from cells electroporated with wild-type and mutant full-length transcripts and RT–PCR amplification of genomic and subgenomic mRNAs was carried out to check whether a low level of RNA replication and subgenomic mRNA transcription occurred in cells transfected with the mutant transcripts.

First, RT–PCR amplification of the negative strand RNA was performed to check if RNA replication occurred in these transfected cells. The primer pair was chosen so that the IBV sequence from 14931 to 15600 nt would be amplified by the RT–PCR reaction. If replication of viral RNA occurred, a 670 bp PCR fragment would be expected. As shown in Figure 3.16, RT–PCR fragments amplified from both positive (lanes 2, 5 and 8) and negative (lanes3, 6 and 9) strand RNA templates were obtained from cells transfected with both wild type and mutant transcripts including Y87A and G98D. The amount of the negative strand RNA was approximately half of that of the positive strand RNA (Figure 3.16). This result demonstrates that detection of the negative strand RNA in cells transfected with wild-type and mutant Y87A, G98D constructs by RT–PCR is due to the

replication of viral RNA. These results confirm that transcription of the negative strand RNA has taken place in cells transfected with the mutant transcripts.

Second, RT-PCR amplification of subgenomic mRNAs was performed to check if a low level of subgenomic mRNA synthesis could occur in cells transfected with the mutant transcripts. The forward primer used in this reaction corresponds to the leader sequence from 26–46 nt in the genomic RNA and the downstream primers covers IBV sequences from 24784 to 24803 nt. If transcription of subgenomic mRNAs did occur, a 415 bp PCR product corresponding to the 5'- terminal region of the subgenomic mRNA4 and a 1010 bp fragment corresponding to the 5'-terminal region of the subgenomic mRNA3 would be expected. As shown in Figure 3.16, a dominant 415 bp band and a weak 1010 bp band were observed in cells electroporated with wild-type full-length transcripts at 2 days post-electroporation (lane 4). Sequencing of the PCR fragments confirmed that they represent the correct sequences of the corresponding regions of the subgenomic mRNAs 3 and 4, respectively. The same PCR products were not detected in cells electroporated with Y87A and G98D mutant transcripts at 72 hours post-electroporation (Figure 3.16, lanes7 and 10). The failure to detect negative stranded sgRNAs in cells transfected with the mutant transcripts show that the Y87A and G98D mutations lead to the disruption of subgenomic RNA transcription.

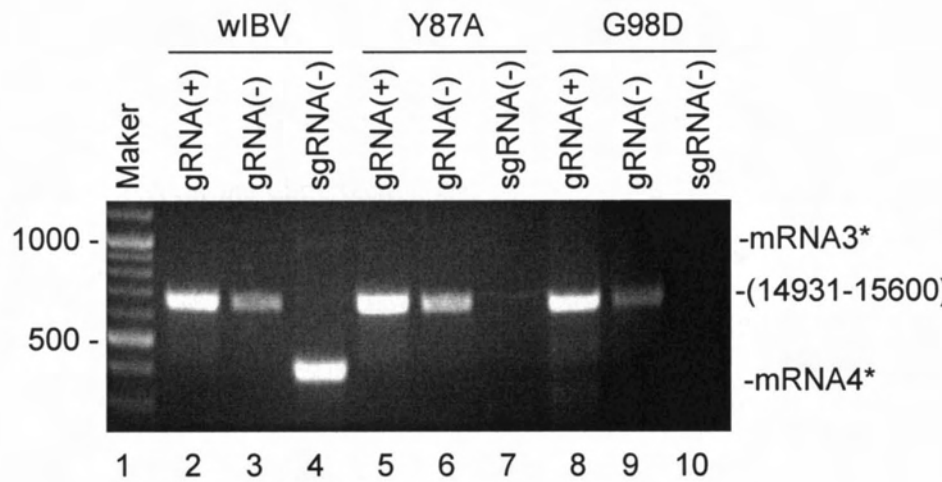

Fig.3.16. **Analysis of negative strand RNA replication and subgenomic RNA transcription in cells transfected with wild-type and mutant full-length transcripts.** Detection of positive, negative strand RNA and negative strand subgenomic RNA synthesis in cells electroporated with wIBV (lanes2, 3 and 4), Y87A (lanes 5, 6 and 7) and G98D (lanes 8, 9 and 10) mutant transcripts. Total RNA was prepared from Vero cells electroporated with in vitro synthesized full-length transcripts 3 days post-electroporation. Regions corresponding to 14931-15600 nt of the positive (+), negative (–) sense IBV RNA and regions corresponding to the 5′ -terminal 415 and 1010 nucleotides of the subgenomic mRNA 4 and 3, respectively, were amplified by RT–PCR and analyzed on 1.2% agarose gel. Lane 1 shows DNA markers. Numbers on the left indicate nucleotides in bases.

3.3.5 Destabilization of the IBV nsp9 homodimer by introducing point mutations into the C-terminal α-helical region correlating with the defects of I95N and G98D mutant constructs in viral RNA replication and infectivity

Biochemical analysis of the effect of the K10A, K31A, Y51A, K90, I95N and G98D mutations on the dimerization and RNA-binding activity of the IBV nsp9 was then carried out to understand the detailed mechanisms of these point mutations on the replication and infectivity of IBV. As dimerization of nsp9 protein is thought to be critical for its RNA binding activity, the effect of these mutations on the formation of nsp9 homodimer was first studied. For this purpose, wild type and the mutant constructs with a 6-His tag at their N-terminus were cloned into a bacterial expression vector, expressed in *E. coli* and purified to near homogeneity. Efforts were made to express the Y87A mutant protein in the same system. However, very low, if any, expression of the mutant protein was consistently observed for some unknown reason (data not shown). This mutant construct was not included in the subsequent studies. After removing the 6-His tag, the purified proteins were treated with 0-2% of glutaraldehyde, a short self-polymerizing reagent that reacts with lysine, tyrosine, histidine and tryptophan residues, and analyzed by SDS-PAGE. The results showed gradually increased detection of the homodimer following cross-linking of wild type and mutant proteins with increasing concentrations of the cross-linking agent (Fig.3.17).

Interestingly, it was noted that the G98D mutant protein showed much less, if any, dimer formation without cross-linking with glutaraldehyde (Fig.3.17). The I95N mutant protein also showed significantly reduced dimer formation under the same conditions (Fig.3.17). These results suggest that the I95N and G98D mutations may destabilize the IBV nsp9 homodimer.

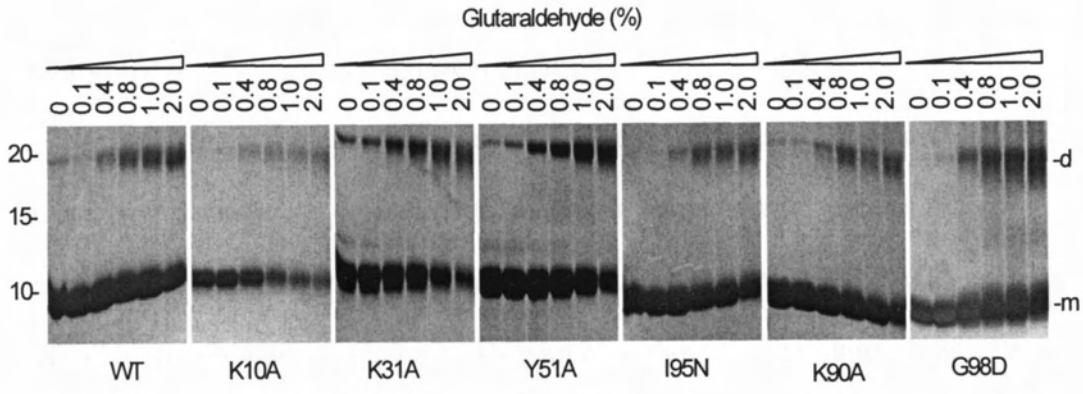

Fig.3.17. Analysis of dimerization of wild type mutant IBV nsp9 protein after chemical cross-linking. The purified wild type and mutant nsp9 proteins were treated with 0-2 % of glutaraldehyde, and analyzed by SDS-15% polyacrylamide gel. The monomeric (m) and dimeric (d) forms of the protein are indicated. Numbers on the left indicate molecular masses in kilodalton.

This possibility was further studied in the following two ways. First, the purified wild type and mutant proteins were analyzed by gel filtration after removing the 6-His tag. The results showed the detection of two peaks for wild type and five out of the six mutants (K10A; Y31A, K51A, K90A and I95N) using standard proteins as markers (Fig.3.18). Analysis of the two peaks by mass spectrometry confirmed that they indeed represent the nsp9 monomers and dimers, respectively. However, only one peak was observed in the G98D mutant protein (Fig.3.19). Once again, analysis by mass spectrometry confirmed that it represents the nsp9 monomers containing the right point mutation. In addition, SDS-PAGE analysis of wild type and mutant nsp9 (G98D) with or without His tag showed same result as their gel filtration data (Fig.3.20 and Fig.3.21).

Second, wild type and the I95N and G98D mutant nsp9 were cloned into a mammalian expression vector with either a Flag or a Myc tag at the N-terminus. The Flag-tagged wild type nsp9 were co-expressed with the Myc-tagged wild type nsp9, I95N and G98D mutants, respectively. The association of wild type nsp9 protein with either wild type or mutant nsp9 proteins was analyzed by coimmunoprecipitation experiment with anti-Flag antibody. The immuno-precipitated proteins were separated on SDS-PAGE and analyzed by Western blotting with either anti-Flag or anti-Myc antibody. As shown in Fig.3.22, Western blot analysis of total cell lysates showed the detection of similar amounts of wild type and mutant nsp9 proteins either expressed on their own or co-expressed with the Flag-tagged wild type nsp9 (Fig.3.22, top panel). Analysis of

the precipitates with anti-Flag antibody showed the detection of approximately equal amounts of the Flag-tagged wild type nsp9 either expressed on its own or co-expressed with the Myc-tagged wild type and mutant nsp9 (Fig.3.22, middle panel). Analysis of the same precipitates with anti-Myc antibody showed efficient detection of the Myc-tagged wild type nsp9 only when it was co-expressed with the Flag-tagged nsp9 protein (Fig.3.22, bottom panel, lane 5). Interestingly, much reduced detection of the Myc-tagged I95N was observed when it was co-expressed with the Flag-tagged wild type nsp9 (Fig.3.22, bottom panel, lane 6), demonstrating that this point mutation destabilizes the nsp9 homodimer. When the Myc-tagged G98D construct was co-expressed with the Flag-tagged wild type nsp9, the mutant protein was not detected in the co-immunoprecipitation experiment (Fig.3.22, bottom panel, lane 7). Taken together, these results confirm that the G98D mutation totally abolishes the nsp9 homodimer formation.

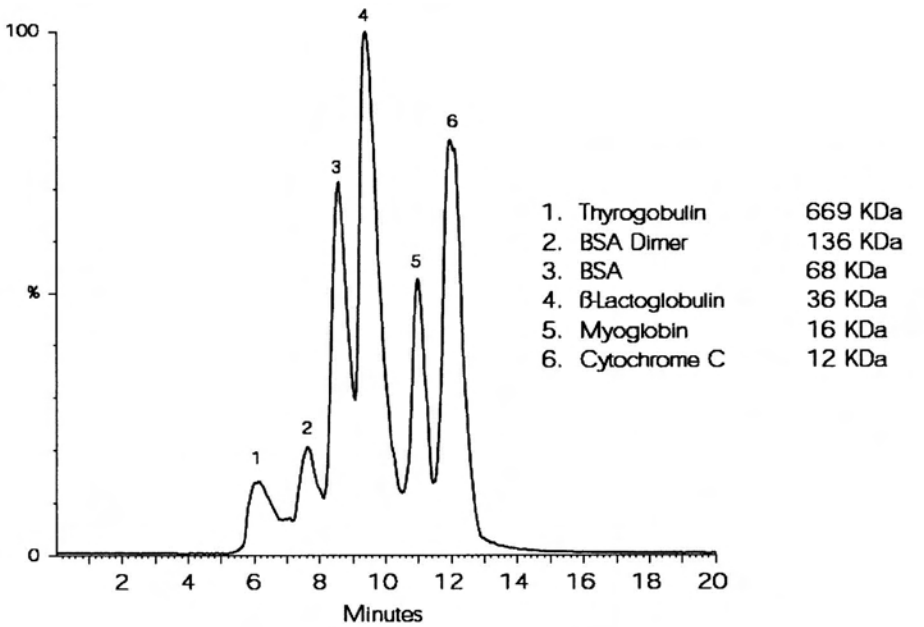

Fig.3.18. LC/MS analysis of protein standards using BioSuite™ 250, 5µm high resolution (HR) SEC column. The gel-filtration assay of the proteins in the figure was performed using BioSuite™ 250 HR SEC column (7.8×300mm, Waters). The figure was adopted from the following website: http://www.waters.com. Date analysis from our study was performed with reference to these standard proteins analysis.

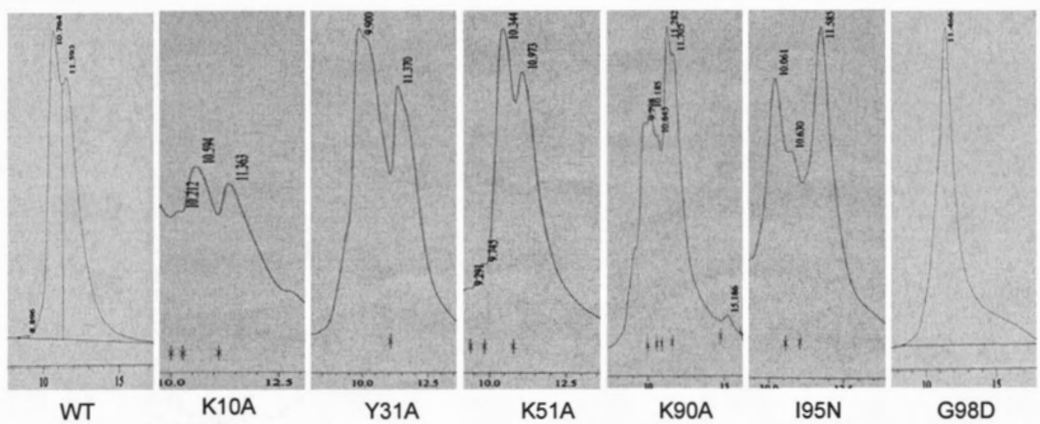

Fig.3.19. Analysis of wild type and mutant nsp9 proteins by gel-filtration. The purified wild type and mutant nsp9 proteins were analyzed by gel filtration assay using BioSuiteTM 250 HR SEC column (7,8×300mm, Waters) on Shimadszu chromatograph (LC-10ATvp) equipped with a photodiode array detector (SPD-M20A). The column was equilibrated at a flow rate of 1 ml/minutes with PBS buffer at room temperature. The protein samples (300µl) were injected at a given concentration and detected. The first peak was formed by the nsp9s dimer (~24 kDa), and the second peak the monomer (~12kDa).

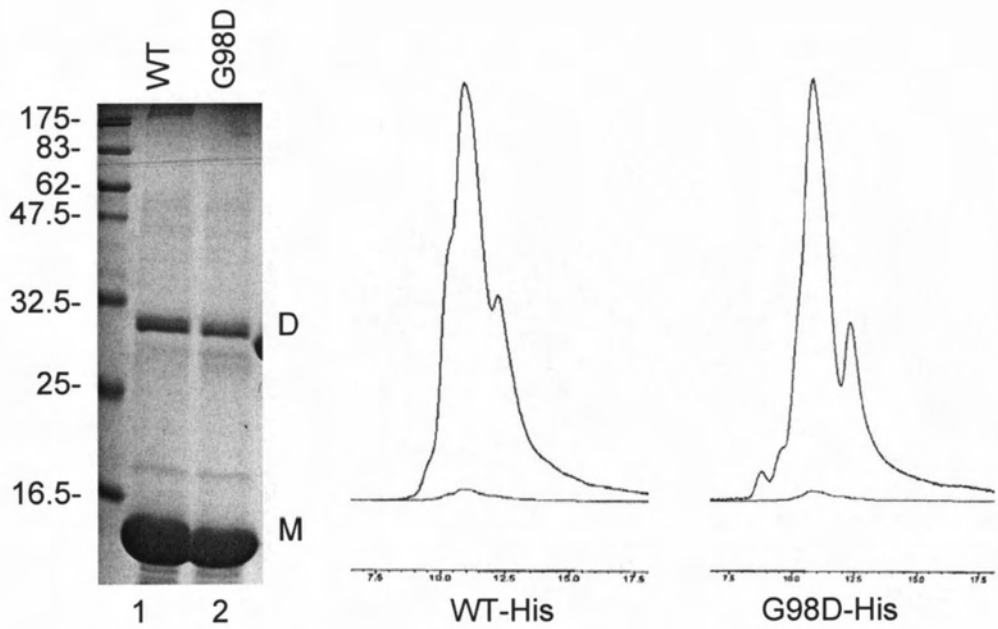

Fig.3.20. Gel-filtration analysis of the purified wild type (WT) and mutant nsp9 protein (G98D) with His-tag. SDS-PAGE analysis of nsp9 with lane WT (wild type nsp9) and lane 2 (G98D) corresponding to the peaks on HPLC trace. M and D represent monomer and dimer. The first peak on HPLC trace was formed by the dimers of wild type and mutant nsp9 (~29 kDa), the second peak indicates monomer (~14kDa).

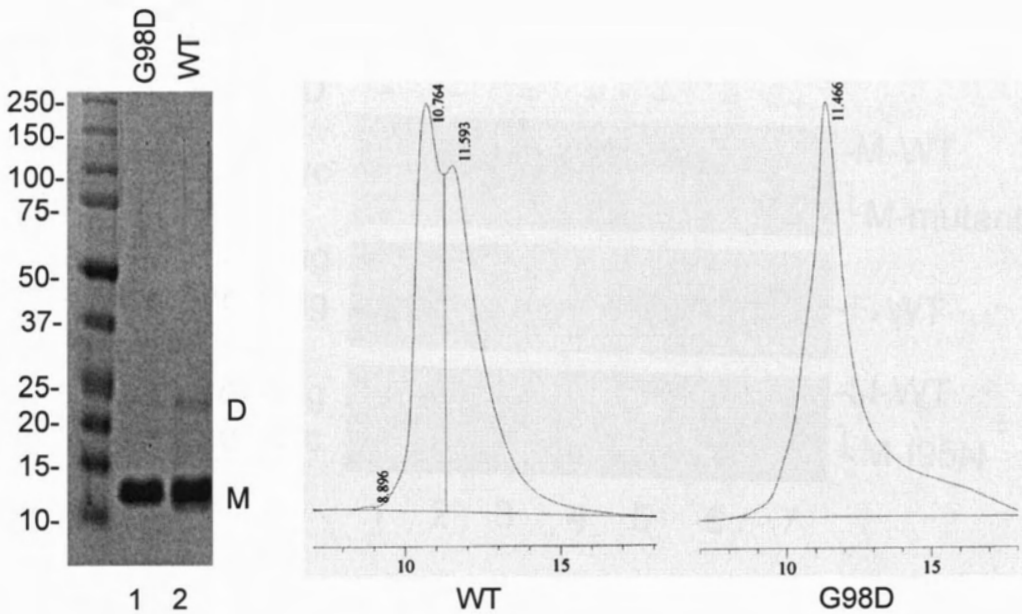

Fig.3.21. Gel-filtration analysis of the purified wild type and mutant nsp9 protein without His-tag. SDS-PAGE analysis of nsp9 with lane 1 G98D and lane 2 WT (wild type nsp9) corresponding to the peaks on HPLC trace. M and D represent monomer and dimer. The first peak was formed by the wild type nsp9 dimer (~24 kDa), the second peak indicates monomer (~12kDa). The only one peak represents the monomer of mutant nsp9 G98D.

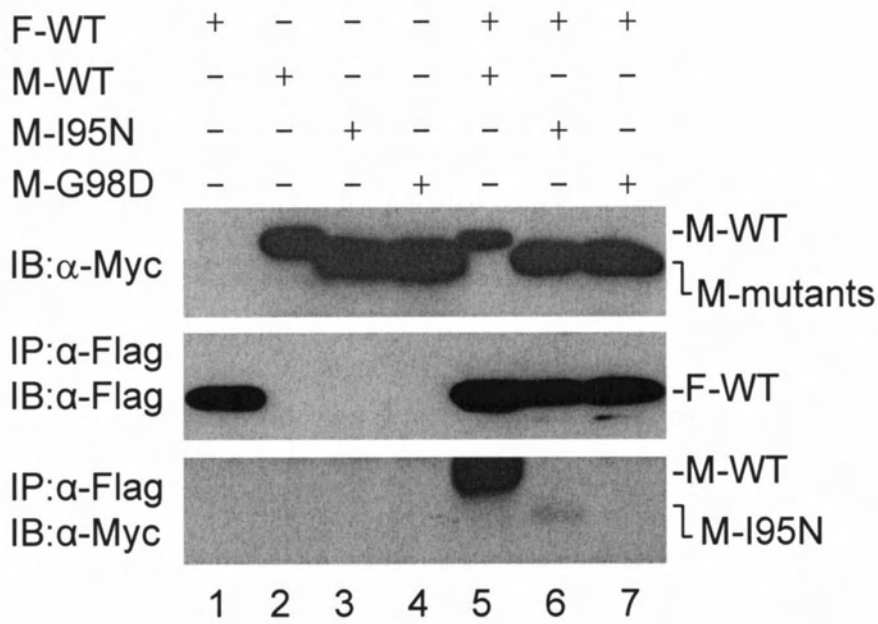

Fig.3.22. Mutational analysis of amino acid residues essential for dimerization of IBV nsp9 protein. HeLa cells overexpressing the Flag-tagged wild type nsp9 protein alone (lane 1), the Myc-tagged wild type nsp9 protein alone (lane 2), the Myc-tagged mutate nsp9 protein (I95N) alone (lane 3), the Myc-tagged mutate nsp9 protein (G98D) alone (lane 4), the Flag-tagged wild type and Myc-tagged wild type nsp9 protein (lane 5), the Flag-tagged wild type nsp9 protein and Myc-tagged mutate nsp9 (I95N) protein (lane 6), the Flag-tagged wild type nsp9 protein and Myc-tagged mutate nsp9 (G98D) protein (lane 7). Cotransfected proteins were separated in SDS–PAGE and analyzed by Western blotting with anti-Myc antibody (top panel). Polypeptides were immunoprecipitated with anti-Flag antibody, separated by SDS–PAGE, and analyzed by Western blotting with anti-Flag antibody (middle panel). Polypeptides were immunoprecipitated with anti-Flag antibody, separated by SDS–PAGE, and analyzed by Western blotting with anti- Myc antibody (bottom panel).

3.3.6 Analysis of the effect of point mutations in the IBV nsp9 protein on its RNA-binding activity

The effect of these mutations on the single strand RNA-binding activity of the IBV nsp9 was then investigated by Northwestern blotting analysis. Approximately equal amounts of the purified wild type and G98D mutant proteins were separated on SDS–PAGE either before or after removal of the 6x His tag (Fig.3.23, top panel). Once again, formation of reasonable amounts of dimer was detected in the purified wild type protein (Fig.3.23, top panel, lane 3). After transfer to a Hybond C extra membrane, the RNA-binding activities of wild type and G98D mutant proteins were analyzed by Northwestern blot with two probes corresponding, respectively, to the positive- and negative-sense 3'-UTR of IBV. The results showed that both wild type and G98D mutant proteins with the 6xHis tag could efficiently bind to either positive- or negative RNA probes (Fig.3.23, middle and bottom panels, lanes 1 and 2). It was noted that efficient detection of the dimeric form of the two proteins was achieved when either probe was used (Fig.3.23, middle and bottom panels, lanes 1 and 2), suggesting preferential binding of the probes to the homodimer of the protein. After removal of the 6xHis tag, both the monomeric and dimeric forms of the purified wild type protein could still efficiently bind to either probe (Fig.3.23, middle and bottom panels, lane 3). However, very weak, if any, binding of the G98D mutant protein to either probe was observed after removal of the 6x His tag (Fig.3.23, middle and

bottom panels, lane 4), suggesting that this point mutation abolishes the RNA-binding activity of the IBV nsp9 protein.

The RNA-binding activity of wild type and all mutant proteins was then analyzed by three independent experiments. As a representative gel shown in Fig.3.24, the K10A and K90A mutations greatly reduced the RNA-binding activity of the protein to both probes (lanes 2 and 5). The K51A mutant protein showed moderately reduced binding activity (Fig.3.24, lane 4), and the Y31A and I95N mutant proteins showed marginally reduced binding activity to both probes (Fig.3.24, lanes 3 and 6). The binding efficiency of wild type and all mutant proteins to both probes was quantified by densitometry measurement of relative bands from three independent experiments and the relative RNA-binding efficiencies of the mutant proteins to wild type protein are shown in Fig.3.25. As can be seen, the G98D mutant protein showed 0 and 4% binding efficiencies to the positive and negative probes, respectively (Fig.3.25). The K10A and K90A mutants showed approximately 10% binding efficiency to both probes (Fig.3.25). The K51A mutant protein showed approximately 35 and 55% binding efficiencies to the positive and negative probes, respectively (Fig.3.25). The Y31A and I95N mutant proteins showed 80 to 100% binding efficiencies to both probes (Fig.3.25).

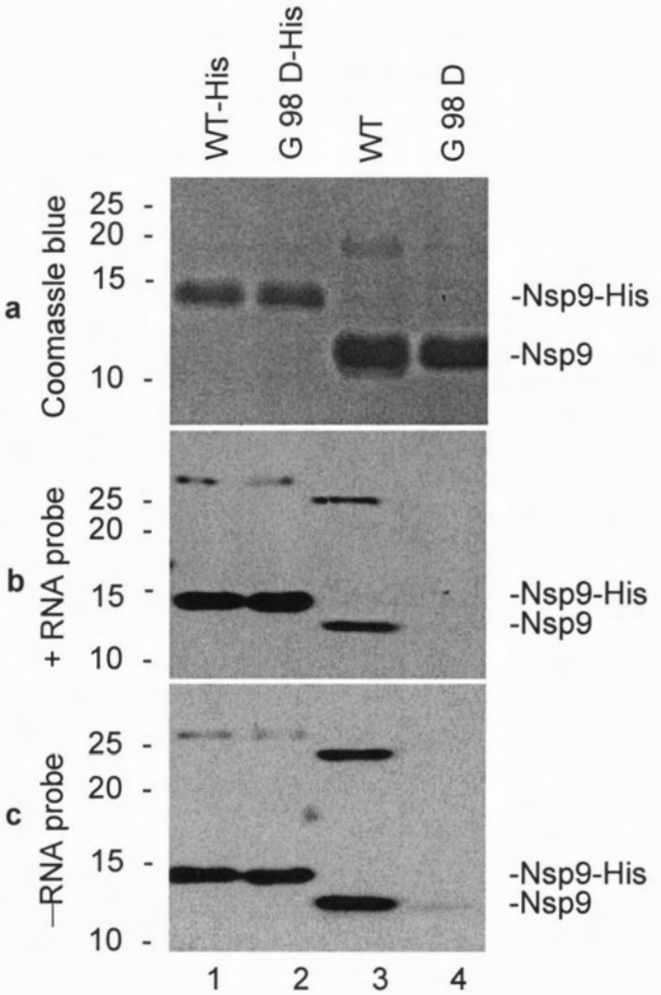

Fig.3.23. Northwestern analysis of the RNA binding activity of wild type and G98D mutant nsp9 protein. The purified wild type and G98D mutant nsp9 protein with or without the 6xHis tag were separated on two SDS-15 % polyacrylamide gels. One gel was directly detected by staining with Commassie blue (top panel), and the second was transferred to Hybond C extra membrane. The RNA-binding activity was probed with either positive (middle panel) or negative (bottom panel) sense, digoxin-labelled RNA corresponding to 26,539–27,608 nucleotides of the IBV genome. The bands corresponding to the dimeric form with the His tag (d-His), the dimeric form without the His tag (d), the monomeric form with His tag (m-His) and the monomeric form without the His tag (m) are indicated. Numbers on the left indicate molecular masses in kilodalton.

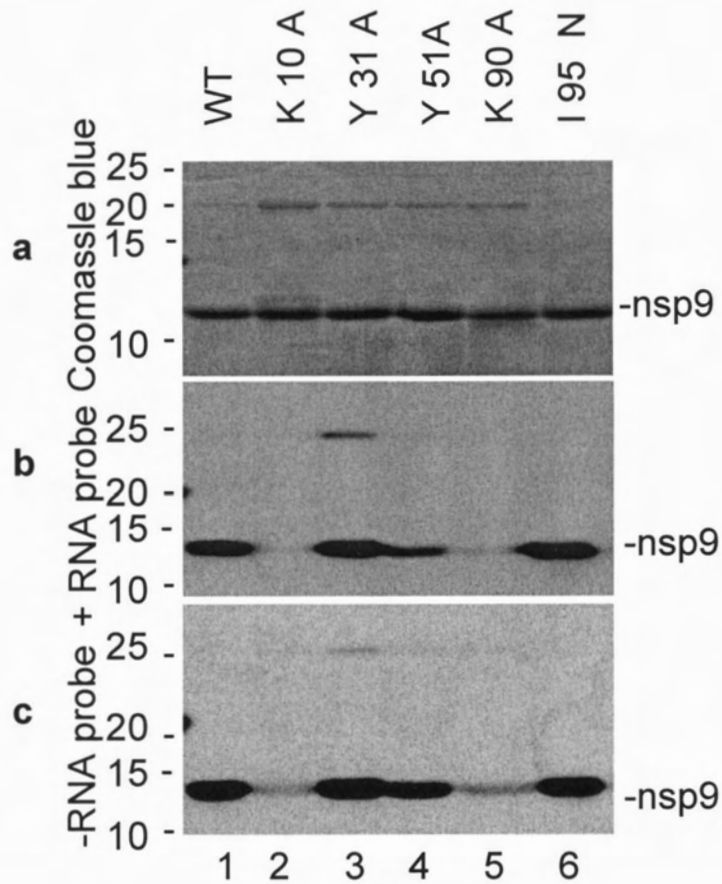

Fig.3.24. Northwestern analysis of the RNA binding activity of wild type and K10A, Y31A, K51A, K90A and I95N mutant nsp9 protein. The purified wild type and mutant nsp9 protein without the 6xHis tag were separated on two SDS-15 % polyacrylamide gels. One gel was directly detected by staining with Commassie blue (top panel), and the second was transferred to Hybond C extra membrane. The RNA-binding activity was probed with either positive (middle panel) or negative (bottom panel) sense, digoxin-labelled RNA corresponding to 26,539–27,608 nucleotides of the IBV genome. The bands corresponding to the dimeric form without the His tag (d) and the monomeric form without the His tag (m) are indicated. Numbers on the left indicate molecular masses in kilodalton.

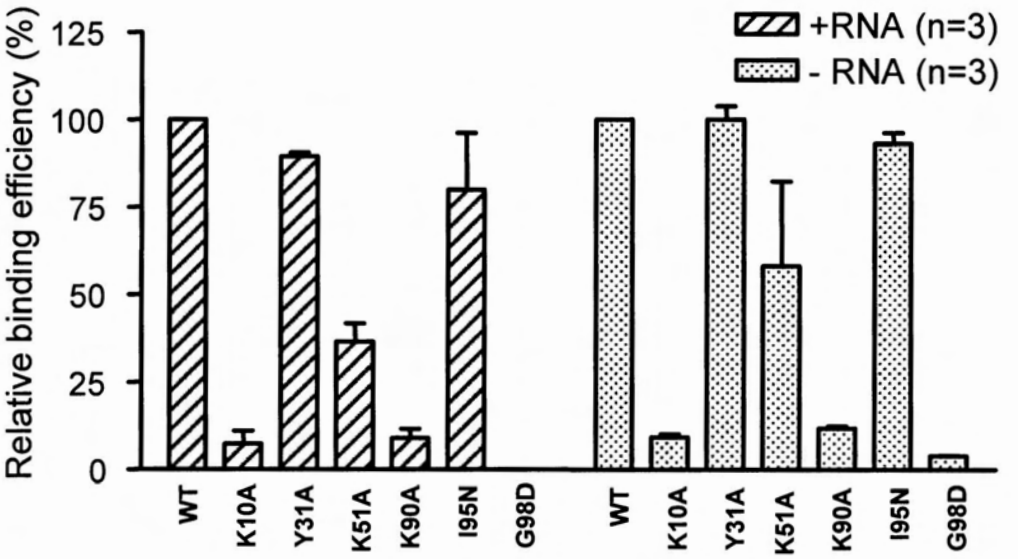

Fig.3.25. Relative binding efficiency of mutant proteins. The relative binding activities of wild type and mutant nsp9 protein to either positive or negative sense probes were quantified by densitometry measurement of individual bands in three independent Northwestern blot experiments, as shown above. The binding activity of wild type nsp9 protein to both probes was treated as 100 %.

3.3.7. No detectable interaction between the IBV nsp9 protein and the RNA-dependent RNA polymerase (nsp12) and RNA helicase (nsp13)

To further study the mechanisms underlying the functional roles of nsp9 in coronavirus replication and infectivity, we next set up to investigate if the IBV nsp9 protein could physically interact with other replicase proteins by co-immunoprecipitation experiment. The two proteins chosen for this study are the putative RNA-dependent RNA polymerase (nsp12) and RNA helicase (nsp13). The Flag-tagged wild type nsp12 were first co-expressed with the Myc-tagged wild type nsp9, I95N and G98D, respectively, and the potential interaction of the nsp12 protein with the wild type and two mutant nsp9 proteins was analyzed by coimmunoprecipitation experiment with anti-Flag antibody. The immunoprecipitated proteins were separated on SDS-PAGE and analyzed by Western blotting with either anti-Flag or anti-Myc antibody. Western blot analysis of the total cell lysates with anti-Myc antibody showed the presence of similar amounts of the Myc-tagged wild type and mutant proteins either expressed on their own or co-expressed with the Flag-tagged nsp12 (Fig.3.26, top panel). Analysis of the precipitates with anti-Flag antibody showed the detection of approximately equal amounts of the Flag-tagged nsp12 either expressed on its own or co-expressed with the Myc-tagged wild type and mutant nsp9 (Fig.3.26, middle panel). However, analysis of the same precipitates with anti-Myc

antibody showed no detection of the Myc-tagged wild type nsp9 only when it was co-expressed with the Flag-tagged nsp9 protein (Fig.3.26, bottom panel, lane 5). Very similar results were observed in cells co-expressing the Flag-tagged nsp13 with either wild type or mutant nsp9 (Fig.3.27). These data confirm that the IBV nsp9 protein may be unable to directly interact with nsp12 and nsp13.

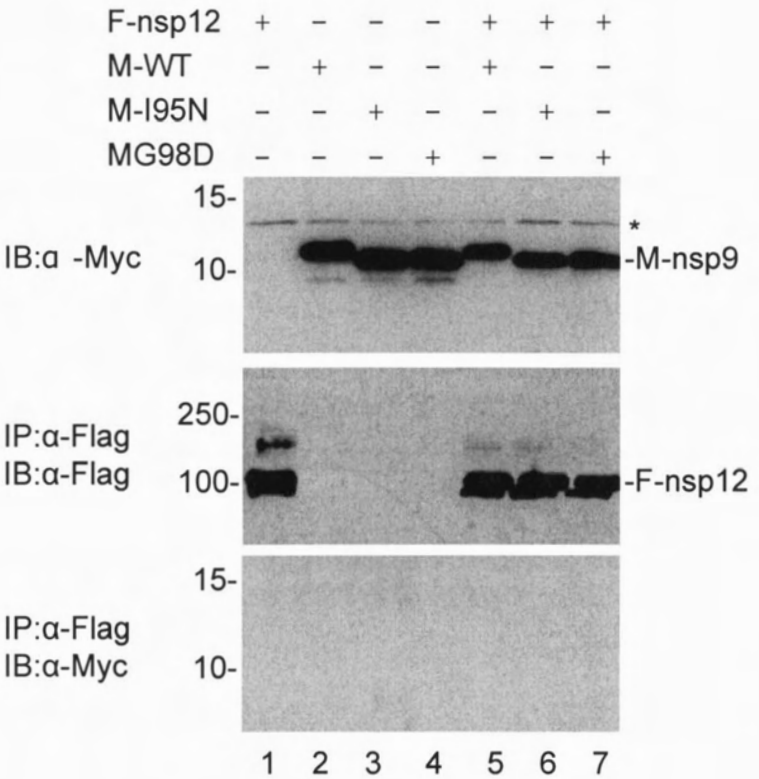

Fig.3.26. Characterization of the interaction between RDRP and nsp9. HeLa cells overexpressing the Flag-tagged RDRP alone (lane 1), the Myc-tagged wild type nsp9 protein alone (lane 2), the Myc-tagged mutate nsp9 protein (I95N) alone (lane 3), the Myc-tagged mutate nsp9 protein (G98D) alone (lane 4), the Flag-tagged RDRP and Myc-tagged wild type nsp9 protein (lane 5), the Flag-tagged RDRP and Myc-tagged mutate nsp9 (I95N) protein (lane 6), the Flag-tagged RDRP and Myc-tagged mutate nsp9 (G98D) protein (lane 7). Cotransfected proteins were separated in SDS–PAGE and analyzed by Western blotting with anti-Myc antibody. Polypeptides were immunoprecipitated with anti-Flag antibody, separated by SDS–PAGE, and analyzed by Western blotting with anti-Flag antibody and anti-Myc antibody.

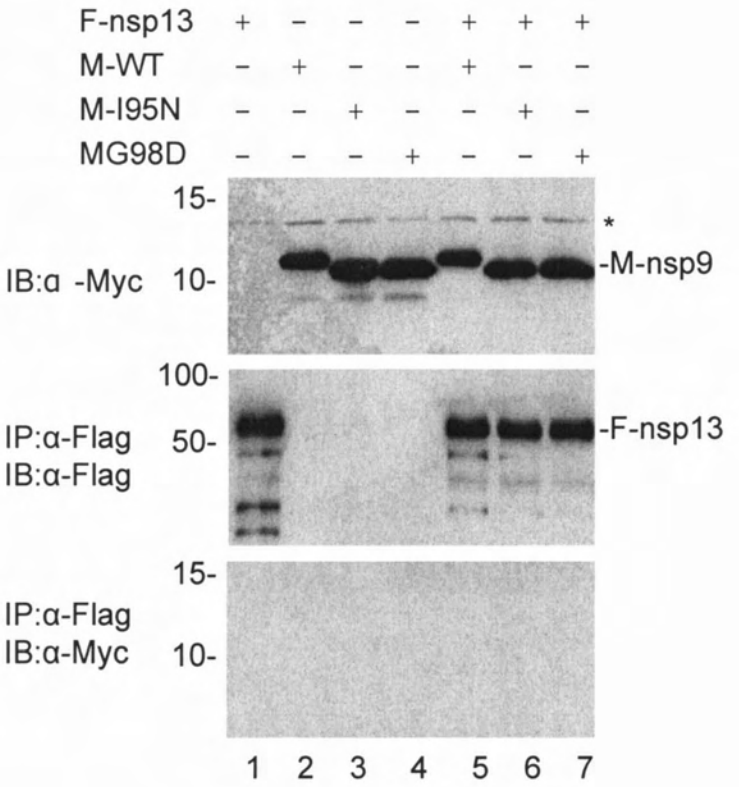

Fig.3.27. Characterization of the interaction between helicase and nsp9. HeLa cells overexpressing the Flag-tagged helicase protein alone (lane 1), the Myc-tagged wild type nsp9 protein alone (lane 2), the Myc-tagged mutate nsp9 protein (I95N) alone (lane 3), the Myc-tagged mutate nsp9 protein (G98D) alone (lane 4), the Flag-tagged helicase and Myc-tagged wild type nsp9 protein (lane 5), the Flag-tagged helicase and Myc-tagged mutate nsp9 (I95N) protein (lane 6), the Flag-tagged helicase and Myc-tagged mutate nsp9 (G98D) protein (lane 7). Cotransfected proteins were separated in SDS–PAGE and analyzed by Western blotting with anti-Myc antibody. Polypeptides were immunoprecipitated with anti-Flag antibody, separated by SDS–PAGE, and analyzed by Western blotting with anti-Flag antibody and Myc antibody.

CHAPTER 4

GENERAL DISCUSSION

AND FUTURAL DIRECTION

4.1 Main Conclusion

Four main conclusions can be drawn based on this thesis study.

(1) An infectious clone was established by in vitro ligation of five fragments spanning the entire IBV genome. The fragment were obtained by RT-PCR of total RNA extracted from Vero cells infected with a Vero cell-adapted IBV Beaudette strain (p65) (Shen et al., 2003, 2004; Fang et al., 2005). Recombinant virus derived from the infectious clone replicated efficiently and displayed similar growth kinetics, plaque morphology, and cytopathology in Vero cells as did wild-type IBV Beaudette strain.

(2) A G-C point mutation at nucleotide position 15,526 of helicase protein was found to be lethal to the infectivity of the in vitro-synthesized full-length transcripts on Vero cells. No infectious virus could be rescued from Vero cells electroporated with transcripts containing this mutation. It demonstrated that a domain with previously unassigned function within helicase protein may play an essential role in coronavirus replication although the mutation does not locate within the two function domains of the protein..

(3) Substitution of a conserved Gly (G98) residue in the C-terminal α-helix with an Asp greatly destabilized the IBV nsp9 homodimer. Introduction of the same mutation into an infectious IBV clone system showed that the mutation totally abolishes the transcription of subgenomic RNA and no infectious virus

could be recovered, demonstrating that dimerization is critical for the function of this replicase protein.

(4) The G98D point mutation also abolishes the RNA-binding activity of IBV nsp9 protein. Mutation of a semi-conserved Ile (I95) residue in the same region showed moderately destabilizing effect on the IBV nsp9 homodimer but minimal effect on its RNA-binding activity. Meanwhile, mutations of some positively charged residues in the β-barrel regions of the IBV nsp9 protein significantly reduced its RNA-binding activity, but with no obvious effect on dimerization of the protein, suggesting that formation of the nsp9 homodimer may play functions not directly related to the RNA-binding activity of the protein.

4.2 Establishment of a Full-length Infectious cDNA System Derived from IBV

4.2.1 The assembly of full-length genomic cDNA by in vitro ligation of smaller subcloned cDNA and recovery of infectious viruses by introduction of the in vitro-synthesized transcripts into cells

The assembly of full-length genomic cDNA by in vitro ligation of smaller, more stable subcloned cDNA, generation full-length transcripts in vitro using a Bacteriophage DNA-dependent RNA polymerase, and recovery of infectious viruses by introduction of the in vitro-synthesized transcripts into cells, was applied first by

Rice et al (1989) in yellow fever virus, a flavivirus. However, for coronaviruses, this scheme had to be executed on a much great scale, with five to seven fragments instead of two due to their large genome size. This approach was first used in coronaviruses by Yount et al (2000) and has been proved that is a rapid and reliable way to construct infectious clones from large RNA viruses. Since then it has been successfully used to construct infectious clones for several coronaviruses, including TGEV, MHV, SARS-CoV, and IBV (Youn et al., 2005a, 2005b; Yount et al., 2000, 2003).

In this study, a full-length infectious cDNA system was established by in vitro ligation of five fragments spanning the entire IBV genome which obtained by RT PCR of total RNA extracted from Vero cells infected with a Vero cell-adapted IBV Beaudette strain (p65) (Shen et al., 2003, 2004; Fang et al., 2005) . To facilitate this approach, the innovation was developed to directly assemble fragments by means of nonsymmetric overhangs generated by enzyme *BsmBI* and *BsaI.* This ensured that the fragments became connected in a predetermined order by ligation, without the generation of rearranged byproducts (Yount, B et al., 2000). Recombinant virus derived from the infectious construct replicated efficiently and displayed similar growth kinetics, plaque morphology, and cytopathology in Vero cells as did wild-type IBV Beaudette strain.

4.2.2 Two point mutations which locate in PLP and 3CLP domains, respectively affect neither the recovery of virus nor the infectivity of the resued virus.

During development of an infectious IBV clone, the G433C (E - Q) point mutation near the catalytic center of the PLP domain in Nsp3 was found to affect neither the recovery of infectious virus from the full-length synthesized in vitro transcripts nor the infectivity of the rescued virus. Similarly, efficient recovery of infectious virus from the in vitro transcripts containing the G9230A (G - E) point mutation in the 3CLP was obtained. The two mutant viruses are genetically stable and show similar growth properties with the wild type recombinant virus. Even though the two mutations are located in or near the catalytic centers of the two viral proteinases, the mutations did not alter their enzymatic activities. This relatively high degree of tolerance to mutations in non-essential regions of important functional proteins would minimize the occurrence of lethal mutations during the replication cycles of RNA viruses and increase the adaptability of these viruses to a changed environment. However, a G–C point mutation at nucleotide position 15526 was found to be lethal to the infectivity of IBV on Vero cells. When the in vitro-synthesized full-length transcripts containing this mutation were introduced into Vero cells, no infectious virus was rescued. Upon correction of the mutation, infectious virus was recovered.

4.3 Severe Phenotypic Defect in Subgenomic RNA Transcription and the Infectivity of IBV Caused by a Point Mutation R132P in the Helicase Domain of IBV

4.3.1 Overview of the property of coronaviral and other nidoviral helicase in function activity and gene organization

Coronaviral and other nidoviral helicase domains are unique among the known positive-stranded RNA virus homologs in that they are linked in a single protein to an N-terminal binuclear zinc-binding domain consisting of 12 conserved Cys/His residues (Gorbalenya et al. 1989; Heusipp et al, 1997) (Fig.4.1). The zinc-binding domain of the arterivirus nsp10 helicase was shown previously to be involved in diverse processes of the viral life cycle, such as genome replication, mRNA transcription, and virion biogenesis (van Dinten et al, 2000). Nidovirus helicases also differ from other positive-stranded RNA viral helicases in that they occupy a position in the viral polyprotein downstream of the RNA-dependent RNA polymerase (RdRp). This arrangement is unique among positive-stranded RNA viruses, in which the helicase protein generally precedes the RdRp in the viral polyprotein (Koonin et al, 1993).

Also, biochemical data revealed functional differences between the nidovirus (Bautista et al, 2002; Seybert et al, 2000) and the well-characterized superfamily 2

helicases of pesti- and flaviviruses, supporting the idea that coronavirus (and nidovirus) helicases serve functions in the viral life cycle that are distinct from those of other RNA viral helicases. Multiple enzymatic activities have been assigned to the Nsp13 helicase protein now. These include RNA and DNA duplex-unwinding activities, NTPase and dNTPase activities, and an RNA 5triphosphatase activity that might be involved in the formation of the 5′ -cap structure of viral RNAs (Ivanov et al., 2004).

The protein is comprised of two domains: a putative N-terminal zinc binding domain, which spans the N terminal region of the protein from approximately amino acids 1 to 77, and a C-terminal helicase domain covering the C-terminal part of the protein from amino acids 279 to the C terminal end (Ivanov et al., 2004) (Fig.4.1). A Ser - Pro substitution located immediately downstream of the putative zinc binding domain of Nsp10, the equivalent RNA helicase protein in equine arteritis virus (EAV), caused defect in subgenomic mRNA transcription (van Dinten et al., 1997, 2000). More detailed analysis of the zinc binding domain of Nsp10 from EAV and Nsp13 from human coronavirus 229E by mutagenesis studies showed that this domain could modulate the enzymatic activities of the helicase domain (Seybert et al., 2005). Through this regulatory role and some yet to be discovered mechanisms, the zinc binding domain is shown to be critically involved in the replication and transcription of coronavirus RNA.

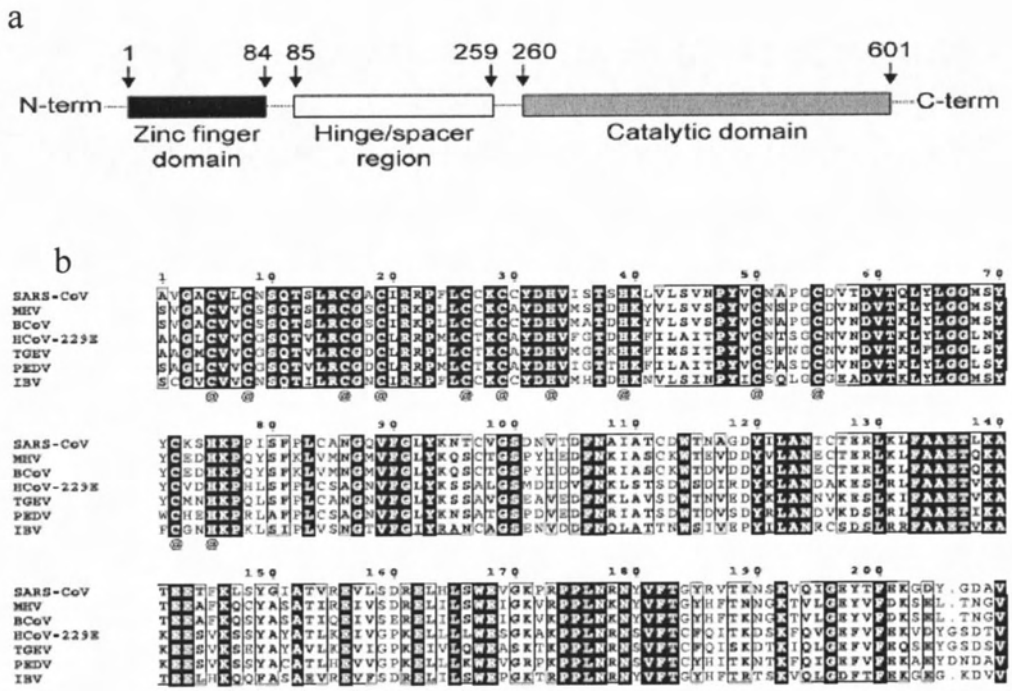

Fig.4.1 Sequence comparison of the region between amino acids 1 and 210 of helicase proteins from seven different coronaviruses. (Konstantin A. Ivanov et al., 2004). (**a**) The diagram shows the two domains of IBV nsp13: the N-terminal zinc finger domain and the C-terminal catalytic domain. (**b**) The nsp13 sequences of SARS-CoV (isolate Frankfurt 1; accession no. AY291315), mouse hepatitis virus (MHV, strain A59; NC_001846), bovine coronavirus (BCoV, isolate LUN; AF391542), human coronavirus 229E (HCoV-229E; X69721), porcine epidemic diarrhea virus (PEDV, strain CV777; AF353511); transmissible gastroenteritis virus (TGEV, strain Purdue 46; AJ271965), and avian infectious peritonitis virus (IBV, strain Beaudette; M95169) were derived from the replicative polyproteins of these viruses, whose sequences were obtained from the DDBJ, EMBL, and GenBank databases. Near the N terminus, the 12 conserved Cys and His residues predicted to form a binuclear zinc-binding cluster (77) are indicated by @.

4.3.2 Subgenomic RNA Transcription and the infectivity of IBV abolished severely by a point mutation R132P in the helicase domain of IBV

In the process of developing an infectious IBV clone from a Vero cell-adapted IBV Beaudette strain using the approach mentioned above, a G - C point mutation at nucleotide position 15,526 was found to be totally defective in subgenomic RNA transcription, a phenotype similar to, but appears to be much more severe than, the Ser - Pro mutation in EAV (van Dinten et al., 1997, 2000). Mutation of the Arg132 residue to a positively charged amino acid (Lys) does not affect the infectivity of the in vitro-synthesized transcripts as well as the growth properties of the rescued virus. However, mutation of the Arg132 residue to Leu, a conserved residue at the same position in most of other known coronaviruses, impaired the recovery rate of the in vitro synthesized transcripts. The recovered mutant virus showed much smaller-sized plaques. The R132 residue is located 57 amino acids downstream of the last His (H75) residue in the putative zinc binding domain (Fig.3.7a) and 147 amino acids upstream of the helicase motif 1 (Seybert et al., 2005). So far, no functional domain has been found in this region of the helicase protein.

4.3.3 Possible explanation for severe phenotypic defect in subgenomic RNA transcription and infectivity of IBC caused by the R132P substitution

Why the R132P substitution, located outside of the two functional domains of the helicase protein, shows severe phenotypic defect in subgenomic RNA transcription and the infectivity of IBV is not clear at the moment. Three possibilities were considered.

First, R132 may be part of the N-terminal zinc binding domain. As no studies have been attempted to define the boundary of the two domains, it is not even certain that an independent domain with unique function may exist in this region. R132P mutant virus shares certain phenotypic similarity to the Ser - Pro mutant EAV, such as the absence of subgenomic mRNA transcription (van Dinten et al., 1997, 2000), suggesting that the two mutations might disrupt a similar function of the helicase protein. However, as biochemical characterization of the effect of R132P mutation on the enzymatic activities of IBV Nsp13 helicase protein is currently lacking, it would be difficult to draw a conclusion that the two mutants share mechanistically similar characteristics.

Second, R132 is located in a region with a high degree of amino acid conservation in all known coronaviruses. Since the main defect of R132P mutant virus is in the subgenomic RNA transcription, one possibility is that this region may be involved

in the subgenomic RNA synthesis by interacting with host or other viral functional proteins. Alternatively, as a positively charged amino acid is required to maintain the full function of the protein, it would be possible that this region may be involved in binding of the helicase protein to viral RNA during RNA replication and transcription.

Finally, mutation to a Pro would lead to the disruption of the three dimensional structures of the two domains. Biochemical characterization of the involvement of this region in the enzymatic activities of the protein and determination of its three dimensional structures are underway to address these possibilities.

4.4 Functional Analysis of the IBV Nsp9 Protein in Viral Replication and Infectivity

The crystal structure of SARS-CoV nsp9 is shown that this protein is dimeric and has nucleic acid-binding activity. The RNA binding activity of nsp9 is not strongly RNA sequence specific and is through the wrapping of ssRNA around the nsp9 dimer (Egloff et al., 2004). Analysis of the sequence conservation across known coronaviruses reveals that the N and C terminal region of the protein are more conserved than the central core region, and the two key glycines (Gly100 and Gly 104) are strictly conserved. Structurally, residue G98 in IBV nsp9 corresponds to the G100 residue in the SARS-CoV nsp9 protein (Fig.3.11) and is strictly conserved across the whole family of coronaviruses (Geoff et al., 2004).

In this study, systematic mutagenesis of nsp9 was carried out based on recent structural studies to study the functional roles of this protein in coronavirus RNA replication and infectivity.

4.4.1 Destabilization of IBV nsp9 homodimer by introducing a point mutation into the C-terminal region of nsp9

The results from this study showed that formation of stable nsp9 homodimer is essential for its functionality in coronavirus RNA replication and transcription. Substitution of a conserved G98 residue in the C-terminal α-helix with a negatively charged amino acid (Asp) greatly destabilized the IBV nsp9 homodimer and abolished the RNA-binding activity of the protein. Consequently, introduction of the same mutation into the infectious IBV clone system showed that the mutation abolished the transcription of subgenomic RNA and no infectious virus could be rescued. Interestingly, mutation of a semi-conserved Ile (I95) residue in the same region showed minimal effect on the RNA-binding activity of the protein and moderately destabilizing effect on the homodimer. Introduction of this mutation into the IBV infectious clone system showed the recovery of a mutant virus with severe growth defects, supporting that dimerization is critical for the function of this replicase protein.

In previous structural studies, the topology of nsp9 protein was shown to most closely resemble the domains of the 3C-like proteinase ($3CL^{pro}$) which belongs to

the serine proteinase superfamily (Berman et al., 2000). Structure alignments revealed that it best matches to the domain II of the coronavirus $3CL^{pro}$ and subdomian I of the picornaviral $3C^{pro}$, suggesting that the two groups of proteins may share certain evolutionary relationship and may play some regulatory functions (Sutton et al., 2004). The direct correction of the RNA replicability and infectivity of IBV with the stability of the nsp9 homodimer confirms that dimer is the functional form of the protein. Interestingly, the functionally active unit of the coronavirus $3CL^{pro}$ is also a dimeric form of the protein (Anand et al., 2004).

4.4.2 RNA binding activity of nsp9 was disrupted by introduced point mutations into the domain within the IBV nsp9

Positive stranded RNA viruses replicate in the cytoplasm of infected cells and encode viral RNA binding proteins. RNA binding proteins play a key role in post-transcriptional regulation, participating in splicing, mRNA transport and localization, mRNA stability and translation. They present a wide array of promising targets for anti-viral therapeutics.

It is intriguing that mutation of the G98 residue to an Asp totally blocks the dimerization and RNA-binding activity of the protein. As the RNA-binding assay used in this study involves binding of RNA probes to the denatured, momomeric form of the nsp9 protein, it is quite unlikely that the loss of RNA-binding activity for this mutant is the direct consequence of destabilization of the nsp9 homodimer

by this point mutation. One possibility is that the C-terminal domain is directly involved in the binding of RNA. Alternatively, this point mutation may alter the overall folding of the protein. To rule out this possibility, the purified G98D and several other mutant proteins were examined by circular dichroism, showing similar spectra for these mutant proteins (data not shown).

Nsp9 protein is a nucleic acid-binding protein. The structural characteristics of nsp9 suggested that its nucleic acid-binding activity is not strictly sequence-specific (Egloff, et al., 2004; Sutton et al., 2004). The nsp9 protein may bind RNA through wrapping of the ssRNA around the nsp9 dimer (Egloff, et al., 2004; Sutton et al., 2004). In this study, we show that mutations of some positively charged residues in the β-barrel regions could significantly reduce the RNA-binding activity of the protein. However, introduction of the same mutations into the viral genome showed only mild or moderate effects on the growth and infectivity of the rescued mutant viruses, though positive correlation between the lowered binding activity and the reduced infectivity of the mutant viruses was observed. It seems that mutations that destabilized the nsp9 homodimer render more profound effect on IBV infectivity than mutations that reduced the RNA-binding activity of the protein per se. We are currently uncertain if this may reflect the limitation of the assay used to analyze the RNA-binding activity of the protein in the study. On the other hand, it would suggest that formation of the nsp9 homodimer may play functions not directly related to the RNA-binding activity of the protein.

One possibility is that dimerization of the protein may facilitate its interaction with other viral replicase proteins or host cell proteins involved in the viral replication cycle.

Nsp9 is a putative component of the replication complex. In cells infected with MHV, nsp9 is localized in the perinuclear region together with other proteins of the replication complex (Bost et al., 1999). RdRp was shown to coimmunoprecipitate with $3CL^{pro}$, nsp8 and nsp9 (Brockway et al., 2003). Biophysical evidence has also been presented for an interaction between nsp9 and nsp8 of MHV (Sutton et al., 2004). Interaction between other replicase proteins was also documented. For example, a co-crystal structure of SARS-CoV nsp7 with nsp8 revealed a complex of eight monomers of each protein forming a hollow cylindrical structure. This hexadecameric assembly was proposed to be able to encircle an RNA template, possibly acting as a processivity factor for the RNA polymerase (Zhai et al., 2005). Structural analysis indicated that nsp9 may play multiple roles in coronavirus replication cycle, and its interaction with other proteins may be essential for the formation of the viral replication complex together with its ability to interact with RNA (Egloff, et al., 2004; Sutton et al., 2004). However, we were unable to demonstrate direct interaction between IBV nsp9 and the two putative essential components of the replication complex, RdRp and RNA helicase in the overexpression system. It suggests that formation of the replication complex may involve other viral and host cell components, including

the viral RNA template. Further study would be required to address this interesting issue.

4.4.3 Disruption of subgenomic RNA transcription caused by mutant nsp9 G98D

According to our data, G98D abolished the transcription of subgenomic RNA and severely affects recombinant virus recovery. Introduction a mutation of Tyr (Y87) residue which had same effect as G98D in recombinant recovery in the same region, this mutant Y87A destroyed the transcription of subgenomic RNA, supporting that this repliase protein involved in the viral replication cycle.

4.4.4 Involvement of Nsp9 in viral replication is not through direct interaction with RDRP and helicase

Nsp9 is a putative component of the replication complex. In cells infected MHV, nsp9 is localized in the perinuclear region together with other proteins of the replication complex (Bost et al., 1999). RDRP was shown to coimmunoprecipitate with $3CL^{pro}$, nsp8 and nsp9 (Brockway et al., 2003). Biophysical evidence has also been presented for an interaction between nsp9 and nsp8 of MHV (Sutton et al., 2004). For example, a co-crystal structure of SARS-CoV nsp7 with nsp8 revealed a complex of eight monomers of each protein forming a hollow

cylindrical structure. This hexadecameric assembly was proposed to be able to encircle an RNA template, possibly acting as a processivity factor for the RNA polymerase (Zhai et al., 2005).

Structural analysis indicated that nsp9 may play multiple roles in coronavirus replication cycle, and its interaction with other proteins may be essential for the formation of the viral replication complex together with its ability to interact with RNA (Egloff et al., 2004; Sutton et al., 2004). In this study, two experiments were performed to test the possibility of the interaction between nsp9 and two viral proteins which involve in viral replication cycle. However, we were unable to demonstrate direct interaction between IBV nsp9 and the two putative essential components of the replication complex, RdRp and RNA helicase in the overexpression system. It suggests that formation of the replication complex may involve other viral and host cell components, including the viral RNA template. Further study would be required to address this interesting issue.

4.5 Future Direction

Future studies will focus on the following four aspects:

1. The precise function of nsp9 in the replication cycle of coronavirus

a. Interaction of nsp9 with other viral components in the replication complex

Nsp9 is a putative component of the viral replication complex. Biophysical evidence has also been presented for an interaction between nsp9 and nsp8 (Geoff et al., 2004). The MHV nsp9 is most prominent in discrete foci in the perinuclear region of infected cells and colocalises with other proteins, such as, 3C-like protein (3CLpro), N, nsp7, nsp8, and nsp13 that are the components of the viral replication complex (Bost et al., 2000), suggesting its involvement (directly or indirectly) in viral RNA metabolism. In this study we were unable to demonstrate direct interaction of IBV nsp9 and with two essential components of the replication complex, RdRp and RNA helicase in the overexpression system. Whether IBV nsp9 may be complemented with other viral proteins is still an open question. We will further investigate this issue using co-immunoprecipitation and immunoflurescent staining.

b. Interaction of nsp9 with host proteins.

Structural analysis indicated that nsp9 may play multiple roles in coronavirus replication cycle, and its interaction with other proteins may be essential for the formation of the viral replication complex together with its ability to interact with RNA. The possibility that proteins may be involve in formation of replication complex together with nsp9 were be investigated by yeast-two hybrid and other screening methods.

2. Analysis of the biological functions and biochemical properties of IBV nsp9 by more systematic mutagenesis studies

Based on recently structural studies, functional and biochemical importance of some individual residues in the dimerization and RNA binding of nsp9 had investigated in this thesis study. Other conserved residues in all CoV nsp9 proteins, such as: Phe 73, Arg 97, Val 100, Gly 102, Gln 111 etc, may be also able to bind the phosphate backbone to the protein surface (Marie-Pierre., et al., 2004). These individual residues will be studied by systematic mutagenesis to further confirm the importance of individual residues in the dimerizaion and RNA binding activity of IBV nsp9 protein using gel filtration, gel-shift assay, RNA binding assay, and co-immunoprecipitation etc.

3. Relationship between RNA-binding activity and dimerizaion of nsp9

The results in this thesis study showed that formation of stable nsp9 homodimer is essential for its functionality in coronavirus RNA replication and transcription. However, we are unable to confirm whether the formation of the nsp9 homodimer may play functions not directly related to the RNA-binding activity of the protein. This issue will be further investigated through gel-shift assay to confirm the exact relationship between RNA-binding activity and dimerizaion of IBV nsp9.

4. Functional characterization of the R123 mutation in the helicase

In this study, R123 mutation of helicase protein was found to be lethal to the infectivity of the in vitro-synthesized full-length transcripts on Vero cells and demonstrated that a domain with previously unassigned function within helicase protein may play an essential role in coronavirus replication. We are unable to demonstrate that the detrimental effect of mutation R123 on viral replication is due to reduction of the RNA helicase activity directly or other biochemical properties of the protein. In addition, nsp13 of coronavirus contains multiple activities, such as: RNA and DNA duplex-unwinding activities, NTPase and dNTPase activities which probably provide the energy for its translocation along RNA templates, and an RNA 5′-triphosphatase activity that might be involved in the formation of the 5′-cap structure of viral RNAs (Ivanov et al., 2004a). However, R123 mutation which affects viral replication does not locate within the two functional domains of the helicase protein. The precise function of helicase protein damaged by this mutation will be explored in the future.

REFERENCES

Alexander, O. P., Willy, J. M., Spaan., and Eric J. S. (2006) Nidovirus transcription: how to make sense...? *J.Gen Virol.* **87**: 1403–1421.

Almazan, F., Galan, C., and Enjuanes, L. (2004) The nucleoprotein is required for efficient coronavirus genome replication. *J. Virol.* **78**:12683–12688.

Anand, K., Palm, G. J., Mesters, J. R., Siddell, S. G., Ziebuhr, J., and Hilgenfeld, R. (2002) Structure of coronavirus main proteinase reveals combination of a chymotrypsin fold with an extra alpha-helical domain. *EMBO J.* **21**: 3213–3224.

Anand K, Ziebuhr J, Wadhwani P, Mesters JR, and Hilgenfeld R. (2003) Coronavirus main proteinase (3CLpro) structure: basis for design of anti-SARS drugs. Science. 300(5626):1763-1767.

Arbely, E., Khattari, Z., Brotons, G., Akkawi, M., Salditt, T., and Arkin, I.T. (2004) A highly unusual palindromic transmembrane helical hairpin formed by SARS coronavirus E protein. *J. Mol. Biol.* **341**: 769–779.

Baric, R. S., and Sims, A. C. (2005) Development of mouse hepatitis virus and SARS-CoV infectious cDNA constructs. *Curr. Top. Microbiol. Immunol.* **287**: 229–252.

Baric, R. S., and Yount, B. (2000) Subgenomic negative-strand RNA function during mouse hepatitis virus infection. *J. Virol.* **74**: 4039–4046.

Baric, R. S., Nelson, G. W., Fleming, J. O., Deans, R. J., Keck, J. G., Casteel, N., and Stohlman, S. A. (1988) Interactions between coronavirus nucleocapsid protein and viral RNAs: implications for viral transcription. *J. Virol.* **62**: 4280–4287.

Baric. R S., Shieh, C.-K., Stohlman, S. A., and Lai, M. M. C. (1987) Analysis of intracellular small RNAs of mouse hepatitis virus: Evidence for discontinuous transcription. *Virol.* **156**: 342-354.

Bartenschlager, R., and Lohmann, V. (2000) Replication of hepatitis C virus. *J Gen Virol.* **81**: 1631-1648.

Bautista, E. M., Faaberg, K. S., Mickelson, D., and McGruder, E. D. (2002) Functional properties of the predicted helicase of porcine reproductive and respiratory syndrome virus. *Virol.* **298**: 258–270.

Berman, H.M., Westbrook, J., Feng, Z., Gilliland, G., Bhat, T.N., Weissig, H., Shindyalov, I.N., and Bourne, P.E. (2000). The Protein Data Bank. Nucleic Acids Res. 28, 235–242.

Borowski, P., Mueller, O., Niebuhr, A., Kalitzky, M., Hwang, L. H., Schmitz, H., Siwecka, M. A., and Kulikowsk, T. (2000) ATP-binding domain of NTPase/helicase as a target for hepatitis C antiviral therapy. *Acta Biochim Pol.* **47**: 173-180.

Bos, E. C. W., Luytjes, W., van der Meulen, H., Koerten, H. K., and Spaan, W. J. M. (1996) The production of recombinant infectious DI-particles of a murine coronavirus in the absence of helper virus. *Virol.* **218**: 52–60.

Bosch, B. J., Martina, B. E., Van Der Zee, R., Lepault, J., Haijema, B. J., Versluis, C., Heck, A. J., De Groot, R., Osterhaus, A. D., and Rottier, P. J. (2004) Severe acute respiratory syndrome coronavirus (SARS-CoV) infection inhibition using spike protein heptad repeat-derived peptides. *PNAS.* **101**: 8455–8460.

Bost, A.G., Carnahan, R.H., Tao Lu, X., and Denison, M.R. (1999) Four proteins processed from the replicase gene polyprotein of mouse hepatitis virus colocalize in the cell periphery and adjacent to sites of virion assembly. *J. Virol.* **74**: 3379–3387.

Boursnell, M., Binns, M. M., Brown, T., Cavanagh, D., and Tomley, F. M. (1989) Molecular biology of avian infectious bronchitis virus. *Karger, New York.*

Boursnell, M.E.G., Brown, T.D.K., Foulds, I.J., Green, P.F., Tomley, F.M., and Binns, M.M. (1987) Completion of the sequence of the genome of the coronavirus avian infectious bronchitis virus. *J. Gen. Virol.* **68**: 57–77.

Bradburne, A.F. (1970) Antigenic relationships amongst coronaviruses. *Arhiv fur die gesamte Virus forschung.* **31**: 352 – 364.

Brockway, S. M., and Denison, M. R. (2005) Mutagenesis of the murine hepatitis virus nsp1-coding region identifies residues important for protein processing, viral RNA synthesis, and viral replication. *Virol.* **340**: 209–223.

Brown, T.D.K., and Brierly, I. (1995) The coronavirus nonstructural proteins. In: Siddell, S.G. (Ed.), The Coronaviridae. *Plenum Press, New York, NY.* 191–217.

Casais, R., Dove, B., Cavanagh, D., and Britton, P. (2003) A recombinant avian infectious bronchitis virus expressing a heterologous spike gene demonstrates that the spike protein is a determinant of cell tropism. *J. Virol.* **77**: 9084 – 9089.

Casais, R., Davies, M., Cavanagh, D., and Britton, P. (2005) Gene 5 of the avian coronavirus infectious bronchitis virus is not essential for replication. *J. Virol.* **79**: 8065–8078.

Casais, R., Thiel, V., Siddell, S., Cavanagh, D., and Britton, P. (2001) A reverse genetics system for the avian coronavirus infectious bronchitis virus. *J. Virol.* **75**: 12359 – 12369.

Casais, R., Thiel, V., Siddell, S.G., Cavanagh, D., and Britton, P. (2001) Reverse genetics system for the avian coronavirus infectious bronchitis virus. *J. Virol.* **75**: 12359–12369.

Cavanagh, D. (2005) Coronaviridae: a review of coronaviruses and toroviruses, in: Schmidt A., Wolff M.H. (Eds.), Coronaviruses with special emphasis on first insights concerning SARS, *Basel, Birkhäuser.* 1–54.

Cavanagh, D. (1995) In "The Coronaviridae" *Plenum, New York.* 73–113.

Cavanagh, D. (2001) cis-acting sequences required for coronavirus infectious bronchitis virus defective-RNA replication and packaging. *J. Virol.* **75**:125–133.

Cavanagh, D. (2005) Coronaviruses in poultry and other birds. *Avian Pathol.* **34 (6)**: 439-448.

Cavanagh, D. (2003) Severe acute respiratory syndrome vaccine development: experiences of vaccination against avian infectious bronchitis coronavirus. *Avian Pathol.* **32 (6)**: 567–582.

Cavanagh, D., and Davis, P. J. (1988) Evolution of avian coronavirus IBV: Sequence of the matrix glycoprotein gene and intergenic region of several serotypes. *J. Gen. Virol.* **69**: 621–629.

Cavanagh, D., Davis, P. J., and Cook, J. K. A. (1992) Infectious bronchitis virus: Evidence for recombination within the Massachusetts serotype. *Avian Pathol.* **21**: 401–408.

Cavanagh, D., Davis, P. J., Pappin, D. J., Binns, M. M., Boursnell, M. E., and Brown, T. D. (1986b) Coronavirus IBV: Partial amino terminal sequencing of spike polypeptide S2 identifies the sequence Arg-Arg-Phe-Arg-Arg at the cleavage site of the spike precursor propolypeptide of IBV strains Beaudette and M41. *Virus Res.* **4**: 133–143.

Chaigne, B., Escriou, N., van der Werf, S., and Yuen, K.-Y. (2005) Differential maturation and subcellular localization of severe acute respiratory syndrome coronavirus surface proteins S, M and E. *J. Gen. Virol.* **86**: 1423–1434.

Chang, M.S., Lu, Y.T., Ho, S.T., Wu, C.C., Wei, T.Y., Chen, C.J., Hsu, Y.T., Chu, P.C., Chen, C.H., Chu, J.M., Jan, Y.L., Hung, C.C., Fan, C.C., and Yang, Y.C. (2004) Antibody detection of SARS-CoV spike and nucleocapsid protein. *Biochem. Biophys. Res. Commun.* **314**: 931–936

Chang, R.-Y., Hofmann, M. A., Sethna, P. B., and Brian, D. A. (1994) A cis-acting function for the coronavirus leader in defective interfering RNA replication. *J. Virol.* **68**: 8223–8231.

Chang, R.-Y., Krishnan, R., and Brian, D. A. (1996) The UCUAAAC promoter motif is not required for high-frequency leader recombination in bovine coronavirus defective interfering RNA. *J. Virol.* **70**: 2720–2729.

Chang, C. K., Sue, S. C., Yu, T. H., Hsieh, C. M., Tsai, C. K., Chiang, Y. C., Lee, S. J., Hsiao, H. H., Wu, W. J., and Chang, C. F. et al. (2005) The dimer interface of the SARS coronavirus nucleocapsid protein adapts a porcine respiratory and reproductive syndrome virus-like structure. *FEBS Lett.* **579**: 5663–5668.

Chang, R. Y. and Brian, D. A. (1996) cis-Requirement for N-specific protein sequence in bovine coronavirus defective interfering RNA replication. *J. Virol.* **70**: 2201–2207.

Charley, B., and Laude, H. (1988) Induction of alpha interferon by transmissible gastroenteritis coronavirus: Role of transmembrane glycoprotein E1. *J. Virol.* **62**: 8–11.

Chen, H., Gill, A., Dove, B. K., Emmett, S. R., Kemp, C. F., Ritchie, M. A., Dee, M., and Hiscox, J. A. (2005) Mass spectroscopic characterization of the coronavirus infectious bronchitis virus nucleoprotein and elucidation of the role of phosphorylation in RNA binding by using surface plasmon resonance. *J. Virol.* **79**: 1164–1179.

Chen, Y. Y., Shuang, B., Tan, Y. X., Meng, M. J., Han, P., Mo, X. ., Song, Q. S., Qiu, X. Y., Luo, X., Gan, Q. N., Zhang, X., Zheng, Y., Liu, S. A., Wang, X. N., Zhong, N. S., and Ma, D. L. (2005) The protein X4 of severe acute respiratory syndrome-associated coronavirus is expressed on both virusinfected cells and lung tissue of severe acute respiratory syndrome patients and inhibits growth of Balb/c 3T3 cell line. *Chin. Med. J.* **118**: 267–274.

Collins, A. R., Knobler, R. L., Powell, H., and Buchmeier, M. J. (1982) Monoclonal antibodies to murine hepatitis virus-4 (strain JHM) define the viral glycoprotein responsible for attachment and cell–cell fusion. *Virol.* **119**: 358–371.

Cologna, R., and Hogue, B. G. (2000) Identification of a bovine coronavirus packaging signal. *J. Virol.* **74**: 580–583.

Cologna, R., Spagnolo, J. F., and Hogue, B. G. (2000) Identification of nucleocapsid binding sites within coronavirus-defective genomes. *Virol.* **277**: 235–249.

Corse, E. and Machamer, C.E. (2000) Infectious bronchitis virus E protein is targeted to the Golgi complex and directs release of virus-like particles. *J. Virol.* **74**: 4319–4326.

Corse, E. and Machamer, C.E. (2003) The cytoplasmic tails of infectious bronchitis virus E and M proteins mediate their interaction. *Virol.* **312**: 25–34.

Cowley, J. A., Dimmock, C. M., Spann, K. M., and Walker, P. J. (2000) Gill-associated virus of Penaeus monodon prawns: An invertebrate virus with ORF1a and ORF1b genes related to arteri- and coronaviruses. *J. Gen. Virol.* **81**: 1473–1484.

Dalton, K., Casais, R., Shaw, K., Stirrups, K., Evans, S., Britton, P., Brown, T. D. K., and Cavanagh, D. (2001) cis-acting sequences required for coronavirus infectious bronchitis virus defective-RNA replication and packaging. *J. Virol.* **75**: 125–133.

de Haan, C. A. M., de Wit, M., Kuo, L., Montalto-Morrison, C., Haagmans, B. L., Weiss, S. R., Masters, P. S., and Rottier, P. J. M. (2003a) The glycosylation status of the murine hepatitis coronavirus M protein affects the interferogenic

capacity of the virus in vitro and its ability to replicate in the liver but not the brain. *Virol.* **312**: 395–406.

de Haan, C. A., and Rottier, P. J. (2005) Molecular interactions in the assembly of coronaviruses. *Adv Virus Res.* **64**: 165– 230.

de Haan, C. A., Masters, P. S., Shen, X., Weiss, S. and Rottier, P. J. (2002) The group specific murine coronavirus genes are not essential, but their deletion, by reverse genetics, is attenuating in the natural host. *Virol.* **296**: 177–189.

Delmas, B., Gelfi, J., L'Haridon, R., Vogel, L. K., Sjostrom, H., Noren, O., and Laude, H. (1992) Aminopeptidase N is a major receptor for the entero-pathogenic coronavirus TGEV. *Nature* **357** (6377): 417-420.

Delmas, B., and Laude, H. (1990) Assembly of coronavirus spike protein into trimers and its role in epitope expression. *J. Virol.* **64**: 5367–5375.

den Boon, J. A., Snijder, E. J., Locker, J. K., Horzinek, M. C., and Rottier, P. J. M. (1991) Another triple-spanning envelope protein among intracellularly budding RNAviruses: The torovirus E protein. *Virol.* **182**: 655–663.

Dhar, A. K., Cowley, J. A., Hasson, K.W., and Walker, P. J. (2004) Genomic organization, biology, and diagnosis of Taura syndrome virus and yellowhead virus of penaeid shrimp. *Adv. Virus Res.* **63**: 353–421.

Egloff, M. P., Ferron, F., Campanacci, V., Longhi, S., Rancurel, C., Dutartre, H., Snijder, E. J., Gorbalenya, A. E., Cambillau, C., and Canard, B. (2004) The severe acute respiratory syndrome-coronavirus replicative protein nsp9 is a single-stranded RNA-binding subunit unique in the RNA virus world. *PNAS.* **101**: 3792–3796.

Eleouet, J. F., Slee, E. A., Saurini, F., Castagne, N., Poncet, D., Garrido, C., Solary, E. and Martin, S. J. (2000) The viral nucleocapsid protein of transmissible gastroenteritis coronavirus (TGEV) is cleaved by caspase-6 and -7 during TGEV-induced apoptosis. *J. Virol.* **74**: 3975–3983.

Enjuanes, L., Sola, I., Alonso, S., Escors, D., and Zuniga, S. (2005) Coronavirus reverse genetics and development of vectors for gene expression. *Curr. Top. Microbiol. Immunol.* **287**: 161–197.

Enjuanes, L., Spaan, W., Snijder, E., and Cavanagh, D. (2000a) Nidovirales. In "Virus Taxonomy. Seventh Report of the International Committee on Taxonomy of Viruses" (Murphy, F. A., Fauquet, C. M., Bishop, D. H. L., Ghabrial, S. A., Jarvis, A. W., Martelli, G. P., Mayo, M. A., and Summers, M. D., eds.) *Academic Press, New York.* 827–834.

Fang, X., Ye, L., Timani, K. A., Li, S., Zen, Y., Zhao, M., Zheng, H., and Wu Z. (2005) Peptide domain involved in the interaction between membrane protein and nucleocapsid protein of SARS -associated coronavirus. *J Biochem Mol Biol.* **38 (4)**: 381-385.

Farsang, A., Ros, C., Renstrom, L. H., Baule, C., Soos, T., and Belak, S. (2002) Molecular epizootiology of infectious bronchitis virus in Sweden indicating the involvement of a vaccine strain. *Avian Pathol.* **31 (3)**: 229–236.

Fielding, B. C, Gunalan, V., Tan, T. H., Chou, C. F., Shen, S., Khan, S., Lim, S.G., Hong, W., and Tan, Y. J. (2006) Severe acute respiratory syndrome coronavirus protein 7a interacts with hSGT. *Biochem Biophys Res Commun.* **343 (4)**: 1201-1208.

Garwes, D. J., Bountiff, L., Millson, G. C., and Elleman, C. J. (1984) Defective replication of porcine transmissible gastroenteritis virus in a continuous cell line. *Adv. Exp. Med. Biol.* **173**: 79–93.

Gorbalenya, A. E., Koonin, E. V., Donchenko, A. P., and Blinov, V. M. (1989) Coronavirus genome: prediction of putative functional domains in the nonstructural polyprotein by comparative amino acid sequence analysis. *Nucleic Acids Res.* **17**: 4847–4861.

Goldsmith, C. S., Tatti, K. M., Ksiazek, T. G., Rollin, P. E., Comer, J. A., Lee, W. W., Rota, P. A., Bankamp, B., Bellini, W. J., and Zaki, S. R. (2004) Ultrastructural characterization of SARS coronavirus. *Emerg. Infect. Dis.* **10**: 320–326.

Gonzalez, M. E., and Carrasco, L. (2003) Viroporins. *FEBS Lett.* **552**: 28–34.

Gosert, R., Kanjanahaluethai, A., Egger, D., Bienz, K., and Baker, S. C. (2002). RNA replication of mouse hepatitis virus takes place at double-membrane vesicles. *J. Virol.* 76:3697–3708.

Graham, R. L., Sims, A. C., Brockway, S. M., Baric, R. S., and Denison, M. R. (2005) The nsp2 replicase proteins of murine hepatitis virus and severe acute

respiratory syndrome coronavirus are dispensable for viral replication. *J. Virol.* **79**: 13399–13411.

Guy, J. S., Breslin, J. J., Breuhaus, B., Vivrette, S., and Smith, L. G. (2000) Characterization of a coronavirus isolated from a diarrheic foal. *J. Clin. Microbiol.* **38**: 4523–4526.

Haijema, B. J., Volders, H., and Rottier, P. J. M. (2003) Switching species tropism: An effective way to manipulate the feline coronavirus genome. *J. Virol.* **77**: 4528–4538.

Haijema, B. J., Volders, H., and Rottier, P. J. (2004) Live, attenuated coronavirus vaccines through the directed deletion of group-specific genes provide protection against feline infectious peritonitis. *J. Virol.* **78**: 3863 –/3871.

Hatta, M., and Kawaoka, Y. (2003) The NB protein of influenza B virus is not necessary for virus replication in vitro. *J. Virol.* **77**: 6050–6054.

He, R., Leeson, A., Ballantine, M., Andonov, A., Baker, L., Dobie, F., Li, Y., Bastien, N., Feldmann, H., Strocher, U., Theriault, S., Cutts, T., Cao, J., Booth, T. F., Plummer, F. A., Tyler, S., and Li, X. (2004) Characterization of protein-protein interactions between the nucleocapsid protein and membrane protein of the SARS coronavirus. *Virus Res.* **105 (2)**: 121-125.

He, R., Dobie, F., Ballantine, M., Leeson, A., Li, Y., Bastien, N., Cutts, T., Andonov, A., Cao, J., Booth, and T. F., et al. (2004) Analysis of multimerization of the SARS coronavirus nucleocapsid protein. *Biochem. Biophys. Res. Commun.* **316**: 476–483.

He, R., Leeson, A., Andonov, A., Li, Y., Bastien, N., Cao, J., Osiowy, C., Dobie, F., Cutts, T., Ballantine, M., and Li, X. (2003) Activation of AP-1 signal transduction pathway by SARS coronavirus nucleocapsid protein. *Biochem. Biophys. Res. Commun.* **311**: 870–876.

Heusipp, G., Harms, U., Siddell, S. G., and J. Ziebuhr. (1997) Identification of an ATPase activity associated with a 71-kilodalton polypeptide encoded in gene 1 of the human coronavirus 229E. *J. Virol.* **71**: 5631–5634.

Herrewegh, A. A., Smeenk, I., Horzinek, M. C., Rottier, P. J. M., and de Groot, R. J. (1998) Feline coronavirus type II strains 79–1683 and 79–1146 originate

from a double recombination between feline coronavirus type I and canine coronavirus. *J. Virol.* **72**: 4508–4514.

Hiscox, J. A. (2005) Mass spectroscopic characterization of the coronavirus infectious bronchitis virus nucleoprotein and elucidation of the role of phosphorylation in RNA binding by using surface plasmon resonance. *J. Virol.* **79**: 1164–1179.

Hiscox, J. A., Wurm, T., Wilson, L., Britton, P., Cavanagh, D., and Brooks, G. (2001) The coronavirus infectious bronchitis virus nucleoprotein localizes to the nucleolus. *J. Virol.* **75**: 506–512.

Ho, Y., Lin, P. H., Liu, C. Y., Lee, S. P., and Chao, Y.C. (2004) Assembly of human severe acute respiratory syndrome coronavirus- like particles. *Biochem. Biophys. Res. Commun.* **318**: 833–838.

Hodgson, T., Casais, R., Dove, B., Britton, P., and Cavanagh, D. (2004) Recombinant infectious bronchitis coronavirus Beaudette with the spike protein gene of the pathogenic M41 strain remains attenuated but induces protective immunity. *J. Virol.* **78**: 13804–13811.

Hsieh, P. K., Chang, S. C., Huang, C. C., Lee, T. T., Hsiao, C. W., and Kou, Y. H., et al. (2005) Assembly of severe acute respiratory syndrome coronavirus RNA packaging signal into virus-like particles is nucleocapsid dependent. *J Virol.* **79**: 13848–13855.

Huang, P., and Lai, M. M. C. (2001) Heterogeneous nuclear ribonucleoprotein A1 binds to the 3'-untranslated region and mediates potential 5'-3'-end cross talks of mouse hepatitis virus RNA. *J. Virol.* **75**: 5009–5017

Huang, Y., Yang, Z. Y., Kong, W. P., and Nabel, G. J. (2004a) Generation of synthetic severe acute respiratory syndrome coronavirus pseudoparticles: Implications for assembly and vaccine production. *J. Virol.* **78**: 12557–12565.

Fan, H., Amy, O., Yong, W. T., Wang, S., Fang, S. G., Liu, D. X., and Julien., L. (2005) The nucleocapsid protein of coronavirus infectious bronchitis virus: crystal structure of its N-terminal domain and multimerization properties. *Structure*. **13**: 1859-1868.

Hurst, K. R., Kuo, L., Koetzner, C. A., Ye, R., Hsue, B., and Masters, P. S. (2005) A major determinant for membrane protein interaction localizes to the

carboxy-terminal domain of the mouse coronavirus nucleocapsid protein. *J. Virol.* **79**: 13285–13297.

Imbert, I., Guillemot, J. C., Bourhis, J. M., Bussetta, C., Coutard, B., Egloff, M. P., Ferron, F., Gorbalenya, A. E., and Canard, B. (2006) A second, non-canonical RNA-dependent RNA polymerase in SARS coronavirus. *EMBO J.* **25**:4933-42.

Ito, N., Mossel, E. C., Narayanan, K., Popov, V. L., Huang, C., Inoue, T., Peters, C. J., and Makino, S. (2005) Severe acute respiratory syndrome coronavirus 3a protein is a viral structural protein. *J. Virol.* **79**: 3182–3186.

Ivanov, K. A., Hertzig, T., Rozanov, M., Bayer, S., Thiel, V., Gorbalenya, A. E., and Ziebuhr, J. (2004) Major genetic marker of nidoviruses encodes a replicative endoribonuclease. *PNAS.* **101**: 12694–12699.

Ivanov, K. A., Thiel, V., Dobbe, J. C., van der Meer, Y., Snijder, E. J., and Ziebuhr, J. (2004a) Multiple enzymatic activities associated with severe acute respiratory syndrome coronavirus helicase. *J. Virol.* **78**: 5619–5632.

Izeta, A., Smerdou, C., Alonso, S., Penzes, Z., Mendez, A., Plana-Duran, J., and Enjuanes, L. (1999) Replication and packaging of transmissible gastroenteritis coronavirus-derived synthetic minigenomes. *J. Virol.* **73**: 1535–1545.

Jackwood, M. W., Hilt, D. A., Boynton, T., and Callison, S. A. (2004) Molecular analysis of TCoV, SARS-CoV, and IBV: how are they related? In: *4th International Symposium on Avian Corona- and Pneumovirus Infections, Rauischholzhausen, Germany.* 158–165.

Jacobs, L., van der Zeijst, B. A., and Horzinek, M. C. (1986) Characterization and translation of transmissible gastroenteritis virus mRNAs. *J. Virol.* **57**: 1010–1015.

John, R. M. (2002) HeLa cells 50 years on: the good, the bad and the ugly. *Nature Reviews Cancer* **2**: 315-319

Joseph, J. S., Saikatendu, K. S., Subramanian, V., Neuman, B. W., Brooun, A., Griffith, M., Moy, K., Yadav, M. K., Velasquez, J., Buchmeier, M. J., Stevens, R. C., and Kuhn, P. (2006) Crystal structure of nonstructural protein 10 from the SARS coronavirus reveals a novel fold with two zinc-binding motifs. *J. Virol.* **80**: 7894–7901.

Kadare, G., and Haenni, A. L. (1997) Virus-encoded RNA helicases. *J Virol.* **71**: 2583-2590.

Kao, R. Y., *et al.* (2004) Identification of novel small-molecule inhibitors of severe acute respiratory syndromeassociated coronavirus by chemical genetics. *Chem Biol* **11**: 1293-1299.

Kapke, P. A., Tung, F. Y., Hogue, B. G., Brian, D. A., Woods, R. D., and Wesley, R. (1988) The amino-terminal signal peptide on the porcine transmissible gastroenteritis coronavirus matrix protein is not an absolute requirement for membrane translocation and glycosylation. *Virol.* **165**: 367–376.

Kim, J. L., Morgenstern, K. A., Griffith, J. P., Dwyer, M. D., Thomson, J. A., Murcko, M. A., Lin, C., and Caron, P. R. (1998) Hepatitis C virus NS3 RNA helicase domain with a bound oligonucleotide: the crystal structure provides insights into the mode of unwinding. *Structure* **6**: 89-100.

Kim, O. J., Lee, D. H., and Lee, C. H. (2006) Close relationship between SARS-coronavirus and group 2 coronavirus. *J. Microbiol.* **44**: 83–91.

Kim, Y.-N., Jeong, Y. S., and Makino, S. (1993) Analysis of cis-acting sequences essential for coronavirus defective interfering RNA replication. *Virol.* **197**: 53–63.

Klimkait, T., Strebel, K., Hoggan, M. D., Martin, M. A., and Orenstein, J. M. (1990) The human immunodeficiency virus type 1- specific protein vpu is required for efficient virus maturation and release. *J. Virol.* **64**: 621–629.

Koetzner, C. A., Parker, M. M., Ricard, C. S., Sturman, L. S., and Masters, P. S. (1992) Repair and mutagenesis of the genome of a deletion mutant of the coronavirus mouse hepatitis virus by targeted RNA recombination. *J. Virol.* **66**: 1841–1848.

Stadler, K. (2003) SARS — Beginning to understand a new virus. *Nat Rev Micorbiol.* **1**: 209-218.

Koonin, E. V., and Dolja, V. V. (1993) Evolution and taxonomy of positivestrand RNA viruses: implications of comparative analysis of amino acid sequences. *Crit. Rev. Biochem. Mol. Biol.* **28**: 375–430.

Kottier, S. A., Cavanagh, D., and Britton, P. (1995) Experimental evidence of recombination in coronavirus infectious bronchitis virus. *Virol.* **213**: 569–580.

Krijnse Locker, J., Rose, J. K., Horzinek, M. C., and Rottier, P. J. M. (1992b) Membrane assembly of the triple-spanning coronavirus M protein. Individual transmembrane domains show preferred orientation. *J. Biol. Chem.* **267**: 21911–21918.

Kuo, L., and Masters, P. S. (2002) Genetic evidence for a structural interaction between the carboxy termini of the membrane and nucleocapsid proteins of mouse hepatitis virus. *J Virol.* **76**: 4987-4999.

Kuo, L., and Masters, P. S. (2003) The small envelope protein E is not essential for murine coronavirus replication. *J Virol.* **77**: 4597–4608.

Kuo, L., Godeke, G. J., Raamsman, M. J., Masters, P. S., and Rottier, P. J. (2000) Retargeting of coronavirus by substitution of the spike glycoprotein ectodomain: crossing the host cell species barrier. *J. Virol.* **74**: 1393–1406.

Kusters, J. G., Jager, E. J., Niesters, H. G., and van der Zeijst, B. A. M. (1990) Sequence evidence for RNA recombination in field isolates of avian coronavirus infectious bronchitis virus. *Vaccine* **8**: 605–608.

Kwong, A. D., Kim, J. L. and Lin, C. (2000) The Hepatitis C Viruses. *Curr. Top. Microbiol. Imunol.* **242**: 171-196

Lai, M. M. C., and Cavanagh, D. (1997) The molecular biology of coronaviruses. *Adv. Virus Res.* **48**: 1–100.

Lai, M. M. C. (1998) Cellular factors in the transcription and replication of viral RNA genomes: a parallel to DNA-dependent RNA transcription. *Virol.* **244**: 1–12.

Lai, M. M. C. (1992) RNA recombination in animal and plant viruses. *Microbiol. Rev.* **56**: 61–79.

Lai, M. M. C., and K. V. Holmes. (2001) Coronaviridae: the viruses and their replication. In: Fields virology, 4th ed. Knipe, D. M., Howley, P. M., Griffin, D. E., Lamb, R. A., Martin, M. A., Roizman, B., and Straus, S. E., eds. Williams, L., and Wilkins. Philadelphia, PA. 1163–1185.

Lai, M. M. C., and Stohlman, S. A. (1978) RNA of mouse hepatitis virus. *J. Virol.* **26**: 236–242.

Lai, M. M. C., and Stohlman, S. A. (1981) Comparative analysis of RNA genomes of mouse hepatitis viruses. *J. Virol.* **38**: 661–670.

Laude, H., and Masters, P. S. (1995) In "The Coronaviridae" (S. G. Siddell, ed.), *Plenum, New York.* 141–163.

Laude, H., Gelfi, J., Lavenant, L., and Charley, B. (1992) Single amino acid changes in the viral glycoprotein M affect induction of alpha interferon by the coronavirus transmissible gastroenteritis virus. *J. Virol.* **66**: 743–749.

Laude, H., Rasschaert, D., and Huet, J. C. (1987) Sequence and N-terminal processing of the transmembrane protein E1 of the coronavirus transmissible gastroenteritis virus. *J. Gen. Virol.* **68**: 1687–1693.

Law, P. T., Wong, C. H., Au, T. C., Chuck, C. P., Kong, S. K., Chan, P. K., To, K. F., Lo, A. W., Chan, J. Y., Suen,Y. K., Chan, H. Y., Fung, K. P.,Waye, M. M., Sung, J. J., Lo, Y. M., and Tsui, S. K. (2005) The 3a protein of severe acute respiratory syndrome-associated coronavirus induces apoptosis in Vero E6 cells. *J. Gen. Virol.* **86**: 1921–1930.

Leigh, V. V., and Virginia, C. M. (1991) HeLa, a new microbial species. *Evolutionary Theory.* **10**: 71-74

Li, W., Moore, M. J., Vasilieva, N., Sui, J., Wong, S. K., Berne, M. A., Somasundaran, M., Sullivan, J. L., Luzuriaga, K., Greenough, T. C., Choe, H., and Farzan, M. (2003) Angiotensin-converting enzyme 2 is a functional receptor for the SARS coronavirus. *Nature* **426 (6965)**: 450-454.

Li, W., Shi, Z., Yu, M., Ren, W., Smith, C., Epstein, J. H., Wang, H., Crameri, G., Hu, Z., Zhang, H., Zhang, J., McEachern, J., Field, H., Daszak, P., Eaton, B. T., Zhang, S., and Wang, L. F. (2005) Bats are natural reservoirs of SARSlike coronaviruses. *Science* **310**: 676–679.

Li, F. Q., Xiao, H., Tam, J. P., and Liu, D. X. (2005) Sumoylation of the nucleocapsid protein of severe acute respiratory syndrome associated coronavirus. *FEBS Lett.* **579**: 2387–2396.

Liao, C. L., and Lai, M. M. C. (1992) RNA recombination in a coronavirus: Recombination between viral genomic RNA and transfected RNA fragments. *J. Virol.* **66**: 6117–6124.

Liao, Y., Lescar, J., Tam, J. P., and Liu, D. X. (2004) Expression of SARS-coronavirus envelope protein in Escherichia coli cells alters membrane permeability. *Biochem. Biophys. Res. Commun.* **325**: 374–380.

Liao, Y., Yuan, Q., Torres, J., Tam, J. P., and Liu, D. X. (2006) Biochemical and functional characterization of the membrane association and membrane permeabilizing activity of the severe acute respiratory syndrome coronavirus envelope protein. *Virol.* **349**: 264-275.

Lim, K. P., and Liu, D. X. (1998a) Characterization of a papain-like proteinase domain encoded by ORF1a of the coronavirus IBV and determination of the Cterminal cleavage site of an 87 kDa protein. *Adv. Exp. Med. Biol.* **440**: 173–184.

Lim, K. P., and Liu, D. X. (1998b) Characterization of the two overlapping papainlike proteinase domains encoded in gene 1 of the coronavirus infectious bronchitis virus and determination of the C-terminal cleavage site of an 87 kDa protein. *Virol.* **245**: 303–312.

Lim, K. P., Ng, L. F., and Liu, D.X. (2000) Identification of a novel cleavage activity of the first papain-like proteinase domain encoded by open reading frame 1a of the coronavirus avian infectious bronchitis virus and characterization of the cleavage products. *J. Virol.* **74**: 1674–1685.

Lin, Y. J., Liao, C. L., and Lai, M. M. C. (1994) Identification of the cis-acting signal for minus-strand RNA synthesis of a murine coronavirus: implications for the role of minus-strand RNA in RNA replication and transcription. *J. Virol.* **68**: 8131–8140.

Lin, Y.-J., and Lai, M. M. C. (1993) Deletion mapping of a mouse hepatitis virus defective interfering RNA reveals the requirement of an internal and discontiguous sequence for replication. *J. Virol.* **67**: 6110–6118.

Liu, D. X., Shen, S., Xu, H.Y., and Wang, S.F. (1998) Proteolytic mapping of the coronavirus infectious bronchitis virus 1b polyprotein: evidence for the presence of four cleavage sites of the 3C-like proteinase and identification of two novel cleavage products. *Virol.* **246**: 288–297.

Liu, D. X., Tibbles, K. W., Cavanagh, D., Brown, T. D. K., and Brierley, I. (1995) Identification, expression and processing of an 87K polypeptide encoded by ORF1a of the coronavirus infectious bronchitis virus. *Virol.* **208**: 47–54.

Liu, D. X., Xu, H. Y., and Brown, T. D. K. (1997) Proteolytic processing of the coronavirus infectious bronchitis virus 1a polyprotein: identification of a 10 kDa polypeptide and determination of its cleavage sites. *J. Virol.* **71**: 1814–1820.

Loewy, A., Smyth, J., von Bonsdorff, C. H., Liljestrom, P., and Schlesinger, M. J. (1995) The 6-kDa membrane protein of Semliki Forest virus is involved in the budding process. *J. Virol.* **69**: 469– 475.

Lomniczi, B., and Kennedy, I. (1977) Genome of infectious bronchitis virus. *J. Virol.* **24**: 99–107.

Luytjes, W., Gerritsma, H., and Spaan,W. J. M. (1996) Replication of synthetic interfering RNAs derived from coronavirus mouse hepatitis virus-A59. *Virol.* **216**: 174–183.

Machamer, C. E., and Rose, J. K. (1987) A specific transmembrane domain of a coronavirus E1 glycoprotein is required for its retention in the Golgi region. *J. Cell. Biol.* **105**: 1205–1214.

Madan, V., Garcia Mde, J., Sanz, M.A., and Carrasco, L. (2005) Viroporin activity of murine hepatitis virus E protein. *FEBS Lett* **579**: 3607–3612.

Madan, V., Sanz, M. A. and Carrasco, L. (2004) Requirement of the vesicular system for membrane permeabilization by Sindbis virus. *Virol.* **332**: 307–315.

Madu, I. G., Chu, V. C., Lee, H., Regan, A. D., Bauman, B. E., and Whittaker, G, R. (2007). Heparan sulfate is a selective attachment factor for the avian coronavirus infectious bronchitis virus Beaudette. *Avian Dis.* **51**: 45-51.

Egloff, M.-P., Ferron, F., Campanacci, V., Longhi, S., Rancurel, C., Dutartre, H., Snijder, E. J., Alexander, E. G., Cambillau, C., and Canard, B.(2004) The severe acute respiratory syndrome coronavirus replicative protein nsp9 is a single-stranded RNA-binding subunit unique in the RNA virus world. *PNAS.* **101**: 3792-3796.

Marra, M. A., Jones, S. J., Astell, C. R., Holt, R. A., Brooks-Wilson, A., Butterfield, Y. S., Khattra, J., Asano, J. K., Barber, S. A., Chan, S. Y., Cloutier, A., Coughlin, S. M., Freeman, D., Girn, N., Griffith, O. L., Leach, S. R., Mayo, M., McDonald, H., Montgomery, S. B., Pandoh, P. K., Petrescu, A. S., Robertson, A. G., Schein, J. E., Siddiqui, A., Smailus, D. E., Stott, J. M., Yang, G. S., Plummer, F., Andonov, A., Artsob, H., Bastien, N., Bernard, K., Booth, T. F., Bowness, D., Czub, M., Drebot, M., Fernando, L., Flick, R., Garbutt, M., Gray, M., Grolla, A., Jones, S., Feldmann, H., Meyers, A., Kabani, A., Li, Y., Normand, S., Stroher, U., Tipples, G. A., Tyler, S., Vogrig, R., Ward, D., Watson, B., Brunham, R. C., Krajden, M., Petric, M., Skowronski, D. M., Upton, C., and Roper, R. L. (2003) The genome sequence of the SARS-associated coronavirus. *Science.* **300**: 1399–1404.

Masters, J. R. (2002) HeLa cells 50 years on: the good, the bad and the ugly. *Nature Reviews Cancer.* **2**: 315-319.

Masters, P. S. (2006) The molecular biology of coronaviruses. *Adv Virus Res.* **66**: 193-292

Mayer, T., Tamura, T., Falk, M., and Niemann, H. (1988) Membrane integration and intracellular transport of the coronavirus glycoprotein E1, a class III membrane glycoprotein. *J. Biol. Chem.* **263**: 14956–14963.

McInerney, G. M., Smit, J. M., Liljestrom, P., and Wilschut, J. (2004) Semliki Forest virus produced in the absence of the 6K protein has an altered spike structure as revealed by decreased membrane fusion capacity. *Virol.* **325**: 200–206.

McIntosh, K. (1974) Coronaviruses. *A comparative review*. **63**: 85–129

McIntosh, K., Kapikian, A. Z., Hardison, K. A., Hartley, J. W., and Chanock, R. M. (1969) Antigenic relationships among the coronaviruses of man and between human and animal coronaviruses. *J. Immunol.* **102**: 1109 –1118.

Molenkamp, R., and Spaan, W. J. M. (1997) Identification of a specific interaction between the coronavirus mouse hepatitis virus A59 nucleocapsid protein and packaging signal. *Virol.* **239**: 78–86.

Mortola, E., and Roy, P. (2004) Efficient assembly and release of SARS coronavirus-like particles by a heterologous expression system. *FEBS Lett.* **576**: 174–178.

Nal, B., Chan, C., Kien, F., Siu, L., Tse, J., Chu, K., Kam, J., Staropoli, I., Crescenzo-Chaigne, B., Escriou, N., van der Werf, S., and Yuen, K.-Y., et al. (2005) Differential maturation and subcellular localization of severe acute respiratory syndrome coronavirus surface proteins S, M and E. *J. Gen. Virol.* **86**: 1423–1434.

Nash, T. C., and Buchmeier, M. J. (1996) Spike glycoprotein-mediated fusion in biliary glycoprotein-independent cell-associated spread of mouse hepatitis virus infection. *Virol.* **223**: 68-78.

Nelson, G. W., Stohlman, S. A., and Tahara, S. M. (2000) High affinity interaction between nucleocapsid protein and leader/intergenic sequence of mouse hepatitis virus RNA. *J. Gen. Virol.* **81**: 181–188.

Ng, L.F., and Liu, D. X. (1998) Identification of a 24 kDa polypeptide processed from the coronavirus infectious bronchitis virus 1a polyprotein by the 3Clike proteinase and determination of its cleavage sites. *Virol.* **243**: 388–395.

Ng, L. F., and Liu, D. X. (2000) Further characterization of the coronavirus infectious bronchitis virus 3C-like proteinase and determination of a new cleavage. *Virol.* **272**: 27–39.l

Ng, L. F., and Liu, D. X. (2002) Membrane association and dimerization of a cysteinerich, 16-kDa polypeptide released from the C-terminal region of the coronavirus infectious bronchitis virus 1a polyprotein. *J. Virol.* **76**: 6257–6267.

O'Connor, J. B., and Brian, D. A. (1999) The major product of porcine transmissible gastroenteritis coronavirus gene 3b is an integral membrane glycoprotein of 31 kDa. *Virol.* **256**: 152–161.

Ortego, J., Escors, D., Laude, H., and Enjuanes, L. (2002) Generation of a replication-competent, propagationdeficient virus vector based on the transmissible gastroenteritis coronavirus genome. *J Virol.* **76**: 11518–11529.

Oshiro, L. (1973) Coronaviruses. In "Ultrastructure of Animal Viruses and Bacteriophages: An Atlas" (A. J. Dalton and F. Haguenau, eds.), *Academic Press, New York.* 331–343.

Parker, M. M., and Masters, P. S. (1990) Sequence comparison of the N genes of five strains of the coronavirus mouse hepatitis virus suggests a three domain structure for the nucleocapsid protein. *Virol.* **179**: 463–468.

Patel, J. R., Davies, H. A., Edington, N., Laporte, J., and Macnaughton, M. R. (1982) Infection of a calf with the enteric coronavirus strain Paris. *Arch. Virol.* **73**: 319–327.

Paul, S. M. (2006) The molecular biology of coronaviruses. *Adv. Virus Res.* **66**: 193–292.

Pensaert, M. B., Debouck, P., and Reynolds, D. J. (1981) An immunoelectron microscopic and immunofluorescent study on the antigenic relationship between the coronavirus-like agent, CV 777, and several coronaviruses. *Arch. Virol.* **68**: 45 – 52.

Peti, W., Johnson, M. A., Herrmann, T., Neuman, B. W., Buchmeier, M. J., Nelson, M., Joseph, J., Page, R., Stevens, R. C., Kuhn, P., and Wu¨thrich, K. (2005) Structural genomics of the severe acute respiratory syndrome coronavirus: nuclear magnetic resonance structure of the protein nsp7. *J. Virol.* **79**: 12905– 12913.

Prentice, E., Jerome, W. G., Yoshimori, T., Mizushima, N., and Denison, M. R. (2004a).Coronavirus replication complex formation utilizes components of cellular autophagy. *J. Biol. Chem.* **279**:10136–10141.

Putics, A., Filipowicz, W., Hall, J., Gorbalenya, A. E., and Ziebuhr, J. (2005) ADP-ribose-1''-monophosphatase: a conserved coronavirus enzyme that is dispensable for viral replication in tissue culture. *J. Virol.* **79**: 12721–12731.

Raamsman, M. J. B., Krijnse Locker, J., de Hooge, A., de Vries, A. A. F., Griffiths, G., Vennema, H., and Rottier, P. J. M. (2000) Characterization of the coronavirus mouse hepatitis virus strain A59 small membrane protein E. *J. Virol.* **74**: 2333–2342.

Racaniello, V. R., and Baltimore, D. (1981) Cloned poliovirus cDNA is infectious in mammalian cells. *Science* **214**: 916–919.

Ratia, K., Saikatendu, K. S., Santarsiero, B. D., Barretto, N., Baker, S. C., Stevens, R. C., and Mesecar, A. D. (2006) Severe acute respiratory syndrome coronavirus papain-like protease: structure of a viral deubiquitinating enzyme. *PNAS* **103**: 5717–5722.

Ricagno, S., Egloff, M. P., Ulferts, R., Coutard, B., Nurizzo, D., Campanacci, V., Cambillau, C., Ziebuhr, J., and Canard, B. (2006) Crystal structure and

mechanistic determinants of SARS coronavirus nonstructural protein 15 define an endoribonuclease family. *PNAS* **103**:11892-11897.

Rice, C. M., Grakoui, A., Galler, R., and Chambers, T. J. (1989) Transcription of infectious yellow fever RNA from full-length cDNA templates produced by in vitro ligation. *New Biologist* **1**: 285–296.

Rota, P. A., Oberste, M. S., Monroe, S. S., Nix, W. A., Campagnoli, R., Icenogle, J. P., Penaranda, S., Bankamp, B., Maher, K., Chen, M. H., Tong, S., Tamin, A., Lowe, L., Frace, M., DeRisi, J. L., Chen, Q., Wang, D., Erdman, D. D., Peret, T. C., Burns, C., Ksiazek, T. G., Rollin, P. E., Sanchez, A., Liffick, S., Holloway, B., Limor, J., McCaustland, K., Olsen Rasmussen, M., Fouchier, R., Gunther, S., Osterhaus, A. D., Drosten, C., Pallansch, M. A., Anderson, L. J., and Bellini, W. J. (2003) Characterization of a novel coronavirus associated with severe acute respiratory syndrome. *Science* **300**: 1394–1399.

Rottier, P., Brandenburg, D., Armstrong, J., van der Zeijst, B., and Warren, G. (1984) Assembly in vitro of a spanning membrane protein of the endoplasmic reticulum: The E1 glycoprotein of coronavirus mouse hepatitis virus A59. *PNAS* **81**: 1421–1425.

Saikatendu, K. S., Joseph, J. S., Subramanian, V., Clayton, T., Griffith, M., Moy, K., Velasquez, J., Neuman, B. W., Buchmeier, M. J., Stevens, R. C., and Kuhn, P. (2005) Structural basis of severe acute respiratory syndrome coronavirus ADP-ribose-1''-phosphate dephosphorylation by a conserved domain of nsp3. *Structure* (Cambridge) **13**: 1665–1675.

Sanchez, C. M., Izeta, A., Sanchez-Morgado, J. M., Alonso, S., Sola, I., Balasch, M., Plana-Duran, J., and Enjuanes, L. (1999) Targeted recombination demonstrates that the spike gene of transmissible gastroenteritis coronavirus is a determinant of its enteric tropism and virulence. *J. Virol.* **73**: 7607–7618.

Åkerström, S., Mirazimi, Ali., and Tan, Y.-J. (2006) Inhibition of SARS-CoV replication cycle by small interference RNAs silencing specific SARS proteins, 7a/7b, 3a/3b and S. *Antiviral Res.* **73**: 219–227.

Sawicki, D., Wang, T., and Sawicki, S. (2001) The RNA structures engaged in replication and transcription of the A59 strain of mouse hepatitis virus. *J. Gen. Virol.* **82**: 385–396.

Sawicki, S. G., and Sawicki, D. L. (1990) Coronavirus transcription: Subgenomic mouse hepatitis virus replicative intermediates function in RNA synthesis. *J. Virol.* **64**: 1050–1056.

Sawicki, S. G., and Sawicki, D. L. (1998) A new model for coronavirus transcription. *Adv. Exp. Med. Biol.* **440**: 215–219.

Sawicki, S. G., and Sawicki, D. L. (2005) Coronavirus transcription: A perspective. *Curr.Top. Microbiol. Immunol.* **287**: 31–55.

Schaad, M. C., and Baric, R. S. (1994) Genetics of mouse hepatitis virus transcription: Evidence that subgenomic negative strands are functional templates. *J. Virol.* **68**: 8169–8179.

Schelle, B., Karl, N., Ludewig, B., Siddell, S. G., and Thiel, V. (2005) Selective replication of coronavirus genomes that express nucleocapsid protein. *J. Virol.* **79**: 6620–6630.

Schochetman, G., Stevens, R. H., and Simpson, R. W. (1977) Presence of infectious polyadenylated RNA in coronavirus avian bronchitis virus. *Virolo.* **77**: 772–782.

Schwegmann-Wessels, C., and Herrler, G. (2006) Sialic acids as receptor determinants for coronaviruses. *Glycoconj J.* **23** :51-58.

Sethna, P. B., Hofmann, M. A., and Brian, D. A. (1991) Minus-strand copies of replicating coronavirus mRNAs contain antileaders. *J. Virol.* **65**: 320–325.

Sethna, P. B., Hung, S. L., and Brian, D. A. (1989) Coronavirus subgenomic minusstrand RNAs and the potential for mRNA replicons. *PNAS* **86**: 5626–5630.

Seybert, A., Hegyi, A., Siddell, S. G., and Ziebuhr, J. (2000) The human coronavirus 229E superfamily 1 helicase has RNA and DNA duplex-unwinding activities with 50-to-30 polarity. *RNA* **6**: 1056–1068.

Seybert, A., van Dinten, L. C., Snijder, E. J., and Ziebuhr, J. (2000) Biochemical characterization of the equine arteritis virus helicase suggests a close functional relationship between arterivirus and coronavirus helicases. *J. Virol.* **74**: 9586–9593.

Seybert, A., Posthuma, C. C., van Dinten, L. C., Snijder, E. J., Gorbalenya, A. E., and Ziebuhr, J. (2005) A complex zinc finger controls the enzymatic activities of nidovirus helicases. *J. Virol.* **79**: 696–704.

Shi, S. T., Schiller, J. J., Kanjanahaluethai, A., Baker, S. C., Oh, J. W., and Lai, M. M. C. (1999). Colocalization and membrane association of murine hepatitis virus gene 1products and De novo-synthesized viral RNA in infected cells. *J. Virol.* **73**:5957–5969.

Shi Z., and Hu Z. (2007) A review of studies on animal reservoirs of the SARS coronavirus. *Virus Res.* Apr 20; [Epub ahead of print]

Siddell, S. G. (ed.). 1995. The Coronaviridae. *Plenum Press, New York.* 1–10.

Sims, A. C., Ostermann, J., and Denison, M. R. (2000). Mouse hepatitis virus replicase proteins associate with two distinct populations of intracellular membranes. *J. Virol.***74**:5647–5654.

Snijder, E. J., and Meulenberg, J. J. (1998) The molecular biology of arteriviruses. *J. Gen. Virol.* **79**: 961–979.

Snijder, E. J., Bredenbeek, P. J., Dobbe, J. C., Thiel, V., Ziebuhr, J., Poon, L. L. M., Guan, Y., Rozanov, M., Spaan, W. J. M., and Gorbalenya., A. E. (2003) Unique and conserved features of genome and proteome of SARS coronavirus, an early split-off from the coronavirus group 2 lineage. *J. Mol. Biol.* **331**: 991–1004.

Song, H. C., Seo, M. Y., Stadler, K., Yoo, B. J., Choo, Q. L., Coates, S. R., Uematsu, Y., Harada, T., Greer, C. E., Polo, J. M., Pileri, P., and Eickmann, M. et al. (2004) Synthesis and characterization of a native, oligomeric form of recombinant severe acute respiratory syndrome coronavirus spike glycoprotein. *J. Virol.* **78**: 10328–10335.

Soonjeon, Y., Julian, L., Leibowitza, b., and Ellen, W. C. (2004) In vitro assembled, recombinant infectious bronchitis viruses demonstrate that the 5a open reading frame is not essential for replication. *Virol.* **332**: 206-215.

Stern, D. F., and Sefton, B. M. (1982) Coronavirus proteins: Structure and function of the oligosaccharides of the avian infectious bronchitis virus glycoproteins. *J. Virol.* **44**: 804–812.

Stohlman, S. A., Baric, R. S., Nelson, G. N., Soe, L. H., Welter, L. M., and Deans, R. J. (1988) Specific interaction between coronavirus leader RNA and nucleocapsid protein. *J. Virol.* **62**: 4288–4295.

Sturman, L. S. (1977) Characterization of a coronavirus: I. Structural proteins: Effect of preparative conditions on the migration of protein in polyacrylamide gels. *Virol.* **77**: 637–649.

Sturman, L. S., Holmes, K. V., and Behnke, J. (1980) Isolation of coronavirus envelope glycoproteins and interaction with the viral nucleocapsid. *J. Virol.* **33**: 449–462.

Su, D., Lou, Z., Sun, F., Zhai, Y., Yang, H., Zhang, R., Joachimiak, A., Zhang, X. C., Bartlam, M., and Rao, Z. (2006) Dodecameric structure of severe acute respiratory syndrome coronavirus nonstructural protein nsp10. *J. Virol.* **80**: 902–7908.

Sugiyama, K., and Amano, Y. (1981) Morphological and biological properties of a new coronavirus associated with diarrhea in infant mice. *Arch. Virol.* **67**: 241–251.

Surjit, M., Liu, B., Jameel, S., Chow, V. T., and Lal, S. K. (2004) The SARS coronavirus nucleocapsid protein induces actin reorganization and apoptosis in COS-1 cells in the absence of growth factors. *Biochem. J.* **383**: 13–18.

Sutton, G., Fry, E., Carter, L., Sainsbury, S., Walter, T., Nettleship, J., Berrow, N., Owens, R., Gilbert, R., Davidson, A., Siddell, S., Poon, L. L., Diprose, J., Alderton, D., Walsh, M., Grimes, J. M., and Stuart, D. I. (2004) The nsp9 replicase protein of SARS-coronavirus, structure and functional insights. *Structure* **12**: 341–353.

Suzich, J. A., Tamura, J. K., Palmer-Hill, F., Warrener, P., Grakoui, A., Rice, C. M., Feinstone, S. M., and Collett, M. S (1993). Hepatitis C virus NS3 protein polynucleotide-stimulated nucleoside triphosphatase and comparison with the related pestivirus and flavivirus enzymes. *J Virol.* **67**: 6152-6158.

Tan, Y.-J. (2005) The Severe Acute Respiratory Syndrome (SARS)-coronavirus 3a protein may function as a modulator of the trafficking properties of the spike protein. *J Virol.* **10**: 2–5.

Tan, Y.-J., Lim, S.- G., and Hong, W.-J. (2005) Characterization of viral proteins encoded by the SARS-coronavirus genome. *Antiviral Res.* **65**: 69–78.

Tan, Y.-J., Teng, E., Shen, S., Tan, T. H. P., Goh, P.-Y., Fielding, B. C., Ooi, E.-E., Tan, H.-C., Lim, S. G., and Hong, W. (2004c) A novel SARS coronavirus protein, U274, is transported to the cell surface and undergoes endocytosis. *J. Virol.* **78**: 6723–6734.

Hodgson, T., Britton, P., and Cavanagh, D. (2005) Neither the RNA nor the proteins of open reading frames 3a and 3b of the coronavirus infectious bronchitis virus are essential for replication. *J. Virol.* **79**: 13399–13411.

Thiel, V., and Siddell, S. G. (2005) Reverse genetics of coronaviruses using vaccinia virus vectors. *Curr. Top. Microbiol. Immunol.* **287**: 199–227.

Thiel, V., Herold, J., Schelle, B., and Siddell, S. G. (2001a) Infectious RNA transcribed in vitro from a cDNA copy of the human coronavirus genome cloned in vaccinia virus. *J. Gen. Virol.* **82**: 1273–1281.

Thiel, V., Ivanov, K. A., Putics, A., Hertzig, T., Schelle, B., Bayer, S., Weissbrich, B., Snijder, E. J., Rabenau, H., Doerr, H. W., Gorbalenya, A. E., and Ziebuhr, J. (2003a) Mechanisms and enzymes involved in SARS coronavirus genome expression. *J. Gen. Virol.* **84**: 2305–2315.

Thiel, V., Rashtchian, A., Herold, J., Schuster, D. M., Guan, N., and Siddell, S. G. (1997) Effective amplification of 20–kb DNA by reverse transcription PCR. *Anal. Biochem.* **252**: 62–70.

Tresnan, D. B., Levis, R., and Holmes, K. V. (1996) Feline aminopeptidase N serves as a receptor for feline, canine, porcine, and human coronaviruses in serogroup I. *J. Virol* . **70**: 8669-8674.

Valen, L. V., and Virginia C. M. (1991) HeLa, a new microbial species. *Evolutionary Theory.* **10**: 71-74.

van der Most, R. G., and Spaan, W. J. M. (1995) In "The Coronaviridae" (Siddell, S. G. ed.) *Plenum, New York.* 11–31.

van Dinten, L. C., van Tol, H., Gorbalenya, A. E., and Snijder, E. J. (2000) The predicted metal-binding region of the arterivirus helicase protein is involved

in subgenomic mRNA synthesis, genome replication, and virion biogenesis. *J. Virol.* **74**: 5213–5223.

van Dinten, L. C., den Boon, J. A., Wassenaar, A. L., Spaan, W. J., and Snijder, E. J. (1997) An infectious arterivirus cDNA clone: identification of a replicase point mutation that abolishes discontinuous mRNA transcription. *PNAS* **94**: 991–996.

Van Dinten, L.C., van Tol, H., Gorbalenya A. E., Snijder, E. J. (2000) The prodicated metal-binding region of the arterivirus helicase protein is involved in subgenomic mRNA sythesis, genome replication, and virion biogenesis. *J. Virol.* **74**: 5213-5223.

Van Vliet, A. L., Smits, S. L., Rottier, P. J. M., and de Groot, R. J. (2002) Discontinuous and non-discontinuous subgenomic RNA transcription in a nidovirus. *EMBO J.* **21**: 6571–6580.

Vennema, H., Godeke, G.-J., Rossen, J. W. A., Voorhout, W. F., Horzinek, M. C., Opstelten, D.-J. E., and Rottier, P. J. M. (1996) Nucleocapsid-independent assembly of coronavirus-like particles by co-expression of viral envelope protein genes. *EMBO J.* **15**: 2020–2028.

Vennema, H., Rijnbrand, R., Heijnen, L., Horzinek, M. C., and Spaan, W. J. M. (1991) Enhancement of the vaccinia virus/phage T7 RNA polymerase expression system using encephalomyocarditis virus 50-untranslated region sequences. *Gene* **108**: 201–209.

Voss, D., Kern, A., Traggiai, E., Eickmann, M., Stadler, K., Lanzavecchia, A., and Becker, S. (2006) Characterization of severe acute respiratory syndrome coronavirus membrane protein. *FEBS Letters.* **580**: 968–973.

Walker, P. A., Leong, L. E.-C., and Porter, A. G. (1995) Sequence and structural determinants of the interaction between the 5_-noncoding region of picornavirus RNA and rhinovirus protease 3C. *J.Biol.Chem.* **270**: 14510–14516.

Wang, L., Junker, D., and Collisson, E. W. (1993) Evidence of natural recombination within the S1 gene of infectious bronchitis virus. *Virol.* **192**: 710–716.

Watanabe, T., Watanabe, S., Ito, H., Kida, H., and Kawaoka, Y. (2001) Influenza A virus can undergo multiple cycles of replication without M2 ion channel activity. *J. Virol.* **75**: 5656–5662.

Wege, H., Muller, A., and ter Meulen, V. (1978) Genomic RNA of the murine coronavirus JHM. *J. Gen. Virol.* **41**: 217–227.

Weiss, S. R., and Navas-Martin, S. (2005) Coronavirus pathogenesis and the emerging pathogen severe acute respiratory syndrome coronavirus. *Microbiol. Mol. Biol. Rev.* **69**: 635–664.

Wilson, L., McKinlay, C., Gage, P., and Ewart, G. (2004) SARS coronavirus E protein forms cation-selective ion channels. *Virol.* **330**: 322–331.

Wu, X. D., Shang, B., Yang, R. F., Yu, H., Ma, Z. H., Shen, X., Ji, Y. Y., Lin, Y., Wu, Y. D., Lin, G. M., Tian, L., Gan, X. Q., Yang, S., Jiang, W. H., Dai, E. H., Wang, X. Y., Jiang, H. L., Xie, Y. H., Zhu, X. L., Pei, G., Li, L., Wu, J. R., and Sun, B. (2004) The spike protein of severe acute respiratory syndrome (SARS) is cleaved in virus infected VERO-E6 cells. *Cell Res.* **14**: 400–406.

Wurm, T., Chen, H., Hodgson, T., Britton, P., Brooks, G., and Hiscox, J. A. (2001) Localization to the nucleolus is a common feature of coronavirus nucleoproteins, and the protein may disrupt host cell division. *J. Virol.* **75**: 9345–9356.

Xu, H. Y., Lim, K. P., Shen, S., and Liu, D. X. (2001) Further identification and characterization of novel intermediate and mature cleavage products released from the ORF 1b region of the avian coronavirus infectious bronchitis virus 1a/1b polyprotein. *Virol.* **288**: 212–222.

Yamada, Y. K., Yabe, M., Ohtsuki, T., and Taguchi, F. (2000) Unique N-linked glycosylation of murine coronavirus MHV-2 membrane protein at the conserved O-linked glycosylation site. *Virus Res.* **66**: 149–154.

Yao, N., and Weber, P. C. (1998) Helicase, a target for novel inhibitors of hepatitis C virus. *Antivir Ther* **3**: 93-97.

Yeager, C. L., Ashmun, R. A., Williams, R. K., Cardellichio, C. B., Shapiro, L. H., Look, A.T., and Holmes, K. V. (1992) Human aminopeptidase N is a receptor for human coronavirus 229E. *Nature* **357 (6377)**: 420-422.

Youn, S., Collisson, E. W., and Machamer, C. E. (2005a) Contribution of trafficking signals in the cytoplasmic tail of the infectious bronchitis virus spike protein to virus infection. *J. Virol.* **79**: 13209–13217.

Youn, S., Leibowitz, J. L., and Collisson, E. W. (2005) In vitro assembled, recombinant infectious bronchitis viruses demonstrate that the 5a open reading frame is not essential for replication. *Virol.* **332**: 206–215.

Yount, B., Curtis, K. M., and Baric, R. S. (2000) Strategy for systematic assembly of large RNA and DNA genomes: Transmissible gastroenteritis virus model. *J. Virol.* **74**: 10600–10611.

Yount, B., Curtis, K. M., Fritz, E. A., Hensley, L. E., Jahrling, P. B., Prentice, E., Denison, M. R., Geisbert, T. W., and Baric, R. S. (2003) Reverse genetics with a full-length infectious cDNA of severe acute respiratory syndrome coronavirus. *PNAS.* **100**: 12995–13000.

Yount, B., Curtis, K. M., and Baric, R. S. (2000) Strategy for systematic assembly of large RNA and DNA genomes: transmissible gastroenteritis virus model. *J. Virol.* **74**: 10600–10611.

Yount, B., Denison, M. R., Weiss, S. R., and Baric, R. S. (2002) Systematic assembly of a full-length infectious cDNA of mouse hepatitis virus strain A59. *J. Virol.* **76**: 11065–11078.

Yuan, X., Shan, Y., Zhao, Z., Chen, J., and Cong, Y. (2005b) G0/G1 arrest and apoptosis induced by SARS-CoV 3b protein in transfected cells. *Virol. J.* **2**: 66.

Huang, Y., Yang, Z.-Y., Kong, W.-P., and Nabel, G. J. (2004) Generation of Synthetic Severe Acute Respiratory Syndrome Coronavirus Pseudoparticles: Implications for Assembly and Vaccine Production. *J. Virol.* **78**: 12557-12565.

Zeng, R., Ruan, H. Q., Jiang, X. S., Zhou, H., Shi, L., Zhang, L., Sheng, Q. H., Tu, Q., Xia, Q. C., and Wu, J. R. (2004a) Proteomic analysis of SARS associated coronavirus using two-dimensional liquid chromatography mass spectrometry and one-dimensional sodium dodecyl sulfatepolyacrylamide gel electrophoresis followed by mass spectrometric analysis. *J. Proteome Res.* **3**: 549–555.

Zhai, Y., Sun, F., Li, X., Pang, H., Xu, X., Bartlam, M., and Rao, Z. (2005) Insights into SARS-CoV transcription and replication from the structure of the nsp7-nsp8 hexadecamer. *Nat. Struct. Mol. Biol.* **12**: 980–986.

Zhou, M., Williams, A. K., Chung, S. I., Wang, L., and Collisson, E. W. (1996) The infectious bronchitis virus nucleocapsid protein binds RNA sequences in the 3' terminus. *Virol.* **217**: 191-199

Ziebuhr, J. (2005) The coronavirus replicase. *Curr. Top. Microbiol. Immunol.* **287**: 57–94.

Ziebuhr, J., Snijder, E. J., and Gorbalenya, A. E. (2000) Virus-encoded proteinases and proteolytic processing in the Nidovirales. *J. Gen. Virol.* **81**: 853–879.

Ziebuhr, J., and Siddell, S. G. (1999). Processing of the human coronavirus 229E replicase polyproteins by the virus-encoded 3C-like proteinase: Identification of proteolytic products and cleavage sites common to pp1a and pp1ab. *J. Virol.* **73**:177–185.

PUBLICATIONS

Available online at www.sciencedirect.com
ScienceDirect
Virology 358 (2007) 136–147
VIROLOGY
www.elsevier.com/locate/yviro

An arginine-to-proline mutation in a domain with undefined functions within the helicase protein (Nsp13) is lethal to the coronavirus infectious bronchitis virus in cultured cells

Shouguo Fang [a], Bo Chen [b], Felicia P.L. Tay [a], Beng Sern Ng [a], Ding Xing Liu [a,b,*]

[a] *Institute of Molecular and Cell Biology, 61 Biopolis Drive, Proteos, 138673 Singapore*
[b] *School of Biological Sciences, Nanyang Technological University, 60 Nanyang Drive, 637551 Singapore*

Received 5 June 2006; returned to author for revision 30 June 2006; accepted 11 August 2006
Available online 18 September 2006

Abstract

Genetic manipulation of the RNA genomes by reverse genetics is a powerful tool to study the molecular biology and pathogenesis of RNA viruses. During construction of an infectious clone from a Vero cell-adapted coronavirus infectious bronchitis virus (IBV), we found that a G–C point mutation at nucleotide position 15526, causing Arg-to-Pro mutation at amino acid position 132 of the helicase protein, is lethal to the infectivity of IBV on Vero cells. When the in vitro-synthesized full-length transcripts containing this mutation were introduced into Vero cells, no infectious virus was rescued. Upon correction of the mutation, infectious virus was recovered. Further characterization of the in vitro-synthesized full-length transcripts containing the G15526C mutation demonstrated that this mutation may block the transcription of subgenomic RNAs. Substitution mutation of the Arg132 residue to a positively charged amino acid Lys affected neither the infectivity of the in vitro-synthesized transcripts nor the growth properties of the rescued virus. However, mutation of the Arg132 residue to Leu, a conserved residue in other coronaviruses at the same position, reduced the recovery rate of the in vitro-synthesized transcripts. The recovered mutant virus showed much smaller-sized plaques. On the contrary, a G–C and a G–A point mutations at nucleotide positions 4330 and 9230, respectively, causing Glu–Gln and Gly–Glu mutations in or near the catalytic centers of the papain-like (Nsp3) and 3C-like (Nsp5) proteinases, did not show detectable detrimental effect on the rescue of infectious viruses and the infectivity of the rescued viruses.

Keywords: Coronavirus infectious bronchitis virus; Infectious clone; Helicase; Arginine-to-proline mutation; Infectivity

Introduction

Coronaviruses cause severe diseases affecting human and other animal species. In 2003, a novel coronavirus (SARS-CoV) was identified as the causative agent of severe acute respiratory syndrome (SARS) (Marra et al., 2003; Rota et al., 2003). The potential risk to public health posed by SARS-CoV and other coronaviruses and the lack of specific antiviral agents and vaccines have triggered a global research effort to characterize this family of viruses at the molecular and cellular levels. Major advances in studies of the biological functions of individual viral proteins and replication mechanisms are currently being made by genetic manipulation of coronaviral genomes using reverse genetics and targeted recombination approaches (Almazan et al., 2000; Casais et al., 2001, 2003, 2005; Coley et al., 2005; Hodgson et al., 2006; Koetzner et al., 1992; Masters and Rottier, 2005; Sanchez et al., 1999; Thiel et al., 2001; Youn et al., 2005a, 2005b; Yount et al., 2000, 2002, 2003, 2005).

Avian infectious bronchitis virus (IBV), a group 3 coronavirus, causes an acute and contagious disease in chickens with a significant impact on the poultry industry worldwide. IBV contains a 27.6 kb single-stranded, positive-sense RNA genome. In the virus-infected cells, six mRNA species, including the genome-length mRNA 1 and five subgenomic mRNAs (mRNA 2–6), are produced by a discontinuous RNA transcription mechanism. Each mRNA species possesses a 64 nucleotides leader sequence derived from the 5′ end of the

* Corresponding author. Institute of Molecular and Cell Biology, 61 Biopolis Drive, Proteos, 138673 Singapore.
E-mail address: dxliu@imcb.a-star.edu.sg (D.X. Liu).

0042-6822/$ - see front matter © 2006 Elsevier Inc. All rights reserved.
doi:10.1016/j.virol.2006.08.020

genome (Boursnell et al., 1987). Subgenomic mRNAs 2, 3, 4, and 6 encode the four structural proteins, i.e., spike glycoprotein (S), envelope protein (E), membrane protein (M), and nucleocapsid protein (N). The 5′ two-third region of mRNA 1 comprises two large ORFs, 1a and 1b, and encodes two polyproteins. The two polyproteins are proteolytically cleaved by two virus-encoded proteinases, the papain-like and 3C-like proteinases, into 15 functional proteins (Nsp2–Nsp16) (Lim and Liu, 1998a, 1998b; Lim et al., 2000; Liu et al., 1995, 1997, 1998; Ng and Liu, 1998, 2000, 2002; Xu et al., 2001). Compared to other coronaviruses, Nsp1 is absent in IBV but Nsp2 is considerably larger (Lim and Liu, 1998a, 1998b; Liu et al., 1995). In general, IBV shares close similarities in the genome organization, gene expression, and RNA replication with other coronaviruses but is non-infectious to human. These properties make IBV an attractive model system for studying the biology and pathogenesis of coronavirus.

In construction of an infectious IBV clone by in vitro assembly of five cloned RT-PCR fragments from a Vero cell-adapted IBV Beaudette strain, a G–C (G15526C) point mutation at nucleotide position 15,526 was found to be lethal to the infectivity of IBV on Vero cells. No infectious virus could be rescued from Vero cells electroporated with in vitro-synthesized full-length transcripts containing this mutation. As this mutation causes Arg132–Pro mutation in a domain with unknown function within the helicase protein (Nsp13), it implies that this region might play certain roles in the functionality of the helicase protein. On the contrary, a G–C (G4330C) and a G–A (G9230) point mutations at nucleotide positions 4330 and 9230, respectively, causing Glu–Gln and Gly–Glu mutations in or near the catalytic centers of the papain-like (Nsp3) and 3C-like (Nsp5) proteinases, did not impair the infectivity of the in vitro-synthesized transcripts containing these mutations. Further characterization of the in vitro-synthesized full-length transcripts containing the G15526C mutation demonstrated that this mutation blocks the transcription of subgenomic RNAs. Substitution mutation of the Arg132 residue to a positively charged amino acid (Lys) affected neither the infectivity of the in vitro-synthesized transcripts nor the growth properties of the rescued virus. However, mutation of the Arg132 residue to a Leu, which is conserved in most of other coronaviruses at the same position, reduced the viral recovery rate of the in vitro-

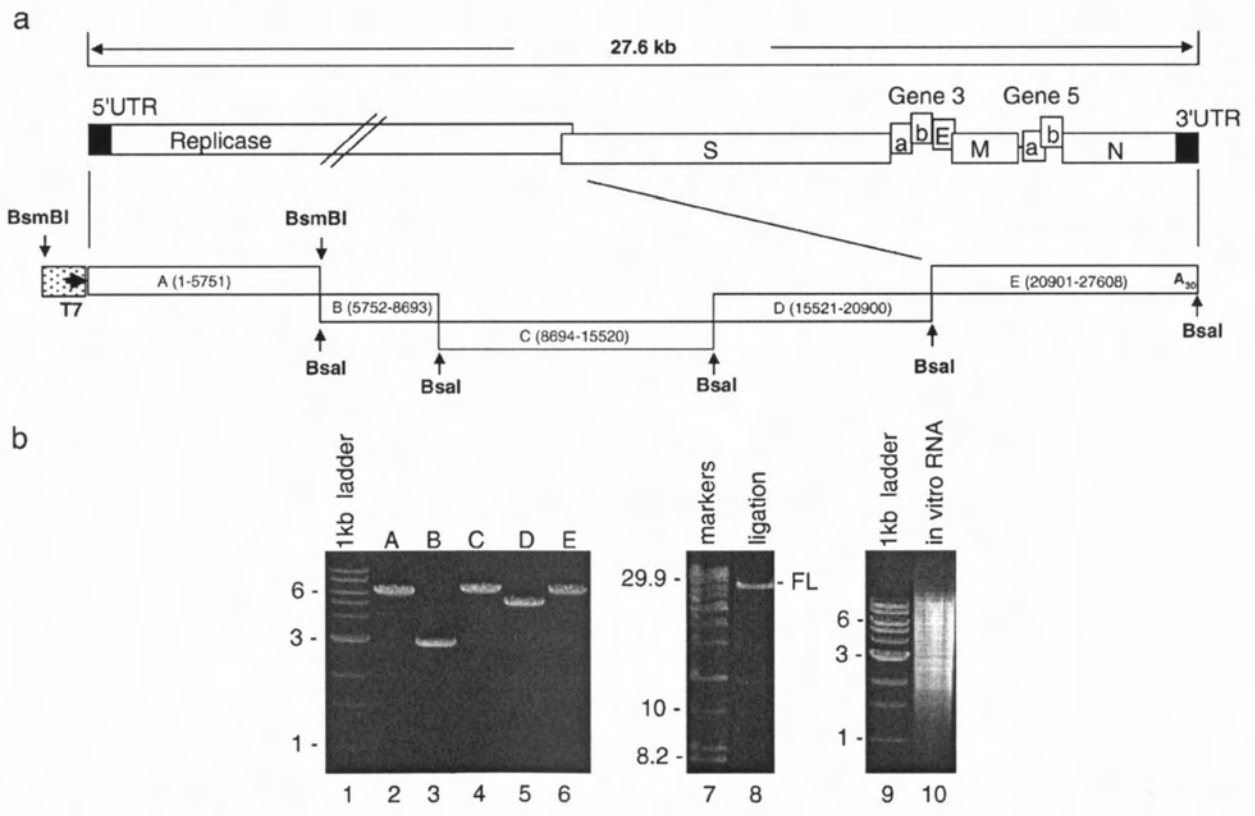

Fig. 1. In vitro assembly of full-length cDNA clone derived from a Vero cell-adapted IBV Beaudette strain. (a) Diagram of the genome organization of IBV. The regions coding for the replicase polyproteins, the structural proteins S, E, M, and N, the accessory proteins 3a, 3b, 5a, and 5b, and the 5′- and 3′-UTR are shown. Also shown are the regions of the five RT-PCR fragments, the T7 promoter at the 5′-end of fragment A, and the 30 As at the 3′-end of fragment E. (b) Preparation of the five cDNA fragments, assembly of the five fragments into a full-length cDNA clone, and in vitro transcription of the full-length transcripts. The five cDNA fragments covering IBV sequences from nucleotides 1–5751 (lane 2), 5752–8693 (lane 3), 8694–15,520 (lane 4), 15,521–20,900 (lane 5), and 20,901–27,608 (lane 6), respectively, were obtained by digestion of corresponding plasmid DNA with either *Bsm*BI or *Bsa*I, purified from agarose gel, and analyzed on a 0.8% agarose gel (lanes 2–6). Equal amounts of the purified fragments were ligated using T4 DNA ligase (lane 7) and analyzed on a 0.4% agarose gel. The in vitro assembled full-length cDNA was used as templates for generation of the full-length in vitro transcripts, which were analyzed on a 0.8% agarose gel (lane 10). Lanes 1, 7, and 9 show DNA markers, and numbers on the left indicate nucleotides in kilobases.

synthesized full-length transcripts. The mutant virus showed much smaller-sized plaques. This study reveals the essential role of a domain with previously unassigned functions within the helicase protein in coronavirus replication.

Results

Construction of a full-length cDNA clone derived from a Vero cell-adapted IBV Beaudette strain by in vitro assembly of five RT-PCR fragments

To construct a full-length IBV clone, five fragments (A to E) spanning the entire IBV genome were obtained by RT-PCR of total RNA extracted from Vero cells infected with a Vero cell-adapted IBV Beaudette strain (p65) (Shen et al., 2003, 2004; Fang et al., 2005). To facilitate the assembly of the full-length cDNA in vitro, restriction sites for either *Bsm*BI or *Bsa*I were introduced into both the 5′ and 3′ ends of the fragments (Fig. 1a). In fragment A, a 19-nucleotide sequence corresponding to the T7 RNA promoter (Table 1) was inserted into the 5′ end of the IBV genome to facilitate in vitro transcription using the T7 polymerase (Fig. 1a). The primers used to amplify these fragments are listed in Table 1. The PCR products were purified from agarose gel and cloned into either pCR-XL-TOPO (Invitrogen) or pGEM-T Easy (Promage) vectors. For the convenience of digestion using the restriction enzyme *Bsm*BI, the *Nhe*I- and *Eco*RI-digested fragment A was subcloned into pKT0 which contains a *Bsm*BI site 400 bp upstream of the T7 promoter sequence (Fig. 1a). Two to three independent clones for each construct were selected for sequencing. The complete sequences of the five fragments, determined by automated nucleotide sequencing, are summarized in Table 2.

The five fragments were then prepared by digestion of the corresponding constructs with either *Bsm*BI or *Bsa*I and purified (Fig. 1b, lanes 2–6). The full-length clone was made by ligation of the purified fragments in vitro (Fig. 1b, lane 8) and used as the template for in vitro transcription. The full-length in vitro-synthesized transcripts were generated using the mMessage mMachine T7 kit (Ambion, Austin, Tex) (Fig. 1b, lane 10). As coronavirus N gene transcripts were shown to enhance the recovery of the rescued virus from the in vitro-synthesized full-length transcripts (Casais et al., 2001; Youn et al., 2005a, 2005b; Yount et al., 2000, 2002), the N transcripts were generated from a linearized pKT0-IBVN construct containing IBV N gene and the 3′-UTR region. The full-length transcripts together with the N transcripts were introduced into Vero cells by electroporation. However, it was consistently observed that no infectious virus could be recovered from cells transfected with the full-length transcripts together with the N transcripts.

Table 2
Comparison of IBV sequences between Vero cell-adapted strain (p65) and the cloned fragments

Position (nt)	p65		Clone	
	nt	aa	nt	aa
Nsp2 (p87)				
2015	A	D	G	**G**[a]
Nsp3 (p195)				
4330	G	E	C	**Q**
4481	C	T	A	**N**
Nsp5 (3CLP)				
9230	G	G	A	**E**
9701–3	-GTG	-G	GTG	G[b]
Nsp6				
10,253	G	S	A	N
10,540	G	D	A	**N**
10,594	G	E	A	**K**
Nsp8 (p24)				
10,942	A	T	C	P
11,362	C	H	T	**Y**
Nsp13 (helicase)				
15,526	G	R	C	**P**
Nsp14 (p58)				
17,033	C	D	T	D
17,674	C	S	T	**L**
18,195	T	Y	C	**H**
18,430	C	S	T	F
N				
26,398	G	A	T	**S**

[a] Unique mutations found only in the cloned fragments.
[b] Same as the published sequences but different from p65.

Rescue of infectious virus by correction of a point mutation (G15526C) located in a domain with unknown function within the helicase protein (Nsp13)

Sequencing comparison of the five fragments with the Vero cell-adapted IBV strain (p65, accession no. DQ001339) shows nucleotide changes at 16 positions (Table 2). Among them, 11

Table 1
Primers used to construct the full-length IBV clone

Clone	Primer	Nucleotide sequence	Location
A	T7-IBV	5′-CGCTAGCTAATACGACTCACTATAGGACTTAAGATAGATATTAATA-3′	1–20
	IBV-5753R	5′-CGGGATC**CGTCTC**GCGACAACACTCTTAAC-3′	5737–5753
B	IBV-5748F	5′-ATTAT**GGTCTC**TGTCGCTAGCTATAAGACCG-3′	5748–5768
	IBV-8694R	5′-G**GGTCTC**GGCCTCAAATTTATCACCTATC-3′	8673–8694
C	IBV-8689F	5′-CGGGATCC**GGTCTC**GAGGCCTACCTTTCAGCG-3′	8689–8706
	IBV-15532R	5′-GCAAAA**GGTCTC**AATGAATCAC-3′	15,511–15,532
D	IBV-15511F	5′-CGGGATCCGTGATTCATT**GAGACC**TTTTGC-3′	15,511–15,532
	IBV-20930R	5′-ACACCTGCAGATGTAACATC-3′	20,911–20,930
E	IBV-20887F	5′-GTTTACACCTCTAAT**GAGACC**ATAG-3′	20,887–20,911
	IBV-27608R	5′-GGAATTC**GGTCTC**G$(T)_{30}$TGCTCTAACTCTATACTAGC-3′	27,589–27,608

caused unique amino acid changes (Table 2). To assess the deleterious effects of these mutations on the infectivity of the full-length clone, correction of some of the mutations was carried out by site-directed mutagenesis. Three point mutations, G4330C, G9230A, and G15526C, were chosen based on the fact that they are located either in or near the catalytic centers of the two viral proteinases or in a region of the RNA helicase protein with undefined functions. Four full-length cDNA clones either with correction of the mutations at all three positions (rIBV) or combination of two positions (e.g., G4330C containing G–C mutation at nucleotide position 4330 but without mutations at the other two positions) were constructed. RNA transcripts generated from the four full-length cDNA clones were introduced into Vero cells together with the N transcripts by electroporation. At 2 days post-electroporation, a typical CPE of the Vero cell-adapted IBV, the formation of giant syncytial cells (Fang et al., 2005), was observed in cells transfected with transcripts generated from cDNA clones rIBV, G4330C, and G9230A. CPE was extended to almost the whole monolayers at 3 days post-electroporation (Fig. 2a). No CPE was observed in cells transfected with transcripts generated from clone G15526C (Fig. 2a).

RT-PCR analysis of the subgenomic mRNA 5 was performed to confirm if CPE observed is caused by the replication of IBV. Sequencing of the RT-PCR fragment generated from cells transfected with rIBV showed correct sequence in the leader/body junction region of the subgenomic mRNA (Fig. 2b). Further sequencing of the RT-PCR fragments covering regions with unique amino acid mutations confirmed the recovery of IBV (rIBV) from the in vitro-synthesized full-length transcripts.

Characterization of the rescued IBV virus (rIBV)

Compared to the parent IBV strains, rIBV contains 8 amino acid mutations (Table 2). To test if these mutations may affect the growth properties and genetic stability of the rescued virus, rIBV was propagated on Vero cells for 5 passages, and the plaque sizes and growth kinetics were determined and compared with wild type IBV p65. In cells infected with

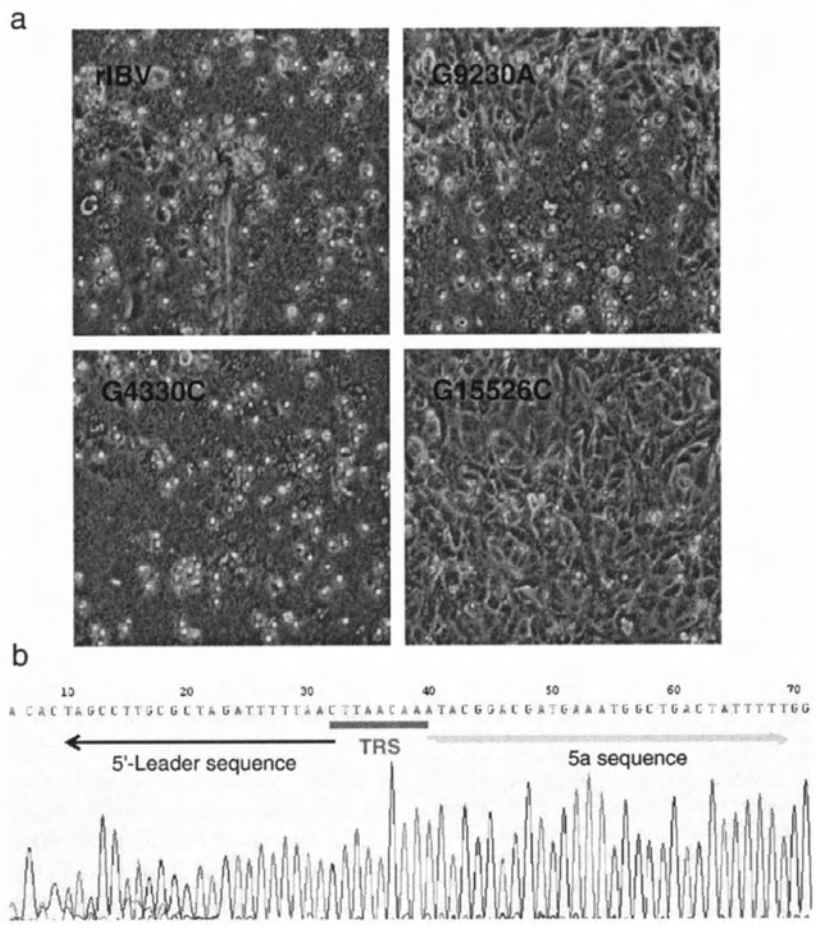

Fig. 2. Recovery of infectious viruses from cells electroporated with in vitro-synthesized full-length transcripts. (a) Vero cells electroporated with in vitro-synthesized transcripts derived from the in vitro assembled full-length clones with or without a point mutation at one of the three positions (G4330C, G9230A, or G15526C). Images were taken at 3 days post-electroporation. (b) Nucleotide sequencing of the leader/body junction of the subgenomic mRNA 5. Total RNA was prepared from Vero cells infected with the recombinant virus rescued from the in vitro-synthesized full-length transcripts 24 h post-infection. The 5′ 400-nucleotide region of the subgenomic mRNA 5 was amplified by RT-PCR and sequenced by automated nucleotide sequencing. The 70 nucleotides flanking the transcription regulatory sequence (TRS) for mRNA 5 are shown.

rIBV, the average plague size is 0.56±0.028 mm, which is slightly smaller than the average plaque size of 0.68±0.034 mm in cells infected with wild type IBV (Fig. 3a). Analysis of the growth curves demonstrated that rIBV exhibited very similar growth properties as the wild type virus (Fig. 3a).

Further characterization of rIBV was subsequently carried out by analysis of viral RNAs and structural proteins. Northern blot and Western blot analyses showed the detection of very similar amounts of viral RNAs (Fig. 3b), and S, N, and M proteins (Fig. 3c) in cells infected with wild type and rIBV, respectively, at 24 h post-infection. When probing with anti-N protein antibodies, other species migrating faster than the full-length products on SDS-PAGE were also observed (Fig. 3c). They may represent premature termination and cleavage products of N protein (unpublished observation). It was also noted that variable amounts of these species were detected in cells infected with wild type and rIBV (Fig. 3c). The significance of these variations is unclear at the moment. Taken together, these results confirm that rIBV is stable and possesses very similar growth properties as wild type IBV.

Absence of subgenomic RNA transcription in cells transfected with G15526C mutant transcripts

As no infectious virus was recovered from cells transfected with G15526C mutant transcripts, RT-PCR amplification of the negative strand RNA was performed to check if RNA replication occurred in these transfected cells. Total RNA was extracted from Vero cells transfected with wild type and G15526C mutant transcripts at 24 and 48 h post-electroporation, respectively. Reverse transcription was performed by using equal amount of RNA and the sense-primer IBV14931-F (5′-$_{14,931}$GCTTATCCACTAGTACATC$_{14,949}$-3′), and PCR was carried out by using the sense-primer IBV14931-F and the antisense-primer IBV15600-R (5′-$_{15,600}$CTTCTCGCACTTCTGCACTAGCA$_{15,578}$-3′). If replication of viral RNA occurred, a 670 bp PCR fragment would be expected. As shown in Fig. 4a, RT-PCR fragments amplified from negative strand RNA templates were obtained from cells transfected with both wild type (lanes 2 and 4) and the mutant transcripts (lanes 3 and 5). Sequencing of the PCR fragments confirmed that they represent the correct sequences. As a negative control, the in vitro-synthesized transcripts were mixed with total RNA extracted from normal Vero cells and were used as a template for RT-PCR. No RT-PCR fragment was detected (Fig. 4a, lane 6), confirming that the detection of negative strand RNA from cells transfected with mutant transcripts is due to the replication of viral RNA. Further quantitation of the negative strand RNA transcription in cells transfected with wild type and G15526C mutant transcripts was carried out by real-time PCR. At 24 and 48 h post-electroporation, transcription of the negative RNA in cells electroporated with wild type transcripts was 24.76- and 945.54-fold, respectively, higher than that in cells electroporated with the G15526C mutant transcripts. These results confirm that transcription of the negative strand RNA has taken place in cells transfected with the mutant transcripts, but with much lower efficiency.

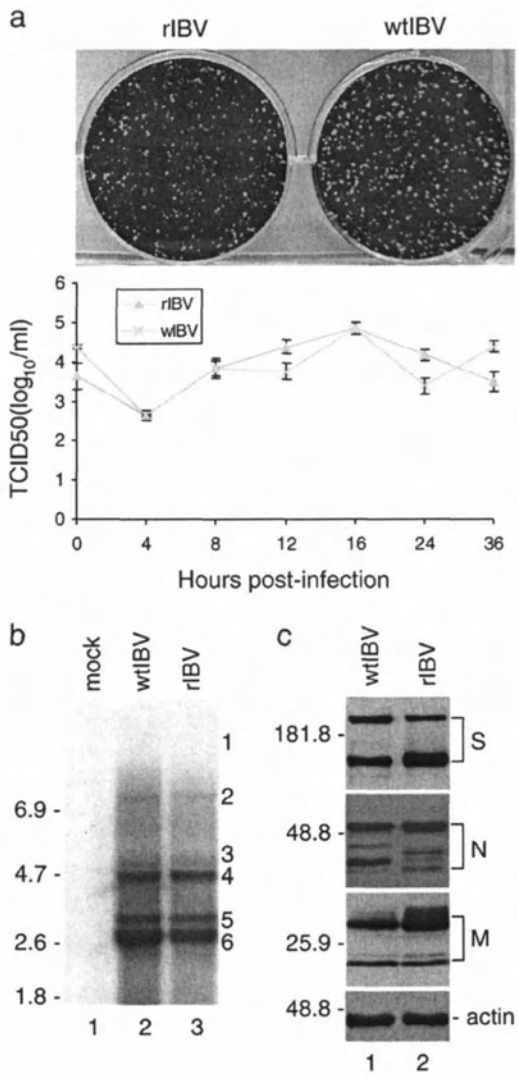

Fig. 3. Analysis of the growth properties of wild type (p65) and rIBV. (a) Plague sizes and one-step growth curves of wild type and rIBV. Monolayers of Vero cells on a 6-well plate were infected with 100 μl of 1000-fold diluted virus stock and cultured in the presence of 0.5% carboxymethy cellulose at 37 °C for 3 days. The cells were fixed and stained with 0.1% toluidine. To determine the one-step growth curves of wild type and rIBV, Vero cells were infected with the viruses and harvested at 0, 4, 8, 12, 16, 24, and 36 h post-inoculation, respectively. Viral stocks were prepared by freezing/thawing of the cells three times, and TCID50 of each viral stock was determined by infecting five wells of Vero cells on 96-well plates in triplicate with 10-fold serial dilution of each viral stock. Error bar shows standard error of the mean. (b) Northern blot analysis of the genomic and subgenomic RNAs in cells infected with wild type and rIBV. Ten micrograms of total RNA extracted from Vero cells infected with wild type and rIBV, respectively, was separated on 1% agarose gel and transferred to a Hybond N+ membrane. Viral RNAs were probed with a Dig-labeled DNA probe corresponding to the 3-end 680 nucleotides of the IBV genome. Total RNA extracted from mock-infected cells was included as negative control. Numbers on the left indicate nucleotides in kilobase, and numbers on the right indicate the genomic and subgenomic RNA species of IBV. (c) Western blot analysis of viral protein expression in cells infected with wild type and rIBV. Vero cells infected with wild type (lane 1) and rIBV (lane 2) were harvested, lysates prepared and separated on SDS-10% polyacrylamide gel. The expression of S, N, and M proteins was analyzed by Western blot with polyclonal anti-S, anti-N, and anti-M antibodies, respectively. The same membrane was also probed with anti-actin antibody as a loading control. Numbers on the left indicate molecular masses in kilodaltons.

RT-PCR amplification of subgenomic mRNAs was carried out to check if a low level of subgenomic mRNA synthesis could occur in cells transfected with the mutant transcripts. Total RNA prepared from the transfected cells 2 days post-electroporation was used in the RT reaction with the sense-primer IBV-leader ($5'$-$_{26}$CTATTACACTAGCCTTGCGCT$_{46}$-$3'$) for the detection of negative-stranded sgRNA, and the antisense-primer IBV24803-R ($5'$-$_{24,803}$CTCTGGATCCAATAACC-TAC$_{24,784}$-$3'$) for the detection of positive-stranded sgRNA. The two primers were then used for PCR. If transcription of subgenomic mRNAs did occur, a 415 bp PCR product corresponding to the 5′-terminal region of the subgenomic mRNA 4 and a 1010 bp fragment corresponding to the 5′-terminal region of the subgenomic mRNA 3 would be expected. As shown in Fig. 4b, a dominant 415 bp band and a weak 1010 bp band were observed in cells electroporated with wild type full-length transcripts at 2 days post-electroporation (lanes 2 and 5). Sequencing of the PCR fragments confirmed that they represent the correct sequences of the corresponding regions of the subgenomic mRNAs 3 and 4, respectively. However, the same PCR products were not detected in cells electroporated with the mutant transcripts (Fig. 4b, lanes 3 and 6). As a negative control, the amplified fragments were not detected in cells without electroporation (Fig. 4b, lane 4). The failure to detect both negative- and positive-stranded sgRNAs in cells transfected with the mutant transcripts show that the G15526C mutation leads to the disruption of subgenomic RNA transcription.

To further demonstrate that the failure to rescue infectious virus from the G15526C mutant transcripts is due to a defect in subgenomic RNA transcription, the full-length clones with and without the G15526C mutation were used to generate recombinant IBV expressing the enhanced green fluorescent protein (EGFP) by replacing the 5a gene with EGFP. Full-length transcripts containing EGFP were synthesized in vitro and introduced into Vero cells together with the N transcripts by electroporation. At 2 days post-electroporation, single CPE with the expression of EGFP was observed in cells transfected with the full-length transcripts without the G15526C mutation

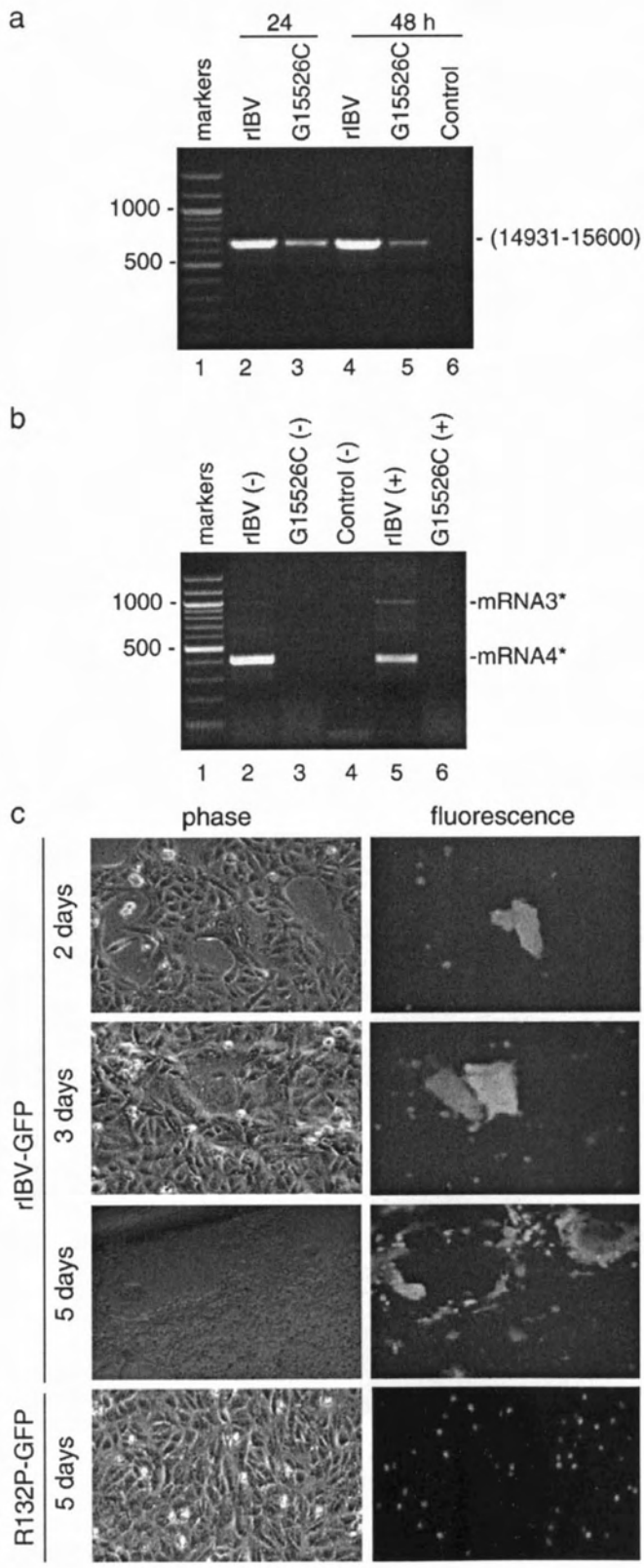

Fig. 4. Analysis of RNA replication in cells electroporated with G15526C mutant transcripts. (a) Detection of negative strand RNA synthesis in cells electroporated with wild type (lanes 2 and 4) and G15526C mutant (lanes 3 and 5) transcripts. Total RNA was prepared from Vero cells electroporated with in vitro-synthesized full-length transcripts at 24 and 48 h post-electroporation, respectively. Region corresponding to nucleotides 14,931–15,600 of the negative (−) sense IBV genomic RNA was amplified by RT-PCR and analyzed on 1.2% agarose gel. Lane 1 shows DNA markers, and lane 6 shows negative control. Numbers on the left indicate nucleotides in bases. (b) Detection of the negative and positive strand subgenomic RNA synthesis in cells electroporated with wild type (lanes 2 and 5) and G15526C mutant (lanes 3 and 6) transcripts. Total RNA was prepared from Vero cells electroporated with in vitro-synthesized full-length transcripts 2 days post-electroporation. Regions corresponding to the 5′-terminal 415 and 1010 nucleotides of the subgenomic mRNA 4 and 3, respectively, were amplified by RT-PCR and analyzed on 1.2% agarose gel. Lane 1 shows DNA markers, and lane 4 shows negative cell control. Numbers on the left indicate the length of DNA in bases. (c) Construction of a recombinant IBV expressing EGFP and further analysis of the effect of G15526C mutation on subgenomic transcription using the recombinant virus. Vero cells electroporated with in vitro-synthesized transcripts derived from the in vitro assembled full-length clones containing EGFP either with or without G15526C mutation. Phase-contrast and fluorescent images were taken 2, 3, and 5 days post-electroporation, respectively.

(Fig. 4c). Gradually increased CPE and fluorescent cells were observed from 3 to 5 days post-electroporation (Fig. 4c). At 5 days post-electroporation, CPE and fluorescent cells were extended to almost the whole monolayer (Fig. 4c). However, it was consistently observed that much less infectious virus was recovered from cells transfected with this construct. Furthermore, the recombinant virus rapidly lost infectivity when passaged on Vero cells; the recovered virus maintains minor infectivity only for one passage. In cells transfected with the full-length transcripts containing the G15526C mutation, neither CPE nor cells expressing EGFP were observed (Fig. 4c), demonstrating that G15526C mutation led to total demolition of the EGFP expression. As EGFP could be expressed only if subgenomic RNAs were synthesized but can be observed even if a single cell was transfected and expressed the protein to a certain level, these results reinforce the conclusion that the G15526C mutation blocks subgenomic RNA transcription.

Mutational analysis of the R132 residue of the helicase protein

G15526C mutation resulted in the substitution mutation of the R132 with a Pro (R132P) of the helicase protein. Sequence comparison of the IBV helicase protein with other known coronaviruses showed that R132 residue is located adjacent to a conserved motif (Fig. 5a). In all sequenced coronaviruses, only IBV has a charged amino acid (R132) at this position (Fig. 5a). To assess if a positive charge amino acid at this position is essential for the function of the protein, mutation of R132 to a Lys (R132K) was carried out. Meanwhile, a conserved Leu residue (Ile in the case of TGEV) was found at this position in all other coronaviruses, mutation of R132 to a Leu (R132L) was also included.

In vitro full-length transcripts containing the R132K and R132L mutations were electroporated into Vero cells. As shown in Fig. 5b, transcripts generated from wild type (R132) and R132K mutant constructs showed very similar infectivity after introduction into Vero cells. Typical CPE was observed in large areas of the monolayers at 3 days post-electroporation (Fig. 5b), and recombinant viruses were recovered. However, R132L transcripts were found to be less infectious. In cells electroporated with transcripts generated from this mutant, typical CPE was observed in much restricted areas of the monolayer at 3 days post-electroporation (Fig. 5b).

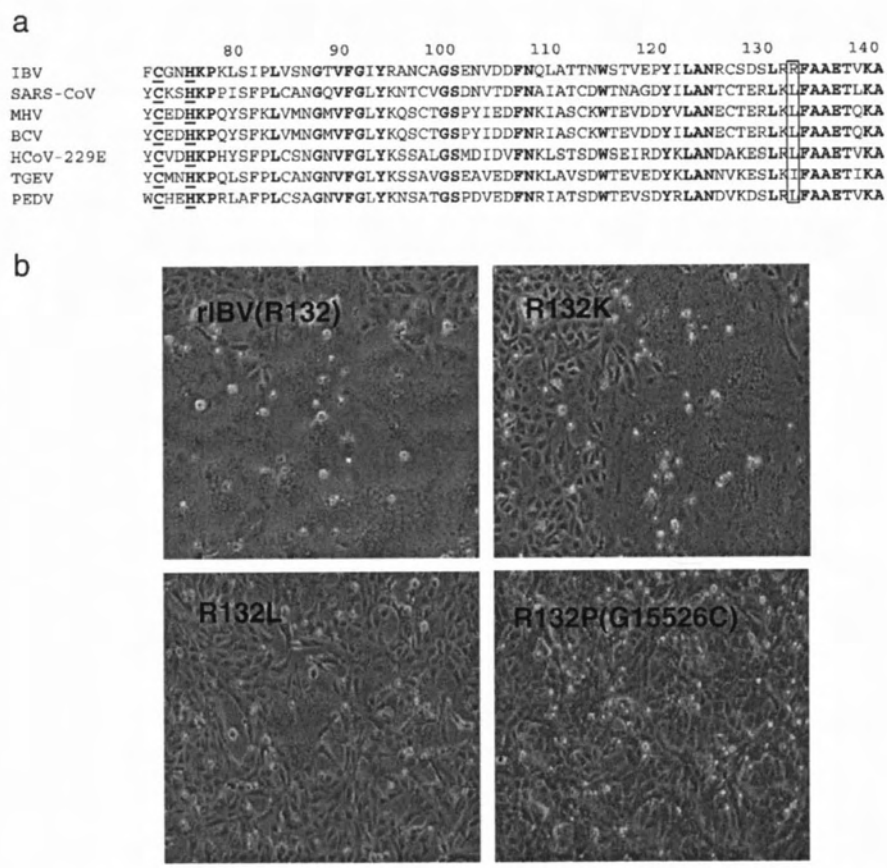

Fig. 5. Mutational analysis of the R132 residue of the helicase protein. (a) Sequence comparison of the region between amino acids 70 and 140 of helicase proteins from seven different coronaviruses. The identical amino acids are shown in bold, and the last Cys/His residues of the zinc-binding domain are shown in bold and underlined. Also shown are the R132 residue in IBV and the equivalent amino acids in other coronaviruses (boxed). (b) Vero cells electroporated with in vitro-synthesized transcripts derived from wild type recombinant IBV (rIBV), R132K, R132L, and R132P (G15526C) constructs. Phase-contrast images were taken 3 days post-electroporation.

Genetic stability and growth kinetics of R132K and R132L mutant viruses

The growth properties of the R132K and R132L mutant viruses on Vero cells were tested by analysis of plaque sizes and growth curves of passage 5 mutant viruses. Compared to cells infected with wild type recombinant virus (average plaques size is 0.56±0.028), plaques with similar size were observed in cells infected with the R132K mutant virus (Fig. 6a). The average plaque size in cells infected with R132K mutant virus is 0.59±0.029 mm. In cells infected with the R132L mutant virus, much smaller-sized plaques were observed (Fig. 6a). The average plaque size in cells infected with this mutant virus is 0.24±0.017 mm. However, analysis of the growth curves of wild type and mutant viruses demonstrated that the mutant viruses exhibited very similar, or even better, growth properties as the wild type recombinant virus (Fig. 6a).

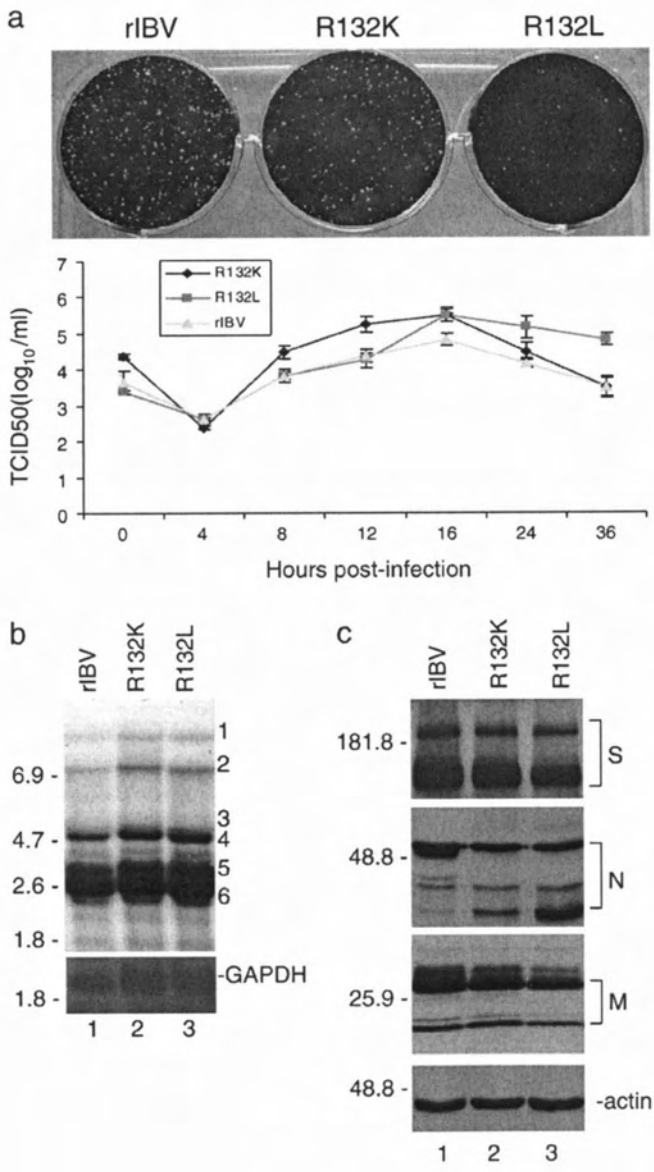

Fig. 6. Analysis of the growth properties of rIBV, R132K, and R132L mutant viruses. (a) Plague sizes and one-step growth curves of rIBV, R132K, and R132 mutant viruses. Monolayers of Vero cells on a 6-well plate were infected with 100 μl of 100-fold diluted virus stock and cultured in the presence of 0.5% carboxymethy cellulose at 37 °C for 3 days. The cells were fixed and stained with 0.1% toluidine. To determine the one-step growth curves of rIBV, R132K, and R132L mutant viruses, Vero cells were infected with the viruses and harvested at 0, 4, 8, 12, 16, 24, and 36 h post-inoculation, respectively. Viral stocks were prepared by freezing/thawing of the cells three times, and TCID50 of each viral stock was determined by infecting five wells of Vero cells on 96-well plates in triplicate with 10-fold serial dilution of each viral stock. Error bar shows standard error of the mean. (b) Northern blot analysis of the genomic and subgenomic RNAs in cells infected with rIBV, R132K, and R132L mutant viruses. Ten micrograms of total RNA extracted from Vero cells infected with rIBV, R132K, and R132L mutant viruses, respectively, was separated on 1% agarose gel and transferred to a Hybond N+ membrane. Viral RNAs were probed with a Dig-labeled DNA probe corresponding to the 3-end 680 nucleotides of the IBV genome. Numbers on the left indicate nucleotides in kilobase, and numbers on the right indicate the genomic and subgenomic RNA species of IBV. (c) Western blot analysis of viral protein expression in cells infected with wild type and R132 mutant viruses. Vero cells infected with wild type recombinant IBV (lane 1), R132K (lane 2), and R132L (lane 3) were harvested, lysates prepared, and separated on SDS-10% polyacrylamide gel. The expression of S, N, and M proteins was analyzed by Western blot with polyclonal anti-S, anti-N, and anti-M antibodies, respectively. The same membrane was also probed with anti-actin antibody as a loading control. Numbers on the left indicate molecular masses in kilodaltons.

The R132K and R132L mutant viruses were subsequently characterized by analysis of viral RNAs and structural proteins. Northern blot analysis showed the detection of very similar amounts of genomic and subgenomic RNAs in cells infected with rIBV and the two mutant viruses at 24 h post-infection (Fig. 6b). Similarly, Western blot analysis of cells infected with rIBV, R132K, and R132L mutant viruses showed that similar amounts of S, N, and M proteins were detected at 24 h post-infection (Fig. 6c, lanes 1–3). When probing with anti-N protein antibodies, other species migrating faster than the full-length products on SDS-PAGE were also observed (Fig. 6c). They may represent premature termination and cleavage products of N protein (unpublished observation). It was also noted that variable amounts of these species were detected in cells infected with wild type and different mutants (Fig. 6c).

The genetic stability of R132K and R132L mutant viruses was tested by propagation of the viruses on Vero cells for 5 passages. Sequencing analysis of the fifth passages of the two mutant viruses showed that the mutations are stable. No reversion to the original sequences or mutation to other nucleotides was found in the position.

Discussion

In vitro assembly of full-length coronavirus clones, generation of full-length transcripts in vitro using a bacteriophage DNA-dependent RNA polymerase, and recovery of infectious viruses by introduction of the in vitro-synthesized transcripts into cells, first used by Yount et al. (2000), are a rapid and reliable approach to construct infectious clones from large RNA viruses. It has been successfully used to construct infectious

clones for several coronaviruses, including transmissible gastroenteritis virus (TGEV), mouse hepatitis virus (MHV), SARS-CoV, and IBV (Youn et al., 2005a, 2005b; Yount et al., 2000, 2003). In the process of developing an infectious IBV clone from a Vero cell-adapted IBV Beaudette strain using this approach, a G–C point mutation at nucleotide position 15,526 was found to be lethal to the infectivity of the in vitro-synthesized full-length transcripts on Vero cells. No infectious virus could be rescued from Vero cells electroporated with transcripts containing this mutation. This mutation causes Arg132–Pro substitution in a domain within the helicase protein (Nsp13) with undefined functions, indicating that this domain may be essential for the functionality of the helicase protein.

Multiple enzymatic activities have been assigned to the Nsp13 helicase protein. These include RNA and DNA duplex-unwinding activities, NTPase and dNTPase activities, and an RNA 5′-triphosphatase activity that might be involved in the formation of the 5′-cap structure of viral RNAs (Ivanov et al., 2004). The protein is comprised of two domains: a putative N-terminal zinc binding domain, which spans the N-terminal region of the protein from approximately amino acids 1 to 77, and a C-terminal helicase domain covering the C-terminal part of the protein from amino acids 279 to the C-terminal end (Ivanov et al., 2004). A Ser–Pro substitution located immediately downstream of the putative zinc binding domain of Nsp10, the equivalent RNA helicase protein in equine arteritis virus (EAV), caused defect in subgenomic mRNA transcription (van Dinten et al., 1997, 2000). More detailed analysis of the zinc binding domain of Nsp10 from EAV and Nsp13 from human coronavirus 229E by mutagenesis studies showed that this domain could modulate the enzymatic activities of the helicase domain (Seybert et al., 2005). Through this regulatory role and some yet to be discovered mechanisms, the zinc binding domain is shown to be critically involved in the replication and transcription of coronavirus RNA.

In this study, introduction of the in vitro-synthesized full-length transcripts containing the G15526C (R132P) mutation was shown to be totally defective in subgenomic RNA transcription, a phenotype similar to, but appears to be much more severe than, the Ser–Pro mutation in EAV (van Dinten et al., 1997, 2000). Mutation of the Arg132 residue to a positively charged amino acid (Lys) does not affect the infectivity of the in vitro-synthesized transcripts as well as the growth properties of the rescued virus. However, mutation of the Arg132 residue to Leu, a conserved residue at the same position in most of other known coronaviruses, impaired the recovery rate of the in vitro-synthesized transcripts. The recovered mutant virus showed much smaller-sized plaques. The R132 residue is located 57 amino acids downstream of the last His (H75) residue in the putative zinc binding domain (Fig. 5a) and 147 amino acids upstream of the helicase motif 1 (Seybert et al., 2005). So far, no functional domain has been found in this region of the helicase protein.

Why the R132P substitution, located outside of the two functional domains of the helicase protein, shows severe phenotypic defect in subgenomic RNA transcription and the infectivity of IBV is not clear at the moment. Three possibilities were considered. First, R132 may be part of the N-terminal zinc binding domain. As no studies have been attempted to define the boundary of the two domains, it is not even certain that an independent domain with unique function may exist in this region. R132P mutant virus shares certain phenotypic similarity to the Ser–Pro mutant EAV, such as the absence of subgenomic mRNA transcription (van Dinten et al., 1997, 2000), suggesting that the two mutations might disrupt a similar function of the helicase protein. However, as biochemical characterization of the effect of R132P mutation on the enzymatic activities of IBV Nsp13 helicase protein is currently lacking, it would be difficult to draw a conclusion that the two mutants share mechanistically similar characteristics. Second, R132 is located in a region with a high degree of amino acid conservation in all known coronaviruses. Since the main defect of R132P mutant virus is in the subgenomic RNA transcription, one possibility is that this region may be involved in the subgenomic RNA synthesis by interacting with host or other viral functional proteins. Alternatively, as a positively charged amino acid is required to maintain the full function of the protein, it would be possible that this region may be involved in binding of the helicase protein to viral RNA during RNA replication and transcription. Finally, mutation to a Pro would lead to the disruption of the three dimensional structures of the two domains. Biochemical characterization of the involvement of this region in the enzymatic activities of the protein and determination of its three dimensional structures are underway to address these possibilities.

The G433C (E–Q) point mutation near the catalytic center of the PLP domain in Nsp3 affects neither the recovery of infectious virus from the full-length synthesized in vitro transcripts nor the infectivity of the rescued virus. Similarly, efficient recovery of infectious virus from the in vitro transcripts containing the G9230A (G–E) point mutation in the 3CLP was obtained. The two mutant viruses are genetically stable and show similar growth properties with the wild type recombinant virus. Even though the two mutations are located in or near the catalytic centers of the two viral proteinases, the mutations did not alter their enzymatic activities. This relatively high degree of tolerance to mutations in non-essential regions of important functional proteins would minimize the occurrence of lethal mutations during the replication cycles of RNA viruses and increase the adaptability of these viruses to a changed environment.

Materials and methods

Cells and virus

Vero cells were cultured at 37 °C in minimal essential medium (MEM) supplemented with 10% fetal bovine serum (FBS), penicillin (100 units/ml), and streptomycin (100 μg/ml). A Vero cell-adapted IBV Beaudette strain (65 passages on Vero cells (p65)) (Shen et al., 2003, 2004; Fang et al., 2005) was propagated in Vero cells in FBS-free MEM.

Reverse transcription (RT)-polymerase chain reaction (PCR), cloning, and sequencing

Five fragments spanning the entire IBV genome were obtained by RT-PCR from Vero cells infected with the Vero cell-adapted IBV p65 at a multiplicity of approximately 1. Briefly, total cellular RNA was extracted from the infected Vero cells with TRI Reagent (Molecular Research Center, Inc.), according to the manufacturer's instructions. Reverse transcription was performed with Expand Reverse Transcriptase (Roche) using reverse primers IBV-5753R, IBV-8694R, IBV-15532R, IBV-20930R, and IBV-27608R (Table 1). Each cDNA fragment was amplified from RT products by PCR using KOD Hot Start DNA polymerase according to the manufacturer's instructions (Novagen). The PCR products were purified from agarose gels and cloned into pCR-XL-TOPO (Invitrogen) or pGEM-T Easy (Promage) vectors. Subsequently, fragment A was removed from pCR-XL-TOPO by digestion with *Nhe*I and *Eco*RI and subcloned into pKT0 vector.

Two to three independent clones of each fragment were selected and sequenced by automated sequencing using specific primers and the ABI dye termination sequencing method. Sequence comparison, assembly, and analysis were performed by using BLAST and DNA STAR software.

PCR mutagenesis

Mutations were introduced into the corresponding fragments by using QuickChange site-directed mutagenesis kit (Stratagene) and confirmed by sequencing of the whole fragments.

In vitro assembly of full-length cDNA clones

Plasmids were digested with either *Bsm*BI (fragment A) or *Bsa*I (fragments B, C, D, and E). The digested plasmids were separated on 0.8% agarose gels containing crystal violet. Bands corresponding to each of the fragments were cut from the gels and purified with QIAquick gel extraction kit (QIAGEN Inc.).

Fragments A and B, and fragments C, D, and E were first ligated with T4 DNA ligase at 4 °C overnight. The two reaction mixtures were then mixed and further ligated at 4 °C overnight. The final ligation products were extracted with phenol/chloroform/isoamyl alcohol (25:24:1), precipitated with ethanol, and detected by electrophoresis on 0.4% agarose gels.

In vitro transcription and electroporation

Full-length transcripts were generated in vitro using the mMessage mMachine T7 kit (Ambion, Austin, TX) according to the manufacturer's instructions with certain modifications. Briefly, 30 μl of transcription reaction with a 1:1 ratio of GTP to cap analog was sequentially incubated at 40.5 °C for 25 min, 37.5 °C for 50 min, 40.5 °C 25 min and 37.5 °C for 20 min.

The N transcripts were generated by using a linearized pKTO-IBVN containing IBV N gene and the 3′-UTR region as templates. A 1:2 ratio of GTP to cap analog was used for the transcription of IBV N gene.

Introduction of in vitro-synthesized transcripts into Vero cells by electroporation

The in vitro-synthesized full-length and N transcripts were treated with DNaseI and purified with phenol/chloroform. Vero cells were grown to 90% confluence, trypsinized, washed twice with cold PBS, and resuspended in PBS. RNA transcripts were added to 400 μl of Vero cell suspension in an electroporation cuvette and electroporated with one pulse at 450 V, 50 μF with a Bio-Rad Gene Pulser II electroporator. The transfected Vero cells were cultured overnight in 1% FBS-containing MEM in a 60 mm dish or a six-well plate and further cultured in MEM without FBS.

Analysis of the negative strand and subgenomic RNAs by RT-PCR, real-time PCR

Total RNA was extracted from Vero cells electroporated in in vitro-synthesized transcripts after treatment with DNaseI, using TRI Reagent (Molecular Research Center, Inc.) at 24 or 48 h post-electroporation. Reverse transcription was performed with Expand Reverse Transcriptase (Roche) using equal amount of RNA. After optimization, real-time PCR was performed using LightCycler FastStart DNA Master SYBR Green I kit according to the manufacturer's instructions (Roche).

Northern blot analysis

Vero cells were infected with wild type and mutant viruses at a multiplicity of approximately 1, and total RNA was extracted from the infected cells. Ten micrograms of RNA was added to a mixture of 1× MOPS, 37% formaldehyde, and formamide and incubated at 65 °C for 20 min before subjected to gel electrophoresis. The segregated RNA bands were transferred onto a Hybond N+ membrane (Amersham Biosciences) via capillary action overnight and fixed by UV crosslinking (Stratalinker). Hybridization of Dig-labeled DNA probes was carried out at 50 °C in hybridization oven overnight. Membranes were washed 3 times for 15 min each with the probe buffer, before proceeding to detection with CDP-Star (Roche) according to the manufacturer's instructions.

Western blot analysis

Vero cells were infected with wild type and mutant viruses at a multiplicity of approximately 1. Total proteins extracted from the infected Vero cells were lysed with 2× SDS loading buffer in the presence of 200 mM DTT plus 10 mM of iodoacetamide and subjected to SDS-PAGE. Proteins were transferred to PVDF membrane (Stratagene) and blocked overnight at 4 °C in blocking buffer (5% fat free milk powder in PBST buffer). The membrane was incubated with 1:2000 diluted primary antibodies in blocking buffer for 2 h at room temperature. After washing three times with PBST, the membrane was incubated with 1:2000 diluted anti-mouse or anti-rabbit IgG antibodies conjugated with horseradish peroxidase (DAKO) in blocking buffer for 1 h at room temperature. After washing three times

with PBST, the polypeptides were detected with a chemiluminescence detection kit (ECL, Amersham Biosciences) according to the manufacturer's instructions.

Growth curve and plaque sizes of the recombinant viruses on Vero cells

Confluent monolayers of Vero cells on six-well plates were infected with 100 µl of 100-fold diluted virus stock. After 1 h of incubation at 37 °C, cells were washed twice with PBS and cultured in 3 ml of MEM containing 0.5% carboxymethy cellulose for 3 days. The cells were fixed and stained with 0.1% toluidine.

Vero cells were infected with wild type and recombinant IBV and harvested at different times post-infection. Viral stocks were prepared by freezing/thawing of the cells three times. The 50% tissue culture infection dose (TCID50) of each sample was determined by infecting five wells of Vero cells on 96-well plates in duplicate with 10-fold serial dilution of each viral stock.

Acknowledgments

This work was supported by the Agency for Science Technology and Research, Singapore, and by a grant from the Biomedical Research Council (BMRC 03/1/22/17/220), Agency for Science, Technology and Research, Singapore.

References

Almazan, F., Gonzalez, J.M., Penzes, Z., Izeta, A., Calvo, E., Plana-Duran, J., Enjuanes, L., 2000. Engineering the largest RNA virus genome as an infectious bacterial artificial chromosome. Proc. Natl. Acad. Sci. U.S.A. 97, 5516–5521.

Boursnell, M.E.G., Brown, T.D.K., Foulds, I.J., Green, P.F., Tomley, F.M., Binns, M.M., 1987. Completion of the sequence of the genome of the coronavirus avian infectious bronchitis virus. J. Gen. Virol. 68, 57–77.

Casais, R., Thiel, V., Siddell, S.G., Cavanagh, D., Britton, P., 2001. Reverse genetics system for the avian coronavirus infectious bronchitis virus. J. Virol. 75, 12359–12369.

Casais, R., Dove, B., Cavanagh, D., Britton, P., 2003. Recombinant avian infectious bronchitis virus expressing a heterologous spike gene demonstrates that the spike protein is a determinant of cell tropism. J. Virol. 77, 9084–9089.

Casais, R., Davies, M., Cavanagh, D., Britton, P., 2005. Gene 5 of the avian coronavirus infectious bronchitis virus is not essential for replication. J. Virol. 79, 8065–8078.

Coley, S.E., Lavi, E., Sawicki, S.G., Fu, L., Schelle, B., Karl, N., Siddell, S.G., Thiel, V., 2005. Recombinant mouse hepatitis virus strain A59 from cloned, full-length cDNA replicates to high titers in vitro and is fully pathogenic in vitro. J. Virol. 79, 3097–3106.

Fang, S.G., Shen, S., Tay, F.P., Liu, D.X., 2005. Selection of and recombination between minor variants lead to the adaptation of an avian coronavirus to primate cells. Biochem. Biophys. Res. Commun. 336, 417–423.

Hodgson, T., Britton, P., Cavanagh, D., 2006. Neither the RNA nor the proteins of open reading frames 3a and 3b of the coronavirus infectious bronchitis virus are essential for replication. J. Virol. 80, 296–305.

Ivanov, K.A., Thiel, V., Dobbe, J.C., van der Meer, Y., Snijder, E.J., Ziebuhr, J., 2004. Multiple enzymatic activities associated with severe acute respiratory syndrome coronavirus helicase. J. Virol. 78, 5619–5632.

Koetzner, C.A., Parker, M.M., Ricard, C.S., Sturman, L.S., Masters, P.S., 1992. Repair and mutagenesis of the genome of a deletion mutant of the coronavirus mouse hepatitis virus by targeted RNA recombination. J. Virol. 66, 1841–1848.

Lim, K.P., Liu, D.X., 1998a. Characterization of a papain-like proteinase domain encoded by ORF1a of the coronavirus IBV and determination of the C-terminal cleavage site of an 87 kDa protein. Adv. Exp. Med. Biol. 440, 173–184.

Lim, K.P., Liu, D.X., 1998b. Characterization of the two overlapping papain-like proteinase domains encoded in gene 1 of the coronavirus infectious bronchitis virus and determination of the C-terminal cleavage site of an 87 kDa protein. Virology 245, 303–312.

Lim, K.P., Ng, L.F., Liu, D.X., 2000. Identification of a novel cleavage activity of the first papain-like proteinase domain encoded by open reading frame 1a of the coronavirus avian infectious bronchitis virus and characterization of the cleavage products. J. Virol. 74, 1674–1685.

Liu, D.X., Tibbles, K.W., Cavanagh, D., Brown, T.D.K., Brierley, I., 1995. Identification, expression and processing of an 87K polypeptide encoded by ORF1a of the coronavirus infectious bronchitis virus. Virology 208, 47–54.

Liu, D.X., Xu, H.Y., Brown, T.D.K., 1997. Proteolytic processing of the coronavirus infectious bronchitis virus 1a polyprotein: identification of a 10 kDa polypeptide and determination of its cleavage sites. J. Virol. 71, 1814–1820.

Liu, D.X., Shen, S., Xu, H.Y., Wang, S.F., 1998. Proteolytic mapping of the coronavirus infectious bronchitis virus 1b polyprotein: evidence for the presence of four cleavage sites of the 3C-like proteinase and identification of two novel cleavage products. Virology 246, 288–297.

Marra, M.A., Jones, S.J.M., Astell, C.R., Holt, R.A., Brooks-Wilson, A., Butterfield, Y.S.N., Khattra, J., Asano, J.K., et al., 2003. The genome sequence of the SARS-associated coronavirus. Science 300, 1399–1404.

Masters, P.S., Rottier, P.J., 2005. Coronavirus reverse genetics by targeted RNA recombination. Curr. Top. Microbiol. Immunol. 287, 133–159.

Ng, L.F., Liu, D.X., 1998. Identification of a 24 kDa polypeptide processed from the coronavirus infectious bronchitis virus 1a polyprotein by the 3C-like proteinase and determination of its cleavage sites. Virology 243, 388–395.

Ng, L.F., Liu, D.X., 2000. Further characterization of the coronavirus infectious bronchitis virus 3C-like proteinase and determination of a new cleavage. Virology 272, 27–39.

Ng, L.F., Liu, D.X., 2002. Membrane association and dimerization of a cysteine-rich, 16-kDa polypeptide released from the C-terminal region of the coronavirus infectious bronchitis virus 1a polyprotein. J. Virol. 76, 6257–6267.

Rota, P.A., Oberste, M.S., Monroe, S.S., Nix, W.A., Campagnoli, R., Icenogle, J.P., Penaranda, S., et al., 2003. Characterization of a novel coronavirus associated with severe acute respiratory syndrome. Science 300, 1394–1999.

Sanchez, C.M., Izeta, A., Sanchez-Morgado, J.M., Alonso, S., Sola, I., Balasch, M., Plana-Duran, J., Enjuanes, L., 1999. Targeted recombination demonstrates that the spike gene of transmissible gastroenteritis coronavirus is a determinant of its enteric tropism and virulence. J. Virol. 73, 7607–7618.

Seybert, A., Posthuma, C.C., van Dinten, L.C., Snijder, E.J., Gorbalenya, A.E., Ziebuhr, J., 2005. A complex zinc finger controls the enzymatic activities of nidovirus helicases. J. Virol. 79, 696–704.

Shen, S., Wen, Z.L., Liu, D.X., 2003. Emergence of an avian coronavirus infectious bronchitis virus (IBV) mutant with a truncated 3b gene: functional characterization of the 3b gene in pathogenesis and replication. Virology 311, 16–27.

Shen, S., Law, Y.C., Liu, D.X., 2004. A Single amino acid mutation in the spike protein of coronavirus infectious bronchitis virus hampers its maturation and incorporation into virions at the nonpermissive temperature. Virology 326, 288–298.

Thiel, V., Herold, J., Schelle, B., Siddell, S.G., 2001. Infectious RNA transcribed in vitro from a cDNA copy of the human coronavirus genome cloned in vaccinia virus. J. Gen. Virol. 82, 1273–1281.

van Dinten, L.C., den Boon, J.A., Wassenaar, A.L., Spaan, W.J., Snijder, E.J., 1997. An infectious arterivirus cDNA clone: identification of a replicase point mutation that abolishes discontinuous mRNA transcription. Proc. Natl. Acad. Sci. U.S.A. 94, 991–996.

van Dinten, L.C., van Tol, H., Gorbalenya, A.E., Snijder, E.J., 2000. The predicted metal-binding region of the arterivirus helicase protein is involved in subgenomic mRNA synthesis, genome replication, and virion biogenesis. J. Virol. 74, 5213–5223.

Xu, H.Y., Lim, K.P., Shen, S., Liu, D.X., 2001. Further identification and characterization of novel intermediate and mature cleavage products released from the ORF 1b region of the avian coronavirus infectious bronchitis virus 1a/1b polyprotein. Virology 288, 212–222.

Youn, S., Collisson, E.W., Machamer, C.E., 2005a. Contribution of trafficking signals in the cytoplasmic tail of the infectious bronchitis virus spike protein to virus infection. J. Virol. 79, 13209–13217.

Youn, S., Leibowitz, J.L., Collisson, E.W., 2005b. In vitro assembled, recombinant infectious bronchitis viruses demonstrate that the 5a open reading frame is not essential for replication. Virology 332, 206–215.

Yount, B., Curtis, K.M., Baric, R.S., 2000. Strategy for systematic assembly of large RNA and DNA genomes: transmissible gastroenteritis virus model. J. Virol. 74, 10600–10611.

Yount, B., Denison, M.R., Weiss, S.R., Baric, R.S., 2002. Systematic assembly of a full-length infectious cDNA of mouse hepatitis virus strain A59. J. Virol. 76, 11065–11078.

Yount, B., Curtis, K.M., Fritz, E.A., Hensley, L.E., Jahrling, P.B., Prentice, E., Denison, M.R., Geisbert, T.W., Baric, R.S., 2003. Reverse genetics with a full-length infectious cDNA of severe acute respiratory syndrome coronavirus. Proc. Natl. Acad. Sci. U.S.A. 100, 12995–13000.

Yount, B., Roberts, R.S., Sims, A.C., Deming, D., Frieman, M.B., Sparks, J., Denison, M.R., Davis, N., Baric, R.S., 2005. Severe acute respiratory syndrome coronavirus group-specific open reading frames encode nonessential functions for replication in cell cultures and mice. J. Virol. 79, 14909–14922.

Functional Roles and Biochemical Characterization of the Dimerization and RNA-Binding Activity of Nonstructural Protein 9 in the Replication and Infectivity of a Coronavirus

Bo Chen[1], Shouguo Fang[2], James P. Tam[1,3] and Ding Xiang Liu[1,2*]

(Submitted to Journal of Virology)

[1]School of Biological Sciences, Nanyang Technological University, 60 Nanyang Drive, Singapore 637551, [2]Institute of Molecular and Cell Biology, 61 Biopolis Drive, Proteos, Singapore 138673, and [3]The Scripps Research Institute, 5353 Parkside Drive, Jupiter, FL 33458, USA

Running Title: Biochemical and functional characterization of coronavirus nsp9

*Corresponding Author at:
Institute of Molecular and Cell Biology
61 Biopolis Drive, Proteos
Singapore 138673
Tel: 65 65869581
Fax: 65 67791117
E-mail: dxliu@imcb.a-star.edu.sg

ABSTRACT

Coronaviruses devote more than three quarters of their coding capacity to encode two large polyproteins (1a and 1ab polyproteins), which are proteolytically processed into 15-16 mature, nonstructural replicase proteins (nsp1 to 16). These cleavage products are believed to play essential roles in replication of the giant RNA genome of ~30 kb and transcription of a nested set of 5 to 9 subgenomic RNA species by a unique discontinuous transcription mechanism. In this report, one of these replicase proteins, nsp9 of the coronavirus infectious bronchitis virus (IBV) is systematically studied using both biochemical and reverse genetics approaches. The results showed that substitution of a conserved Gly (G98) residue in the C-terminal α-helix with an Asp greatly destabilized the IBV nsp9 homodimer and abolished its RNA-binding activity. Introduction of the same mutation into an infectious IBV clone system showed that the mutation totally abolishes the transcription of subgenomic RNA and no infectious virus could be recovered. Mutation of a semi-conserved Ile (I95) residue in the same region showed moderately destabilizing effect on the IBV nsp9 homodimer but minimal effect on its RNA-binding activity. Introduction of the mutation into the IBV infectious clone system showed recovery of a mutant virus with severe growth defects, supporting that dimerization is critical for the function of this replicase protein. Meanwhile, mutations of some positively charged residues in the β-barrel regions of the IBV nsp9 protein significantly reduced its RNA-binding activity, but with no obvious effect on dimerization of the protein. Introduction of these mutations into the viral genome showed only mild to moderate effects on the growth and infectivity of the rescued mutant viruses.